

001
002
003
004
005
006
007
008
009
010
011
012
013
014
015
016
017
018
019
020
021
022
023
024
025
026
027
028
029
030
031
032
033
034
035
036
037
038
039
040
041
042
043
044
045
046

Microbial symbionts buffer hosts from the demographic costs of environmental stochasticity

Joshua C. Fowler^{1,2*}, Shaun Ziegler³, Kenneth D. Whitney³,
Jennifer A. Rudgers³, Tom E.X. Miller¹

¹*Department of BioSciences, Rice University, Houston, 77005, TX, USA.

²Department of Biology, University of Miami, Miami, 33146, FL, USA.

³Department of Biology, University of New Mexico, Albuquerque, 87131, NM, USA.

*Corresponding author(s). E-mail(s): jcf221@miami.edu;

Contributing authors: shaun.ziegler@gmail.com; whitneyk@unm.edu;

jrudgers@unm.edu; tom.miller@rice.edu;

Phone: 719-359-2960

Author Contributions

J.C.F. contributed to data collection, data analysis, and led manuscript drafting. S.Z. contributed to data collection and manuscript revisions. K.D.W. contributed to research conception, data collection, and manuscript revisions. J.A.R. established transplant plots, contributed to research conception, data collection, and manuscript revisions. T.E.X.M. contributed to research conception, data collection, data analysis, and manuscript revisions.

Data and Code Accessibility

Data will be made accessible as an Environmental Data Initiative package online
DOI: [updated here when available](#). Code for all analysis is available through
<https://github.com/joshuacfowler/Grass-Endophyte-Stochastic-Demography>

Article Type: Letter

Running Title: Symbiont-mediated demographic buffering

Keywords: stochastic demography, plant-microbe interactions, environmental variability, symbiosis, mutualism, long-term data, life history, Epichloë, Poaceae

This file contains: Abstract (150 words), Main Text (5397 words), Figures (1-4); Supporting Information - Supplemental Methods, Supplemental Figures A1-A28, Supplemental Tables S1-S3, References (66)

047

Abstract

048

Species' persistence in increasingly variable climates will depend on resilience
049 against the fitness costs of environmental stochasticity. Most organisms host
050 microbiota that shield against stressors. Here, we test the hypothesis that, by
051 limiting exposure to environmental extremes, microbial symbionts reduce hosts'
052 demographic variance. We parameterized stochastic models using data from a
053 14-year symbiont-removal experiment including seven grass species that host
054 *Epichloë* fungal endophytes. Endophytes reduced variance in fitness by > 10%, on
055 average. Hosts with "fast" life history traits that lacked longevity as an intrinsic
056 buffer benefited most from symbiont-mediated variance buffering. Under current
057 climate conditions, contributions of variance buffering were modest compared to
058 symbiont benefits to mean fitness. However, simulations of increased stochasticity
059 amplified benefits of variance buffering and made it the more important pathway
060 of host-symbiont mutualism than elevated mean fitness. Microbial-mediated
061 variance buffering is likely an important, yet cryptic, mechanism of resilience in
062 an increasingly variable world.

063

064

065

066

067

068

069

070

071

072

073

074

075

076

077

078

079

080

081

082

083

084

085

086

087

088

089

090

091

092

Introduction	093
Global climate change involves heterogenous changes in environmental variability, including changes to precipitation patterns and increases in frequency of extreme weather events [1–3]. Yet, the ecological consequences of increasing variability are less well understood than those of changing climate means, such as long-term warming or drying. Incorporating environmental variability into forecasts of population dynamics can improve predictions of the future [4].	094
Classic theory predicts that long-term population growth rates (equivalently, population mean fitness) will decline under increased environmental stochasticity because the costs of bad years outweigh the benefits of good years – a consequence of nonlinear averaging [5, 6]. For example, in unstructured populations, the long-term stochastic growth rate in a fluctuating environment (λ_s) will always be lower than the arithmetic mean growth rate ($\bar{\lambda}$) by an amount proportional to the environmental variance (σ^2):	095
$\log(\lambda_s) \approx \log(\bar{\lambda}) - \frac{\sigma^2}{2\bar{\lambda}^2} \quad (1)$	096
Populations structured by size or stage similarly experience costs of temporal variability [7, 8]. There are accordingly two pathways to increase population viability in a variable environment: increase the arithmetic mean of growth rate and/or dampen temporal fluctuation in growth rates, also called “demographic buffering”.	097
Both the inherent characteristics of species and the external properties of their environment can buffer demographic fluctuations. These inherent characteristics include life history traits [9], negative correlations among vital rates [10], and transient shifts in population structure [11]. For example, theory predicts that long-lived species, those on the slow end of the slow-fast life history continuum, will be less sensitive to environmental variability than short-lived species [12], a pattern which has empirical support across plants [13, 14] and animals [15, 16]. Demographic variance is also determined by external abiotic factors, such as the magnitude of environmental variability [17] or the degree of environmental autocorrelation [18, 19]. These complex interplay of these factors determines the risks of extinction faced by populations [20] and underlies management strategies promoting ecosystem resilience [21]. Yet little is known about how biotic interactions influence demographic variability or contribute to demographic buffering [22].	098
Most research on biotic interactions has focused on effects on mean demographic performance, yet species interactions also have the potential to influence demographic variance. Inter-specific interactions that dampen variance in sensitive vital rates, such as parental care of juveniles in birds [23] and in primates [24] can improve fitness. Inter-specific interactions are pervasive and have this same potential. Most multicellular organisms host symbiotic microbes that affect growth and performance [25, 26], and many of these are vertically transmitted from maternal hosts to offspring [27]. Vertical transmission links the fitness of hosts and symbionts in a feedback loop that selects for mutual benefits [28]. Many vertically-transmitted microbes are mutualistic and protect hosts from stressful environmental conditions including drought, extreme temperatures, or natural enemies [29, 30]. Some of the best studied examples include	099
	100
	101
	102
	103
	104
	105
	106
	107
	108
	109
	110
	111
	112
	113
	114
	115
	116
	117
	118
	119
	120
	121
	122
	123
	124
	125
	126
	127
	128
	129
	130
	131
	132
	133
	134
	135
	136
	137
	138

139 bacterial symbionts of insects that provide their hosts with thermal tolerance through
140 the production of heat-shock proteins [31], and fungal symbionts of plants that pro-
141 duce anti-herbivore and drought-protective compounds [32–34]. However, these diverse
142 protective symbioses are context-dependent: the magnitude of benefits depends on
143 environmental conditions [35, 36] and thus will vary temporally in a stochastic envi-
144 ronment [37]. We hypothesized that context-dependent benefits from symbionts may
145 buffer hosts against variability through strong benefits during harsh periods and neu-
146 tral or even costly outcomes during benign periods, reducing the impacts of host
147 exposure to extremes and dampening inter-annual variance relative to non-symbiotic
148 hosts (Fig. 1). Variance buffering is a previously unexplored mechanism by which sym-
149 bionts may benefit their hosts instead of or in addition to elevating average fitness,
150 the focus of most previous research.

151 To test the hypothesis that context-dependent benefits of symbiosis buffer hosts
152 from the fitness costs of environmental stochasticity, we used a combination of long-
153 term field experiments and stochastic demographic modeling. We used cool-season
154 grasses and *Epichloë* fungal endophytes as a tractable experimental model in which
155 non-symbiotic plants can be derived from naturally symbiotic plants through heat
156 treatment, providing a contrast of symbiont effects that controls for the confounding
157 influence of host genetic background. *Epichloë* endophytes are specialized symbionts
158 growing intercellularly in the aboveground tissue of ~ 30% of C_3 grass species [38].
159 These fungi are primarily transmitted vertically from maternal plants through seeds
160 [39]. They produce a variety of alkaloids that can protect host plants from natural
161 enemies [40] and drought stress [41].

162 Over 14 years (2007–2021), we collected longitudinal demographic data on the
163 survival, growth, reproduction, and recruitment of all plants within replicated
164 endophyte-symbiotic and endophyte-free populations at our field site in southern Indi-
165 ana, USA. Through taxonomic replication (seven host-symbiont species pairs) we
166 aimed to understand whether host life history traits could explain inter-specific vari-
167 ation in the magnitude of demographic buffering through symbiosis. We used this
168 long-term data to parameterize stochastic population projection models in a hierar-
169 chical Bayesian framework. Specifically, we (1) quantified the effect of symbiosis on
170 the mean and variance of host vital rates (survival, growth and reproduction) and fit-
171 ness, (2) evaluated the relationship between host life history traits and the magnitude
172 of symbiont-mediated variance buffering, (3) determined the relative contribution of
173 symbiont-mediated mean and variance effects to host fitness, and (4) projected how
174 increased environmental stochasticity (expected under future climates) changes the
175 importance of variance buffering as a pathway of host-symbiont mutualism.
176

177 Materials and Methods

178 Study site and species

180 This study was conducted at Indiana University’s Lilly-Dickey Woods Research and
181 Teaching Preserve (39.238533, -86.218150) in Brown County, Indiana, USA. This site
182 is part of the Eastern broadleaf forests of southern Indiana, where the ranges of many
183 understory cool-season grass species overlap. The experiment focused on seven of these
184

grasses (<i>Agrostis perennans</i> , <i>Elymus villosus</i> , <i>Elymus virginicus</i> , <i>Festuca subverticillata</i> , <i>Lolium arundinaceum</i> , <i>Poa alsodes</i> , and <i>Poa sylvestris</i>), each of which hosts a unique species of <i>Epichloë</i> endophyte (Table S1). All are native to eastern North America except the Eurasian species <i>L. arundinaceum</i> .	185
	186
	187
	188
	189
	190
Endophyte removal, plant propagation, and field set-up	191
Seeds from naturally symbiotic populations of the seven focal host species were collected during summer-fall 2006 from Lilly-Dickey Woods and the nearby Bayles Road Teaching and Research Preserve (39.220167, -86.542683). To generate symbiotic (S+) and symbiont-free (S-) plants from the same genetic lineages, seeds from each species were disinfected with a heat treatment described in Table S1 or left untreated. The heat treatment created symbiont-free plants by warming seeds to temperatures at which the fungus becomes inviable but the host seeds can still germinate. Both heat-treated and untreated seeds were surface sterilized with bleach to remove epiphyllous microbes, cold stratified for up to 4 weeks, then germinated in a growth chamber before transfer to the greenhouse at Indiana University where they grew for ~ 8 weeks. We confirmed endophyte status by staining thin sections of inner leaf sheath with aniline blue and examining tissue for fungal hyphae at 200X magnification [42]. We established experimental populations with vegetatively propagated clones of similar sizes (plants ranging from one to six tillers across species). By starting the experiment with plants of similar sizes and the same number of unique genotypes, we aimed to limit any potential effects of heat treatments on initial plant growth [43].	192
	193
	194
	195
	196
	197
	198
	199
	200
	201
	202
	203
	204
	205
	206
	207
	208
	209
	210
	211
	212
	213
	214
	215
	216
Long-term demographic data collection	217
Each summer (2008–2021) we censused all individuals in each plot for survival, growth and reproduction, and added new recruits to the census. Plots contained 13.3 individuals/m ² on average over the course of the experiment. Each census year was a sample of inter-annual climatic variation (n = 14 years, comprising 13 demographic transition years). We censused each species during its peak fruiting stage (May: <i>Poa alsodes</i> , <i>Poa sylvestris</i> ; June: <i>Festuca subverticillata</i> ; July: <i>Elymus villosus</i> , <i>Elymus virginicus</i> , <i>Lolium arundinaceum</i> ; September: <i>Agrostis perennans</i>), such that the censuses were pre-breeding and new recruits came from the previous years' seed production. Leaf litter was cleared out of each plot prior to the census, to aid in locating plants. For each plant remaining from the previous year, we determined survival, measured its size as a count of tillers, and collected reproductive data as counts of reproductive tillers and seed-bearing spikelets on all reproductive tillers to a maximum of three. We also tagged all unmarked individuals that were recruits from the previous years' seed	218
	219
	220
	221
	222
	223
	224
	225
	226
	227
	228
	229
	230

231 production and collected the same demographic data. New recruits typically had one
232 tiller and were non-reproductive. In 2008 through 2010, we took additional counts of
233 seeds per inflorescence for all reproducing individuals in the plots to relate inflorescence
234 and spikelet counts to seed production. In 2018, we stopped collecting data for the
235 exotic *L. arundinaceum*, which had very high survival and low recruitment, and conse-
236 quently very low variation across years. In total across 14 years, the dataset included
237 demographic information for 16,789 individual host-plants and 31,216 transition-year
238 observations.

239 We expected plots to maintain their endophyte status (symbiotic or symbiont-
240 free) because these fungal symbionts are almost exclusively vertically transmitted,
241 and plots were spaced a minimum of 5 m apart, limiting seed dispersal or horizontal
242 transmission of the symbiont between plots. However, we regularly confirmed endo-
243 phyte treatment throughout the lifetime of the experiment by opportunistically taking
244 subsets of seeds from reproductive individuals and scoring them for their endophyte
245 status with microscopy as above. Overall, these scores reflected 98% faithfulness of
246 recruits to their expected endophyte status across species and plots (Fig. S23; Sup-
247 plement data). Additionally, we have rarely observed fungal stromata, the fruiting
248 bodies by which *Epichloë* are potentially transmitted horizontally, provided the fly
249 vector is also present [44]. For *A. perennans*, *F. subverticillata*, *L. arundinaceum*, and
250 *P. alsodes*, we never observed stromata. We observed stromata only infrequently for
251 *E. villosus*, and even more rarely for *E. virginicus* and *P. sylvestris* (Table S2). For
252 these species, stromata have only been observed irregularly across years on 35, 4, and
253 6 plants respectively, making up < 0.3% of all censused plants.

254

255 **Vital rate modeling**

256

257 Equipped with these demographic data, we fit statistical models for adult survival,
258 seedling survival, adult growth, seedling growth, flowering (yes or no), fertility of
259 flowering plants (number of flowering tillers), production of seed-bearing spikelets
260 (number per inflorescence), the average number of seeds per spikelet, and the recruit-
261 ment of seedlings from the preceding year's seed production. We fit these vital rates
262 as generalized linear mixed models in a hierarchical Bayesian framework using RStan
263 [45] which allowed us to isolate endophyte effects on vital rate means and variances,
264 borrow strength across species for some variance components, and propagate uncer-
265 tainty from the individual-level vital rates to population projection models [46]. Each
266 size-structured vital rate model included year effects specific to each species and
267 endophyte-status as well as random plot effects shared across species. The models
268 included the same linear predictor, including two key sets of parameters: one which
269 described the effect of endophyte symbiosis on the mean of that vital rate specific to
270 each species, and another which described the inter-annual variance in the vital rate
271 for symbiotic and symbiont-free plants of each species. The species- and endophyte-
272 status specific random year effects allowed us to quantify the effect of endophytes on
273 inter-annual variance for each vital rate. Other parameters accounted for size struc-
274 ture in the data (defined as the number of tillers) as well as the difference between
275 originally transplanted plants and those which recruited naturally into the plots. Pre-
276 liminary analyses indicated similar model fits between models including linear and

quadratic terms, and so we proceeded with only linear effects. Full details of the vital rate modeling are included in the *Supporting Information Supplemental Methods*. All parameters were given vague priors [47]. We ran each vital rate model for 2500 warm-up and 2500 MCMC sampling iterations with three chains. We assessed model convergence with trace plots of posterior chains and checked for \hat{R} values less than 1.01, indicating low within- and between-chain variation [48, 49]. For those models that showed poor convergence, we extended the MCMC sampling to include 5000 warm-up and 5000 sampling iterations, which was only necessary for seedling growth. We graphically checked vital rate model fit with posterior predictive checks comparing simulated and observed data (Fig. S29-S39).

Stochastic population model

We parameterized stochastic matrix projection models using the fitted statistical vital rate models. Each matrix projection model included two state variables: r_t (the number of newly recruited individuals in year t which we assume to be non-reproductive), and \mathbf{n}_t (a vector including all non-seedling individuals of sizes $x \in \{1, 2, \dots, U\}$, ranging from one to the maximum number of tillers U). We use these two state variables to avoid having to assume demographic equivalence between seedling and non-seedling one-tiller plants. We used the same model structure for each species and endophyte status (not shown in model notation for readability). See Fig. S21 for a generalized life cycle graph.

The number of recruits in year $t + 1$ is given by:

$$r_{t+1} = \sum_{x=1}^U P(x; \boldsymbol{\tau}_P) F(x; \boldsymbol{\tau}_F) K(x; \boldsymbol{\tau}_K) D R(\boldsymbol{\tau}_R) n_t^x \quad (2)$$

The total number of seeds produced by a maternal plant of size x is the product of the size-specific probability of flowering P , the number of reproductive tillers F , the number of spikelets per inflorescence K , and the number of seeds per spikelet D . Multiplying by the probability of transitioning from seed to seedling R gives a per-capita rate of seedling production, which is multiplied by the number of plants of size x (n_t^x , the x^{th} element of \mathbf{n}_t) and summed over all sizes. Each function also depends on the species- and endophyte-specific year random effects for that vital rate ($\boldsymbol{\tau}$, a vector of year-specific values derived from the statistical models).

The number of y -sized plants in year $t + 1$ is given by:

$$n_{t+1}^y = Z(y; \boldsymbol{\tau}_Z) B(\boldsymbol{\tau}_B) r_t + \sum_{x=1}^U S(x; \boldsymbol{\tau}_S) G(x, y; \boldsymbol{\tau}_G) n_t^x \quad (3)$$

where n_{t+1}^y is the y^{th} element of vector \mathbf{n}_{t+1} . The first term on the right hand side of Eqn. 3 represents growth (Z) and survival (B) of seedling recruits. The second term includes the survival of previously x -sized plants and the growth of survivors from size x to y , summed over all x . To avoid predictions of unrealistic growth outside of the observed size distribution, we set a ceiling on the growth function for plants at the 97.5th percentile of observed sizes for each host species [50].

323 Each of the vital rate functions in Eqns. 2 and 3 have separate intercepts and year
 324 random effects for symbiotic and symbiont-free populations, allowing us to calculate
 325 the effect of endophyte symbiosis on the mean, variance, and coefficient of variation
 326 (CV) of λ , the dominant eigenvalue of the year- and endophyte-specific projection
 327 matrix. This model treats climate drivers implicitly through year-specific random
 328 effects. We also developed a climate-explicit version with the addition of parameters
 329 defining the relationship between either annual or growing season drought index and
 330 each vital rate. A full description of climate-explicit methods can be found in the
 331 *Supporting Information Supplemental Methods*.

332

333 Life History Analysis

334

335 We collected metrics describing each host species' life history to test the relationship
 336 between pace of life and variance buffering (Table S2). Using the Rage package [51],
 337 we calculated R_0 , longevity, generation time, Keyfitz entropy, and Demetrius entrooy
 338 from the mean transition matrix for symbiont-free populations. We recorded seed size
 339 as the average lemma length from the Flora of North America [52]. We also calculated
 340 the 99th percentile of maximum observed age for symbiont-free plants from the census
 341 data for each species. Next, we fit Bayesian phylogenetic mixed-effects models using
 342 the brms package [53] to test the relationship between each life history trait and the
 343 effect of symbiosis on the CV of λ (a measure of variance buffering) while controlling
 344 for phylogenetic non-independence between host and symbiont species. We pruned
 345 species-level phylogenies of plants [54] and *Epichloë* fungi [55] to include the focal
 346 species. *Agrostis perennans* was not included in the tree, and so we used the congener
 347 *A. hyemalis*. We defined separate phylogenetic covariance matrices for each pruned
 348 tree. We propagated uncertainty in the estimated variance buffering effect V with a
 349 measurement error model:

350

351

$$V_{MEAN,h} \sim Normal(V_{EST,h}, V_{SD,h}) \quad (4a)$$

352

$$V_{EST,h} \sim Normal(\mu_h, \sigma) \quad (4b)$$

353

$$\mu = \alpha + \beta * trait + \pi_j \quad (4c)$$

354

$$\alpha \sim Normal(0, .5) \quad (4d)$$

355

$$\beta \sim Normal(0, .1) \quad (4e)$$

356

$$\sigma \sim Half - Normal(.04, .01) \quad (4f)$$

357

$$\pi_h \sim MVN(0, \sigma_\pi \mathbf{A}) \quad (4g)$$

358

$$\sigma_\pi \sim Half - Normal(0, .1) \quad (4h)$$

359

360

361

362 Here, V_{EST} is the variance buffering effect for host species h , estimated from the
 363 posterior mean (V_{MEAN}) and standard deviation (V_{SD}), propogating uncertainty asso-
 364 ciated with the effect of symbiosis. The model includes an intercept (α) and a slope
 365 (β) defining the relationship between the variance buffering effect and the life history
 366 trait. The residual standard deviation is given by (σ). We used weakly informative
 367 priors for all parameters except the intercept (α), which was given a large prior
 368 variance to reflect uncertainty in the true value.

prios to aid model convergence. Each prior was centered at zero, except for the residual standard deviation, which we centered at the standard deviation of the estimated variance buffering effect, .04. The phylogenetic random effect (π), which is modeled as a multivariate normal distribution, has a between-species standard deviation (σ_π) structured by the phylogenetic covariance matrix \mathbf{A} . We ran each MCMC sampling chain for 8000 warmup iterations and 2000 sampling iterations. We assessed model convergence as described for the vital rate models.

Mean-variance decomposition

To calculate stochastic population growth rates (λ_s) for each host species and endophyte status we simulated population dynamics for 1000 years by randomly sampling from the 13 annual transition matrices, discarding the first 100 years to minimize the influence of initial conditions. Sampling observed transition matrices produces models that realistically capture inter-annual variation by preserving correlations between vital rates [56]. We tallied the total population size at each time step as $N_t = r_t + \sum_{x=1}^U n_t^x$ and calculated the stochastic growth rate as $\log(\lambda_s) = E[\log(\frac{N_t}{N_{t+1}})]$ [57, 58]. We calculated the total effect of endophyte symbiosis as the difference in λ_s between S+ and S- populations. We propagated uncertainty from the vital rate models to the calculation of λ_s using 500 draws from the posterior distribution of model parameters.

We decomposed the total endophyte effect on λ_s into contributions from effects on vital rate means, variances, and their interaction. Specifically, we repeated the calculation of λ_s for two additional “treatments”: (1) endophyte effects on mean vital rates only, with inter-annual variances shared between S+ and S- at the S- reference level for all vital rates, and (2) endophyte effects on vital rate variances only, with vital rate means shared between S+ and S- at the S- reference level. The combination of all four λ_s treatments (S+ vital rate means and variances, S- means and variances, S+ means with S- variances, S- means with S+ variances) allowed us to quantify to what extent the overall effect of symbiosis derives from changes in vital rates means, variances, and their interaction. The interaction occurs because the variance penalty to stochastic growth is proportional to the arithmetic mean of annual growth rates (see Eq. 1) such that variance is more detrimental for populations with lower average growth rates. To quantify how mean and variance effects of symbionts on mean and variance arise through effects on different vital rates, we performed an additional decomposition described in the *Supporting Information Supplemental Methods*.

To create scenarios of increased variance relative to that observed during the study period, we repeated the stochastic growth rate decomposition, but sampling only subsets of the 13 observed annual transition matrices. We created two scenarios of increased environmental variance by sampling the transition matrices associated with the set of either six or two most extreme λ values. These extreme λ values represent the best and worst years experienced by the plants, using the S- populations as the reference condition. By sampling away from an average year in both directions, the six- and two- years scenarios increased the standard deviation of yearly host growth rates by 1.3 and 2.1 times, respectively, without changing mean growth rates (< 2.3% difference in $\bar{\lambda}$ between simulation treatments, Fig. S50). We performed the same

415 mean-variance decomposition for these scenarios as for the ambient conditions (all 13
416 years sampled) for all host species described above.

417

418 **Results**

419

420 **Symbionts buffer host demographic variance**

421

422 Across the 14 census years, endophytes reduced inter-annual variance for 66% (37/56)
423 of host species-vital rate combinations (average Cohen's D for effects on vital rate stan-
424 dard deviation: -0.15) (Fig. 2A; Fig. S6 - Fig. S18). Endophytes also increased mean
425 vital rates for the majority (36/56) of host species-vital rate combinations (average
426 Cohen's D for effects on vital rate mean: 0.15), and benefits were particularly strong
427 for host survival, plant growth and recruitment (Fig. 2A; Fig. S1 - Fig. S5). The magni-
428 tude of mean and variance effects differed among host species and vital rates. Symbiont
429 effects on vital rate variance are as large and even exceed effects on vital rate means
430 for certain species. For example, endophytes modestly increased mean adult survival
431 (Fig. 2C) and strongly reduced variance in survival (Fig. 2D) for *Festuca subverticil-*
432 *lata*, while for *Poa alsodes*, variance buffering was more apparent in seedling growth
433 and inflorescence production (Fig 2E). Interestingly, certain vital rates showed costs
434 of endophyte symbiosis. Symbiotic individuals of *A. perennans* grew larger than those
435 without endophytes (Fig. 2B), yet endophytes also reduced this species' mean recruit-
436 ment rates (Fig. 2A). Similarly, variance was increased for certain species' vital rates,
437 such as in seedling growth for *Elymus villosus* and *Festuca subverticillata* (Fig. 2A).

438 Because not all vital rates contribute equally to fitness, we used stochastic matrix
439 models to integrate the diverse effects on vital rates described above into comprehen-
440 sive measures for the arithmetic mean and variance of year-to-year fitness (λ_t) and
441 the long-run stochastic growth rate, a geometric average, that integrates both mean
442 and variance (λ_S). On average across host species, the mean fitness of S+ populations
443 increased by more than 10% ($> 92\%$ confidence that endophytes increased $\bar{\lambda}$) and
444 inter-annual variability in fitness was 26% lower ($> 86\%$ confidence that endophytes
445 decreased the coefficient of variation of λ_t) than S- populations (Fig. 3). For some host
446 species, the CV of λ_t declined by more than 62% (*P. alsodes*, *F. subverticillata*), a
447 greater than two-fold reduction, while for others, endophyte effects on variance were
448 substantially smaller (5% lower for *E. villosus*, 13% lower for *A. perennans*), or even
449 positive (37% increase for *E. virginicus*).

450

451 **Faster life histories predict stronger symbiont-mediated 452 variance buffering**

453

454 In support of the prediction that hosts with long lifespans, which are intrinsically
455 buffered from environmental variability, should benefit less from symbiont-mediated
456 variance buffering, we found that hosts with trait values representing slower life history
457 strategies experienced weaker variance buffering from endophytes than those with
458 fast life histories (Fig. 4). Bayesian phylogenetic mixed-effects models, controlling for
459 species' relatedness, indicated that variance buffering was stronger for host species
460 with shorter lifespan (Fig. 4A; 75% probability of positive relationship with empirically

observed maximum plant age) and smaller seeds (Fig. 4B; 73% probability of positive relationship with seed length). Other life history traits similarly had positive, but weaker, support for the prediction that faster life history traits correlate with stronger variance buffering (Fig. S57-S59). Models indicate moderate phylogenetic signal in the effect of variance buffering (average Pagel's λ of 0.26 and of 0.63 from models including host and symbiont phylogenetic covariance respectively). Conclusions about the role of symbiont-mediated demographic buffering in life history evolution are constrained by the narrow range of closely related species in the grass sub-family Pooideae and their co-evolving symbionts.

Contributions from variance buffering are weak relative to mean effects

To evaluate the relative importance of mean fitness benefits and variance buffering as alternative pathways of mutualism, we decomposed the overall effect of the symbiosis on the stochastic growth rate λ_S using simulations from the population models in four configurations. These included either the full symbiosis effect (both mean and variance buffering effects), mean effects alone, variance effects alone, or neither mean nor variance effects. Overall, the full effect of symbiosis on λ_S , averaged across host species, provided strong evidence of grass-endophyte mutualism (99% certainty of a positive total effect on λ_s) (Fig. 5; see Fig. S52 for individual host species). Contributions to this full effect derived from both mean and variance buffering effects, as well as a slightly negative interaction (i.e., the combined influence of mean and variance effects was smaller than the sum of their individual effects). Endophytes' contributions to λ_S from mean effects were four times greater, averaged across species, than contributions from variance buffering (Fig. 5), suggesting that, under the regime of environmental variability represented by our 14-year study, dampened fluctuations in fitness via variance buffering was a far less important element of the benefits of symbiosis than increased mean fitness. Decomposing this result further into contributions through endophytes effects on different vital rates demonstrated that demographic buffering arose primarily from symbionts' effects on host survival and growth, rather than from effects on reproduction (Fig. S53). Results for individual host species were largely consistent with the cross-species trends (Fig S22). The full effect of symbiosis on λ_S was positive for seven out of eight host species, with statistical confidence ranging from 66% to > 99% certainty. The one exception was the host species *P. sylvestris*, for which our analysis indicated that fungal endophytes were effectively neutral in their overall fitness effect (45% and 55% posterior probability of positive and negative effects; Fig S22).

Variance buffering strengthens under increased environmental variability

To simulate increased variability, we repeated the decomposition of λ_S for two alternative forecast scenarios, randomly sampling transition matrices that represented either the six most extreme years experienced by each species or the two most extreme years, subsets of the thirteen transition matrices across the 14-year study period. Increased

507 variability elicited stronger mutualistic benefits of endophyte symbiosis (Fig. 5) than
508 ambient variability (overall effect of the symbiosis increased by > 130%, a 2.3 fold
509 increase). This increase was driven by increased contributions from the variance buffering
510 mechanism (from a 24% contribution in the ambient scenario to a 66% contribution
511 in the most variable scenario) rather than from greater mean effects. In the most
512 variable scenario, the relative importance of mean and variance effects reversed, with
513 variance buffering contributions that were 1.5 times greater than contributions from
514 mean benefits, averaged across species (Fig. 5).

515

516 Discussion

517

518 Across seven host species, eight vital rates, 14 years, and 16,789 individual plants,
519 our analysis provided the first empirical evidence of symbiont-mediated demographic
520 buffering. Our analysis of taxonomically-replicated, long-term field experiments that
521 manipulated the presence/absence of fungal symbionts in plants demonstrated for
522 the first time that heritable microbes can commonly benefit hosts not only through
523 improved mean fitness – the focus of most previous research – but also through buffering
524 against environmental variance. When mean and variance effects of symbionts were
525 considered together, none of the host-symbiont pairings were antagonistic (i.e., with
526 endophytes that both decreased mean fitness and increased variance) (Fig. 3C), sug-
527 gesting that variation across host species and vital rates in mean and variance effects
528 may reflect alternative strategies that yield similar net benefits of endophyte symbiosis.
529 These alternative strategies may explain the long-term stability of these mutualisms

530 Symbiont-mediated demographic buffering is a potential target of selection for
531 improved holobiont fitness [59]. Our results show that by partnering with context-
532 dependent symbionts in variable environments, hosts can supplement their inherent
533 life-history strategy. We found support for the prediction that hosts with fast life cycles
534 that produce many small offspring with low per-capita chance of success benefit from
535 the variance buffering effects of the symbiosis [60, 61]. Considering fungal life history
536 traits, the three host species for which the net mutualism benefit was weakest (*Ely-
537 mus villosus*, *Elymus virginicus*, and *Poa sylvestris*) (Fig. 2C) were the only hosts for
538 which we observed fungal stromata, fruiting bodies capable of horizontal (contagious)
539 transmission (Table S2). This result supports the theoretical expectation that strict
540 vertical transmission drives the evolution of strong host-symbiont mutualism [28, 62].
541 For example, variation in the benefits of host-symbiont mutualism introduces a poten-
542 tial feedback driving the evolution of horizontal transmission under conditions where
543 the interaction benefits are weak or costly [63]. Additionally, imperfect transmission,
544 the production of symbiont-free offspring from a symbiotic maternal individual, occurs
545 in this system (Table S2) and raises interesting questions about how symbiosis may
546 influence evolutionary bet-hedging. Variation in offspring type potentially improves
547 the chances that at least some individuals perform well in any given year [64] which
548 could be explored by loosening the assumption in our analysis of perfect vertical
549 transmission. For *Epichloë* hosts, this offspring variation likely would occur primarily
550 through the production of symbiotic or symbiont-free offspring, as individual hosts
551 are typically home to single haplotypes of asexually reproducing symbionts [65], but
552

across host-microbe systems the diversity of the microbiome may be an important key to expanding phenotypic variance [66]. Our understanding of how life history variation modulates the fitness consequences of microbial symbiosis would profit from tests across a wider span of taxonomic groups [67].¹

Work remains to be done to connect endophyte effects on mean and variance to realistic forecasts of host-symbiont dynamics under global change. Our simulations of increased environmental variability indicated that mutualism with microbial symbionts, and their variance buffering effects in particular, will take on increased importance for hosts under a more variable future climate. However, our analyses treated certain important aspects determining stochastic population growth rates implicitly. First, we amplified interannual variance in yearly fitness rather than realistically connecting the most important climate drivers to each vital rate [68, 69]. Reduced sensitivity to drought, as has been reported for some *Epichloë* symbioses [41], is a candidate mechanism that could generate a signature of variance buffering: drought conditions may have weaker fitness costs for S+ hosts, reducing fluctuations in fitness through time. We performed a climate-explicit analysis that indicated that symbionts reduced sensitivity to annual or growing season drought indices for five of seven host taxa (Supporting Information Text; Fig. S24-S25; Table S3). However, we did not find a strong relationship between the magnitude of variance buffering and relative drought sensitivities, suggesting that other climatic factors or other temporally-varying aspects of the environment may elicit benefits of endophyte symbiosis, including documented resistance to herbivory for six of these host taxa [70, 71]. Identifying the type and timescale of relevant drivers would allow more direct connections between demographic models and outputs from global climate models. The magnitude and autocorrelation of climate variability are likely to impact future population projections [72]. Second, climate-demography relationships may change unpredictably under global climate change. For example, interacting effects of multiple climate drivers and shifting cost-benefits between hosts and symbionts may alter vital rate correlations. Increased positive correlations between vital rates could amplify demographic variance [8, 73], negating demographic buffering provided by symbionts. Finally, the limits of extrapolating spatially and temporally beyond the experimental plots are unknown. While commonly used to build inference about ecological processes and environmental variables, space-for-time substitutions can be misleading [74]. Environmental variability is spatially heterogenous and is expected to both increase and decrease across the broad ranges of our focal species [2]. Locally adapted populations may have divergent responses, making it difficult to predict the fate of the symbiosis.

Conclusion

Ecologists increasingly recognize the importance of symbiotic microbes for host organisms and the populations, communities, and ecosystems in which their hosts reside [75–78]. Despite awareness of these ubiquitous interactions, long-term studies of microbial symbiosis are very rare. Our results provide an important advance to improve forecasts of the responses of populations (and symbionts) to increasing environmental stochasticity under global change, suggesting that, for some host species, microbial

¹Is it worth talking about demographic lability anywhere?

599 symbiosis may compensate for the lack of intrinsic tolerance of variability conferred by
600 “slow” life history traits. We found that, relative to mean fitness benefits, symbiont-
601 mediated variance buffering made weak contributions to host-symbiont mutualism
602 under the current regime of environmental variability. However, demographic buffer-
603 ing is likely to become the dominant benefit that fungal endophytes confer to grass
604 hosts in more variable future environments. Thus, demographic buffering – a cryptic
605 microbial influence that manifests only over long time scales – is poised to become
606 the dominant way in which grasses benefit from symbiosis with fungal endophytes in
607 more variable climates of the future. This result emerges from the context-dependent
608 nature of grass-endophyte interactions, combined with the observation that environ-
609 mental stochasticity generates fluctuation in context. These key ingredients, and thus
610 the potential for symbiont-mediated variance buffering, similarly apply to the diverse
611 host-microbe symbioses across the tree of life.

612

613

614

615

616

617

618

619

620

621

622

623

624

625

626

627

628

629

630

631

632

633

634

635

636

637

638

639

640

641

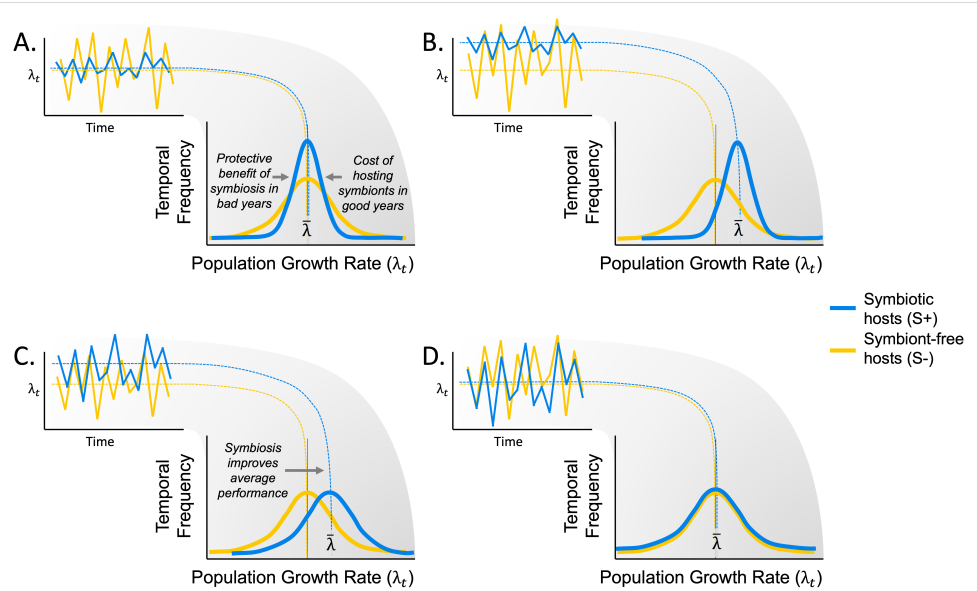
642

643

644

Acknowledgments. We thank Mark Sheehan, Ali Campbell, Kyle Dickens, Blaise Willis, and Sar Lindner for contributions to field data collection. We also thank Volker Rudolf, Daniel Kowal, Lydia Beaudrot and Judie Bronstein for helpful comments on and discussion of this project. This research was supported by the National Science Foundation (grants 1754468 and 2208857).	645 646 647 648 649 650 651 652 653 654 655 656 657 658 659 660 661 662 663 664 665 666 667 668 669 670 671 672 673 674 675 676 677 678 679 680 681 682 683 684 685 686 687 688 689 690
Supplementary information. Supplementary information for this paper includes Supplementary Methods, Figs. A1 to A28, and Tables A1 to A3.	

691 **Figures**



714 **Fig. 1** Hypothesized effects of symbiosis on the mean and variance of annual population growth
 715 rates. (A) Context-dependent symbiosis may provide benefits to hosts during harsh years while being
 716 neutral or costly during benign years. Temporal variance in populations growth rates of symbiotic
 717 host populations (S+; blue lines) is expected to decrease relative to symbiont-free hosts (S-; yellow
 718 lines). (B) Symbiosis may improve average performance across years in addition to reducing temporal
 719 variance. (C) Consistent benefits of symbiosis could improve average performance across years with
 720 no influence on temporal variance. (D) Symbiosis may have an effectively neutral effect on population
 721 growth rates.

737
 738
 739
 740
 741
 742
 743
 744
 745
 746
 747
 748
 749
 750
 751
 752
 753
 754
 755
 756
 757
 758
 759
 760
 761
 762
 763
 764
 765
 766
 767
 768
 769
 770
 771
 772
 773
 774
 775
 776
 777
 778
 779
 780
 781
 782

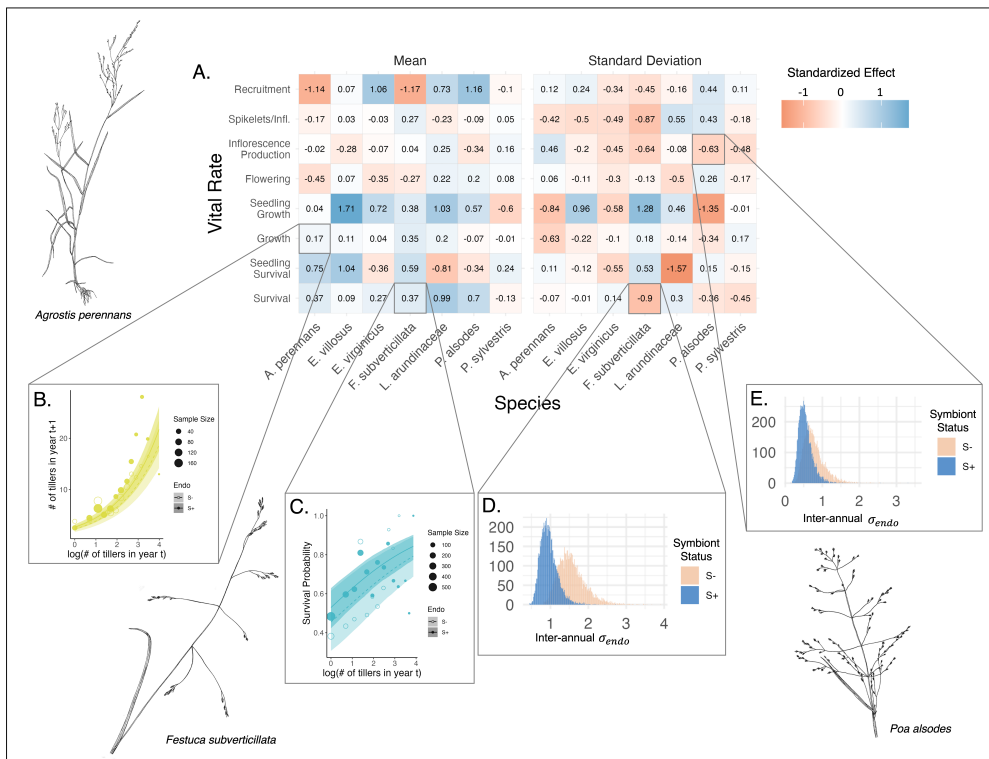


Fig. 2 Endophyte symbiosis altered host vital rates.(A) Shading represents the posterior mean standardized effect size (Cohen's D) of endophyte symbiosis on mean or standard deviation of host vital rates (blue indicates that symbiosis increased the mean or standard deviation and red indicates a reduction). Endophytes' diverse vital rate effects include increased (B) mean growth of *A. perennans* and (C) mean survival probability of *F. subverticillata*. Endophyte presence also reduced inter-annual standard deviation in (D) the survival of *F. subverticillata* and (E) the fertility of *P. alsodes*. In panels B-C, mean vital rate estimates are shown with 80% credible intervals along with data binned by size for symbiotic (S+) and symbiont-free (S-) plants, while panels D-E show estimated posterior distributions of endophyte-status specific inter-annual standard deviation ($\sigma_{\tau_{e,h}}$) for each vital rate for S+ (blue) and S- (beige) populations. Organism silhouettes modified from "Festuca subverticillata" by Cindy Roché and "Agrostis hyemalis" and "Poa alsodes" by Sandy Long ©Utah State University.

783

784

785

786

787

788

789

790

791

792

793

794

795

796

797

798

799

800

Fig. 3 Mean and variance-buffering effects on fitness. Black circles indicate the average effect of endophytes along with 500 posterior draws (smaller colored circles) on the (A) mean and (B) coefficient of variation in λ for each host species as well as a cross species mean. (C) For all hosts, endophytes either reduce variance, increase the mean, or both, and consequently when considering stochastic environments, the interactions are always at least potentially mutualistic.

801

802

803

804

805

806

807

808

809

810

811

812

813

814

815

816

817

818

819

820

821

Fig. 4 Host species with faster life history traits experience stronger effects of symbiont-mediated

822 variance buffering. Regressions between life history traits describing the fast-slow life history continuum

823 ((A) 99th percentile maximum age observed during long term censuses in years; (B) Seed size)

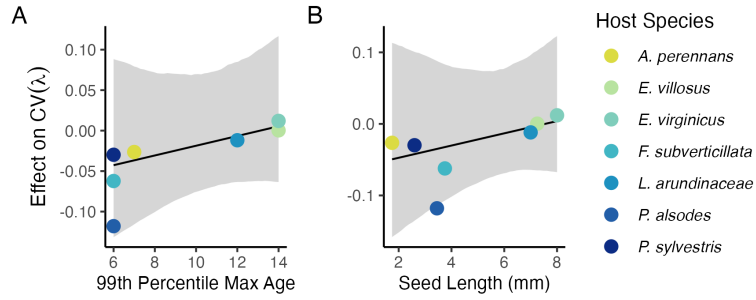
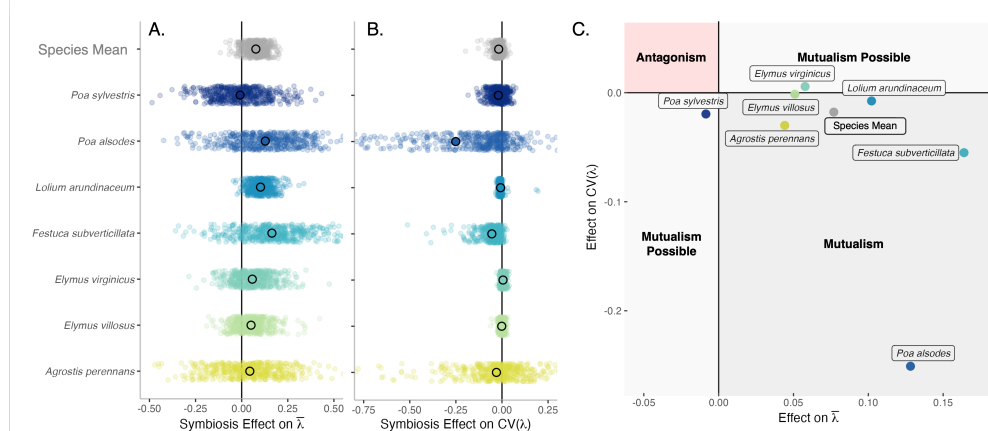
824 and the effect of endophyte symbiosis on the coefficient of variation in population growth rate (λ).

825 Each panel shows the fitted mean relationship (line) along with the 95% credible interval.

826

827

828



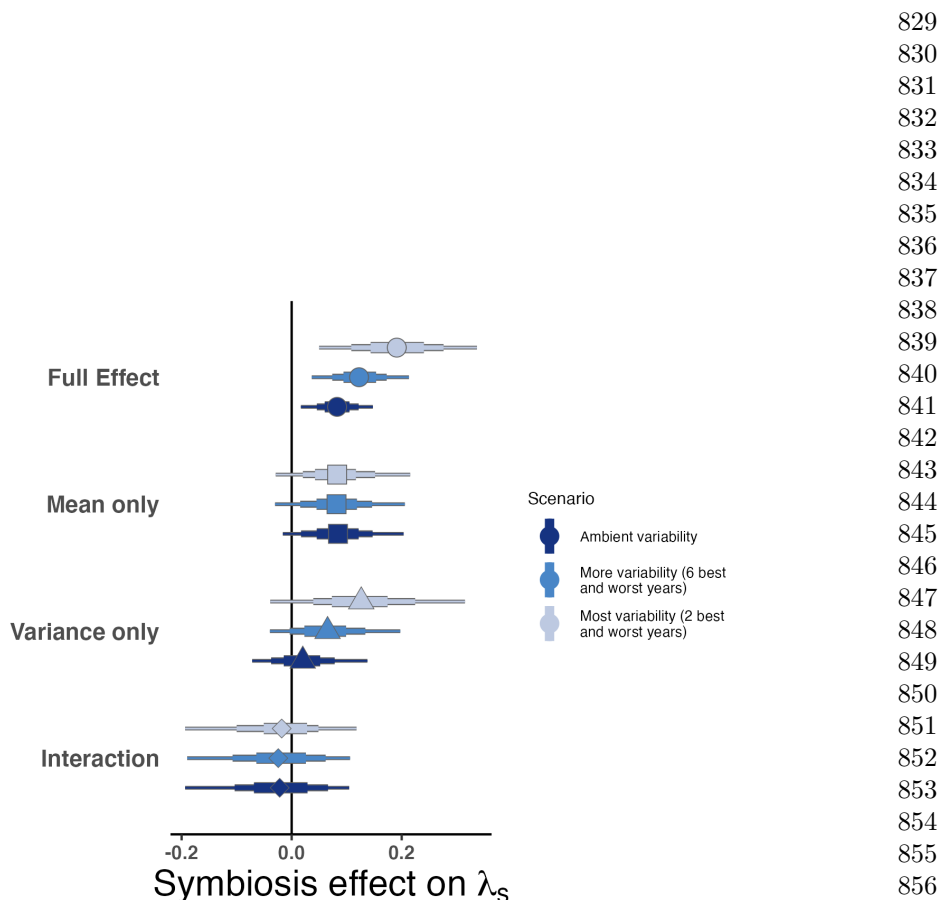


Fig. 5 Cross-species average endophyte contributions to stochastic growth rates under observed and elevated variance. Endophyte symbiosis contributes to the total effect of mutualism on λ_S through benefits to mean growth rates and through variance buffering as well as the interaction between mean and variance effects. Shapes indicate the posterior mean of each contribution averaged across the seven focal symbiota, along with bars for the 50, 75 and 95% credible intervals. The full effect of the symbiosis (circles) becomes more mutualistic under scenarios of increased variance (represented by color shading). Relative to the ambient scenario sampling transition matrices for all 13 transition years during the study period, simulations increased variance by sampling the most extreme six or two years years, leading to increased contributions from variance buffering effects (triangles) and a constant contribution from mean effects (squares).

875 **Supporting Information**

876

877 **Supplemental Methods**

878 **Detailed vital rate modeling**

879
880 We fit vital rates models in a Bayesian hierarchical framework. Statistical models for
881 adult survival, seedling survival, adult growth, seedling growth, flowering (yes or no),
882 fertility of flowering plants (number of flowering tillers), production of seed-bearing
883 spikelets (number per inflorescence), the average number of seeds per spikelet, and the
884 recruitment of seedlings from the preceding year's seed production, were constructed
885 as follows:

886 *Survival* - We modeled survival as a Bernoulli process, where the survival (S) of
887 an individual i in plot p and census year t was predicted by the plot-level endophyte
888 status (e), host species (h), size in the preceding census, and the plant's origin status
889 (whether it was initially transplanted or naturally recruited into the plot).

890

891

892
$$S_{i,p,e,h,t} \sim Bernoulli(\hat{S}_{i,p,e,h,t}) \quad (1a)$$

893
$$\text{logit}(\hat{S}_{i,p,e,h,t}) = \beta_{0_h} + \beta_1 * \text{origin}_i \quad (1b)$$

894
$$+ \beta_{2_h} * \text{endo}_e + \beta_{3_h} * \text{size}_{i,t-1} + \tau_{e,h,t} + \rho_p \quad (1c)$$

895
$$\tau_{e,h,t} \sim \text{Normal}(0, \sigma_{\tau_{e,h}}^2) \quad (1d)$$

896
$$\rho_p \sim \text{Normal}(0, \sigma_\rho^2) \quad (1e)$$

897

898

899 Here, \hat{S} is the survival probability, β_{0_h} is an intercept specific to each host species,
900 β_1 is the effect of the plant's recruitment origin, β_{2_h} is the endophyte effect, β_{3_h} is the
901 size effect, $\tau_{e,h,t}$ is a normally distributed year effect for each species and endophyte
902 status with variance $\sigma_{\tau_{e,h}}^2$, and ρ_p is a normally distributed plot effect with variance
903 σ_ρ^2 ($p(e)$ indicates that plot identity is uniquely associated with an endophyte status).
904 We assume that origin effect β_1 and plot-to-plot variance σ_ρ^2 are shared across host
905 species, allowing us to "borrow strength" across the multi-species dataset; other model
906 parameters are unique to host species. We separately modeled the survival of newly
907 recruited seedlings with a similar model but omitting previous size dependence and
908 origin status.

909 *Growth* - We modeled plant size in census year t (G) with the same linear pre-
910 dictor for the mean as described for survival. Because we measured size as positive
911 integer-valued counts of tillers, we modeled it with a zero-truncated Poisson-inverse
912 Gaussian distribution. This distribution includes a shape parameter λ_G to account for
913 overdispersion in the data. We additionally modeled the growth of newly recruited
914 seedlings separately with a Poisson-inverse Gaussian model omitting size structure
915 and the plants' origin status as with seedling survival.

916 *Flowering* - We modeled whether or not a plant was flowering during the census (P)
917 as a Bernoulli process, with the same linear predictor for the mean as described above
918 for survival except that size dependence for reproductive vital rates was determined
919

920

by the individual's size during the same census year as opposed to its size during the previous year.	921
	922
<i>Fertility</i> - For a plant that was flowering during the census, its fertility was the number of reproductive tillers produced (F), which we modeled as a function of size in the same census period with a zero-truncated Poisson-Inverse Gaussian distribution, with the same linear predictor for the mean as described above.	923
	924
	925
	926
<i>Spikelets per Inflorescence</i> - Spikelet production (K) was recorded as integer counts on up to three inflorescences per reproducing plant. We modeled these data with a negative binomial distribution, with the same linear predictor for the mean as described above.	927
	928
	929
	930
<i>Seed Production per Spikelet</i> - For individuals with recorded counts of seed production, we calculated the number of seeds per spikelet from our counts of seeds and spikelets per inflorescence, and then modeled seeds per spikelet (D) as means of a Gaussian distribution for each species and endophyte status. Because we had less detailed data across years and plants for seed production than for other reproductive vital rates, we omitted both plot and year random effects.	931
	932
	933
	934
	935
	936
<i>Seedling Recruitment</i> - We used a binomial distribution to model the recruitment of new seedlings (R) into the plots from seeds produced in the preceding year, assuming no long-lived seed bank. We included an intercept specific to each host and endophyte status and the same random effects structure as in other models. We estimated the number of seeds per plot in the preceding year by multiplying the total number of reproductive tillers per plant by the mean number of spikelets per inflorescence and mean number of seeds per spikelet (D). For plants with missing fertility or spikelet data, we used the expected number of reproductive tillers (F) or of spikelets per inflorescence from (K), drawing from the full posteriors of our models. We rounded this value to get the estimated seed production for each individual, and finally summed across all reproductive plants in each year and plot to get the total number of seeds produced.	937
	938
	939
	940
	941
	942
	943
	944
	945
	946
	947
	948
	949
Estimating climate drivers of environmental context-dependence	950
To connect the variance buffering effects of endophytes with inter-annual variability in climate, we built climate-explicit stochastic matrix population models from the vital rate data in addition to the climate-implicit model described in the main text. Identifying the potentially complex relationships between vital rates and environmental drivers remains a key challenge for accurate forecasts of the ecological impacts of environmental stochasticity [79]. We first downloaded temperature and precipitation data from a weather station in Bloomington, IN, approx. 27 km from our study site, using the rnoaa package [80]. Compared to other weather stations in the area, the measurements from Bloomington contain the most complete climate record across the study period and are correlated with more local measurements from Nashville, IN for years in which local data are available (total daily precipitation: $R^2 = .76$; mean daily temperature: $R^2 = .94$). The mean annual temperature across the study period was $11.9 C^\circ$ (SD: $1.05 C^\circ$) and the average annual precipitation was 1237.9 mm/year (SD: 204.89 mm/year) (Fig. S24). Given the known role of endophytes in promoting host drought tolerance, we calculated the Standardised Precipitation-Evapotranspiration	951
	952
	953
	954
	955
	956
	957
	958
	959
	960
	961
	962
	963
	964
	965
	966

967 Index (SPEI) for 3 and 12 months preceding each annual censuses, reflecting drought
968 during the growing season and across the year [81]. To calculate SPEI, we used the
969 Thornthwaite equation to model potential evapotranspiration as implemented in the
970 SPEI R package [82]

971 We repeated the process of fitting statistical models for each vital rate as described
972 in **Materials and Methods** with the inclusion of a parameter describing the influ-
973 ence of SPEI. We fit separate vital rate models incorporating either the growing season
974 or annual drought index for each vital rate, except for the model describing the mean
975 number of seeds per inflorescence. This model was fit without climate effects because
976 the data came from only a few years. Initial analyses indicated similar fits for models
977 including only a linear term and those with both linear and quadratic terms describ-
978 ing the relationship between the climate driver and the vital rate response, and so
979 we proceeded with models including only the linear term. We expected that includ-
980 ing climate predictors into the models would explain some inter-annual variance in
981 vital rates, shrinking the variance associated with the fitted year random effects. We
982 assessed model fit with graphic posterior predictive checks and convergence diagnostics
983 as described for the climate-implicit analysis. Finally, we next built matrix projec-
984 tion models incorporating the climate-dependent vital rate functions to assess the
985 response of symbiotic (S+) vs symbiont-free (S-) populations to drought. The model
986 is as described in **Materials and Methods** with the inclusion of parameters describ-
987 ing the slope of the relationship with SPEI. We compared the sensitivity of λ to either
988 annual or seasonal SPEI of S+ populations ($\frac{\Delta\lambda^+}{\Delta SPEI}$) with those of S- populations
989 ($\frac{\Delta\lambda^-}{\Delta SPEI}$)(Fig. S25; Table S).

990 Most species were slightly more responsive to growing season rather than annual
991 drought conditions, and for most species symbiotic populations were less sensitive to
992 SPEI than symbiont-free populations (Fig. S25; Table S3). However, these drought
993 indices did not explain the full extent of inter-annual variability in demographic
994 vital rates. For example, flowering in *A. perennans* had one of the strongest climate
995 signals (82% probability of a positive relationship with SPEI), yet the estimated inter-
996 annual variance $\sigma_{\tau_P}^2$ for symbiont-free plants shrank from 6.7 to 6.1 after including
997 3-month SPEI as a covariate, suggesting that other factors contribute to inter-annual
998 variability.
999

1000 **Vital rate mean-variance decomposition**

1001

1002 We repeated the mean-variance decomposition to quantify the extent that mean and
1003 variance effects on stochastic population growth rates arise through different vital
1004 rates. Specifically, we repeated the calculation of λ_s as described in the main text
1005 for symbiotic populations as well as symbiont-free populations, as well as for four
1006 additional “treatments”. These treatments differentiate between mortality and growth
1007 related vital rates (adult survival, adult growth, seedling survival, and seedling growth)
1008 and reproductive vital rates (probability of flowering, inflorescence production, spikelet
1009 production, seed production, and recruitment). Each treatment held vital rate mean
1010 and interannual variances at the S- reference level across vital rates while introducing
1011 (1) endophyte effects on the vital rate means for survival and growth vital rates only,
1012 (2) endophyte effects on the vital rate variances for survival and growth vital rates

only, (3) endophyte effects on the vital rate means for reproductive vital rates only, and (4) endophyte effects on the vital rate variances for reproductive vital rates only. 1013
The combination of all six λ_s treatments allowed us to quantify to what extent the overall effect of symbiosis derives from changes in mean and variance of mortality and growth versus in reproductive vital rates. To explore how these contributions could be expected to change under increased variability relative to that observed during the study period, we repeated this decomposition under the scenarios of increased variance described in the main text, sampling transition matrices associated with the set of either six or two most extreme λ values. 1014
1015
1016
1017
1018
1019
1020
1021
1022
1023
1024
1025
1026
1027
1028
1029
1030
1031
1032
1033
1034
1035
1036
1037
1038
1039
1040
1041
1042
1043
1044
1045
1046
1047
1048
1049
1050
1051
1052
1053
1054
1055
1056
1057
1058

1059 Supplemental Figures S1-S28

1060

1061

1062

1063

Adult Survival
Data from Original plants only

1064

1065

1066

1067

1068

1069

1070

1071

1072

1073

1074

1075

1076

1077

1078

1079

1080

1081

1082

1083

1084

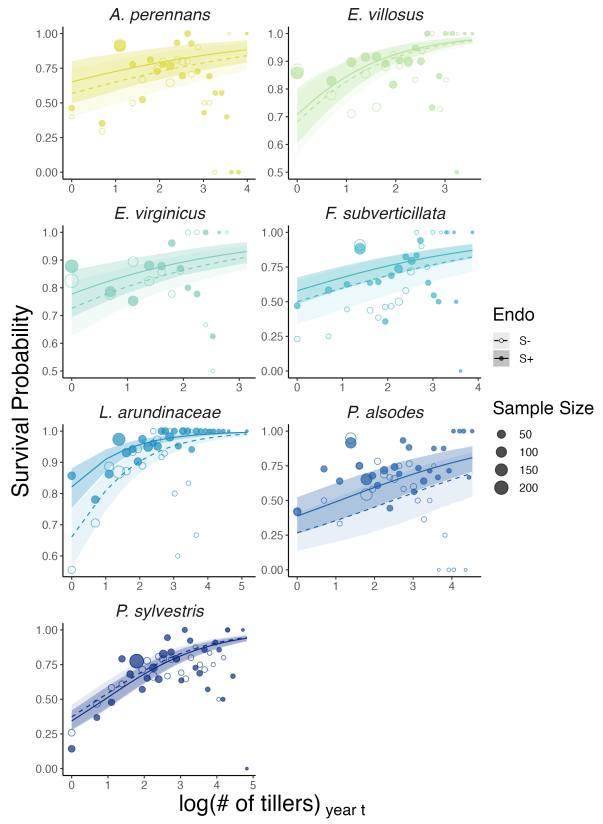
1085

1086

1087

1088

1089



1090 **Fig. S1** Effect of endophyte symbiosis on mean adult survival. Fitted curves represent the size-
1091 specific mean survival probability for original plants along with data binned by size shown as open
1092 circles with a dashed line for symbiont-free (S-) plants, while the solid line and filled circles represent
1093 symbiotic (S+) plants. 80% credible intervals are shown with dark shading for S+, or light shading
1094 for S-.

1095

1096

1097

1098

1099

1100

1101

1102

1103

1104

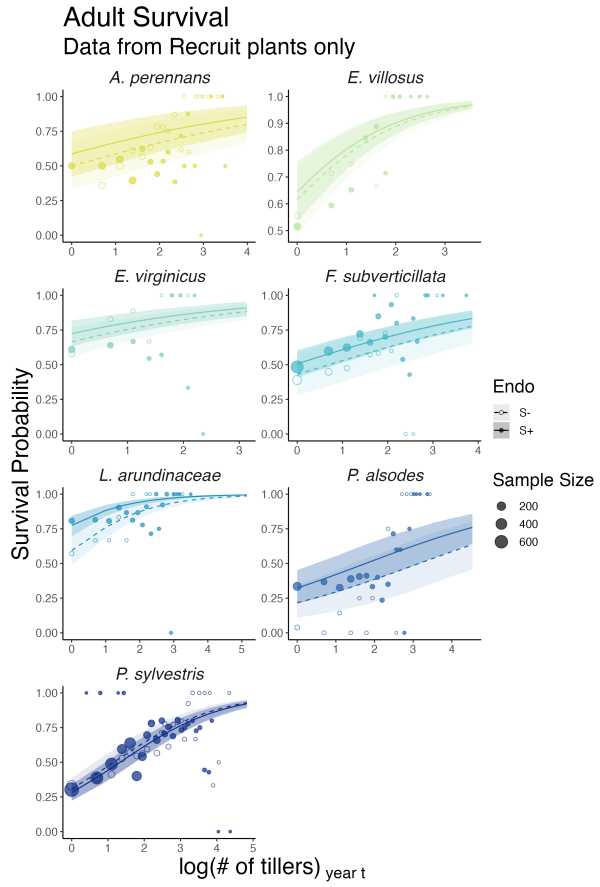
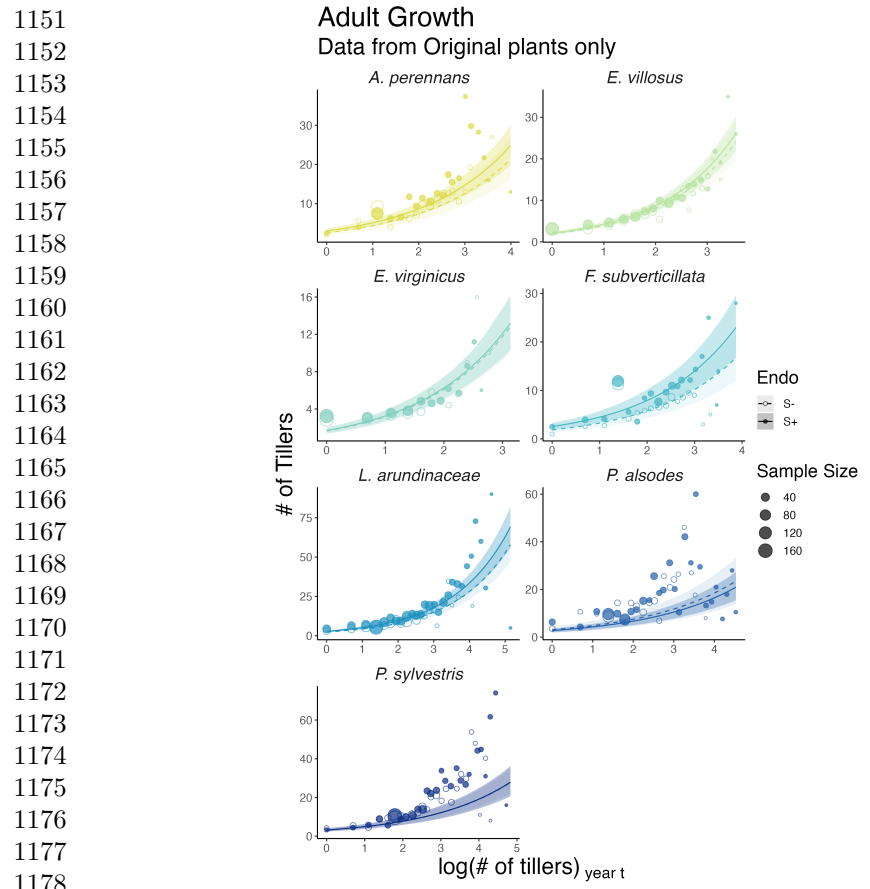


Fig. S2 Effect of endophyte symbiosis on mean adult survival. Fitted curves represent the size-specific mean survival probability for recruited plants along with data binned by size shown as open circles with a dashed line for symbiont-free (S-) plants, while the solid line and filled circles represent symbiotic (S+) plants. 80% credible intervals are shown with dark shading for S+, or light shading for S-.

1105
1106
1107
1108
1109
1110
1111
1112
1113
1114
1115
1116
1117
1118
1119
1120
1121
1122
1123
1124
1125
1126
1127
1128
1129
1130
1131
1132
1133
1134
1135
1136
1137
1138
1139
1140
1141
1142
1143
1144
1145
1146
1147
1148
1149
1150



1179 **Fig. S3** Effect of endophyte symbiosis on mean adult growth. Fitted curves represent the size-specific
1180 mean expected plant size for original plants along with data binned by size shown as open circles with
1181 a dashed line for symbiont-free (S-) plants, while the solid line and filled circles represent symbiotic
1182 (S+) plants. 80% credible intervals are shown with dark shading for S+, or light shading for S-.
1183
1184
1185
1186
1187
1188
1189
1190
1191
1192
1193
1194
1195
1196

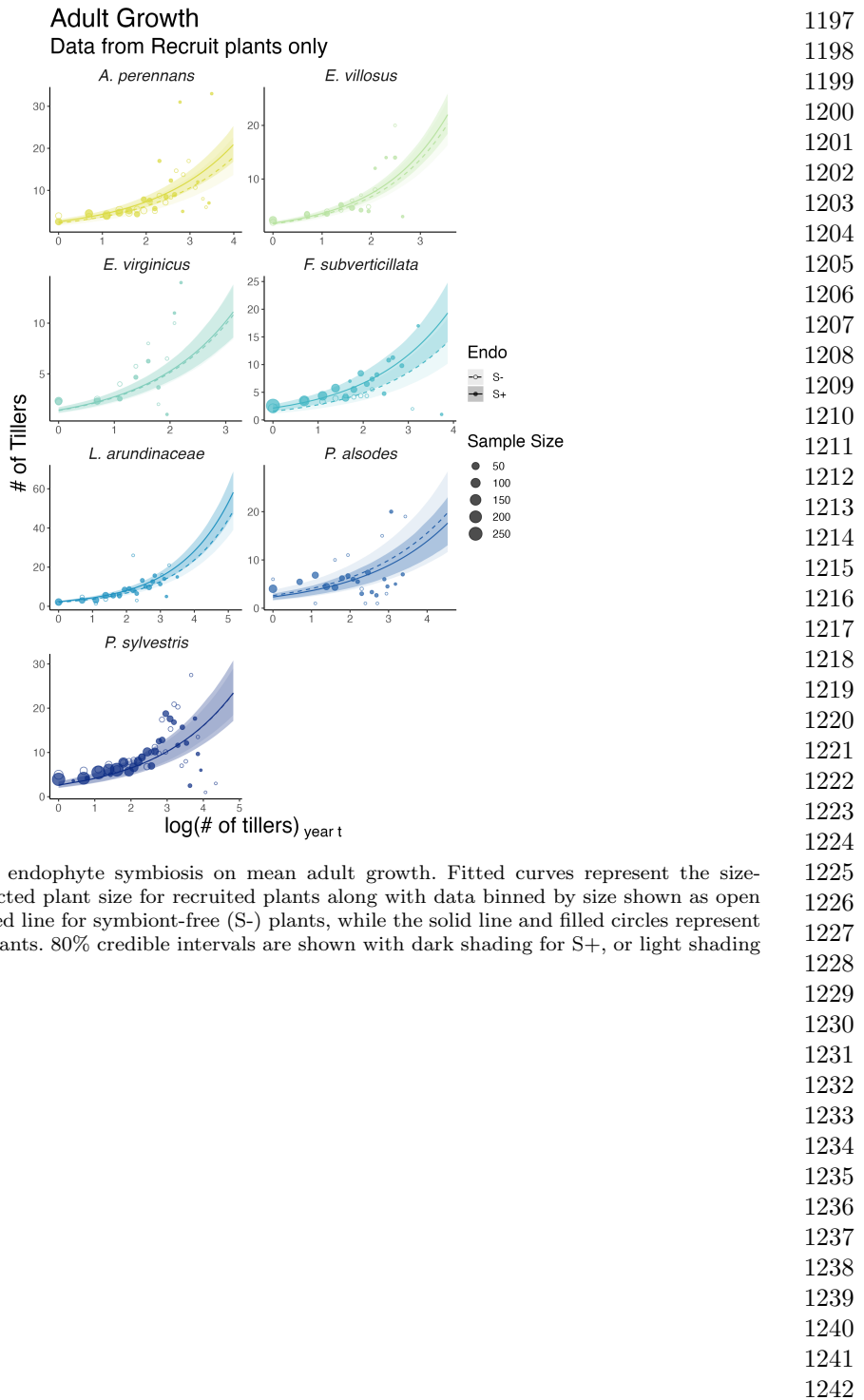
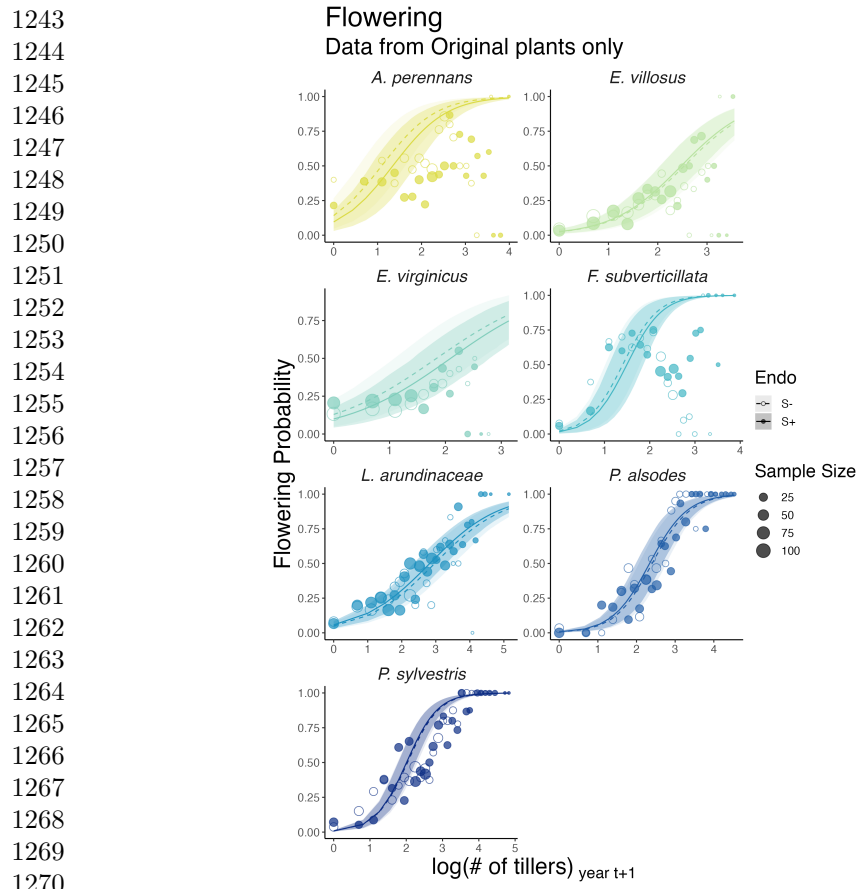
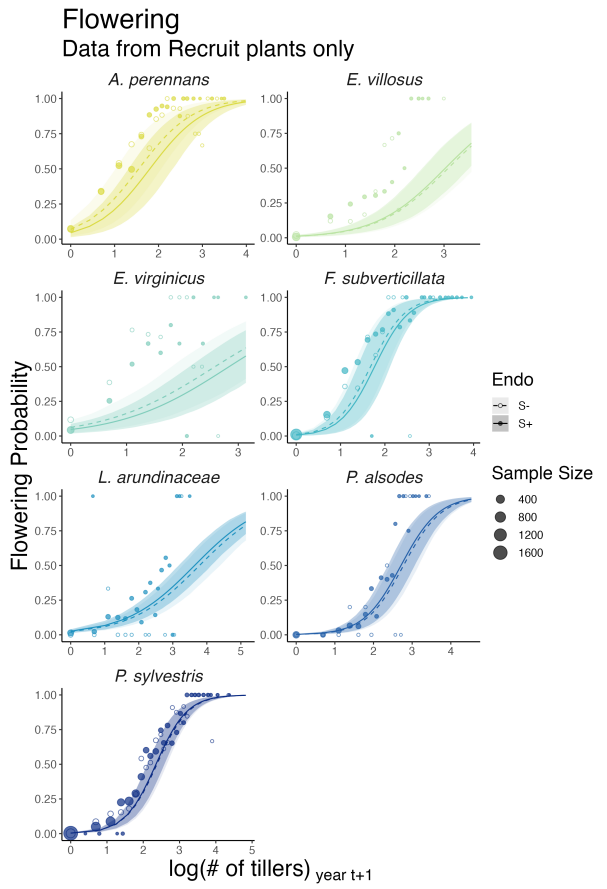


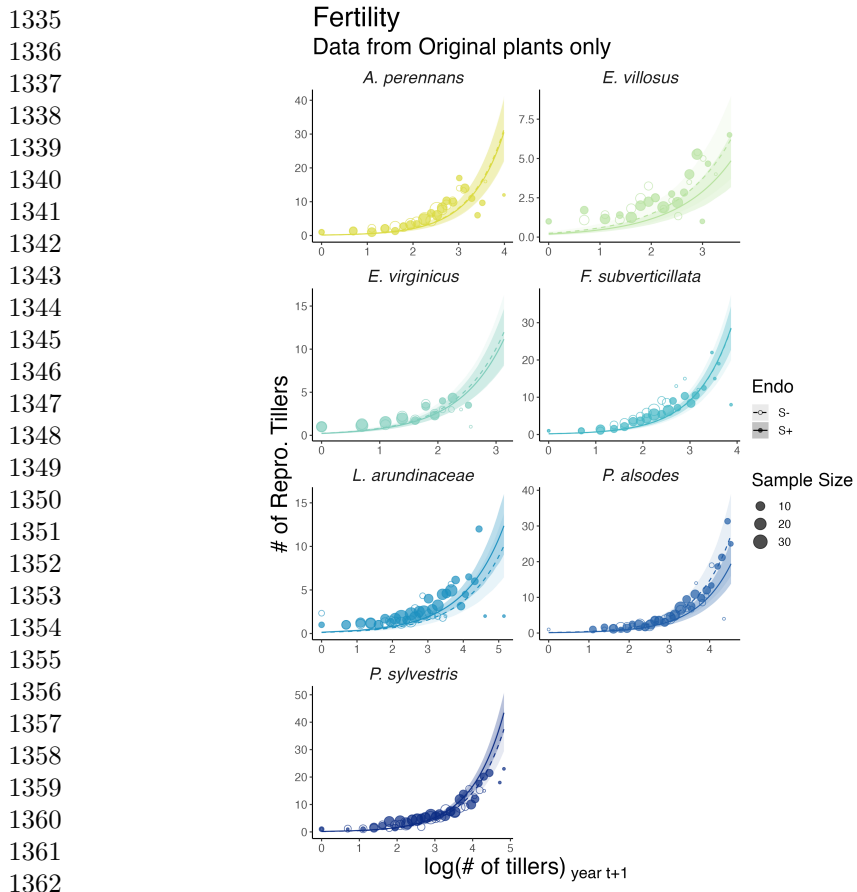
Fig. S4 Effect of endophyte symbiosis on mean adult growth. Fitted curves represent the size-specific mean expected plant size for recruited plants along with data binned by size shown as open circles with a dashed line for symbiont-free (S-) plants, while the solid line and filled circles represent symbiotic (S+) plants. 80% credible intervals are shown with dark shading for S+, or light shading for S-.



1271 **Fig. S5** Effect of endophyte symbiosis on mean flowering. Fitted curves represent the size-specific
 1272 mean flowering probability for original plants along with data binned by size shown as open circles with
 1273 a dashed line for symbiont-free (S-) plants, while the solid line and filled circles represent symbiotic
 1274 (S+) plants. 80% credible intervals are shown with dark shading for S+, or light shading for S-.
 1275
 1276
 1277
 1278
 1279
 1280
 1281
 1282
 1283
 1284
 1285
 1286
 1287
 1288



1289
1290
1291
1292
1293
1294
1295
1296
1297
1298
1299
1300
1301
1302
1303
1304
1305
1306
1307
1308
1309
1310
1311
1312
1313
1314
1315
1316
1317
1318
1319
1320
1321
1322
1323
1324
1325
1326
1327
1328
1329
1330
1331
1332
1333
1334



1363 **Fig. S7** Effect of endophyte symbiosis on mean fertility. Fitted curves represent the size-specific
 1364 mean expected number of flowering tillers for original plants along with data binned by size shown
 1365 as open circles with a dashed line for symbiont-free (S-) plants, while the solid line and filled circles
 1366 represent symbiotic (S+) plants. 80% credible intervals are shown with dark shading for S+, or light
 1367 shading for S-.

1368
 1369
 1370
 1371
 1372
 1373
 1374
 1375
 1376
 1377
 1378
 1379
 1380

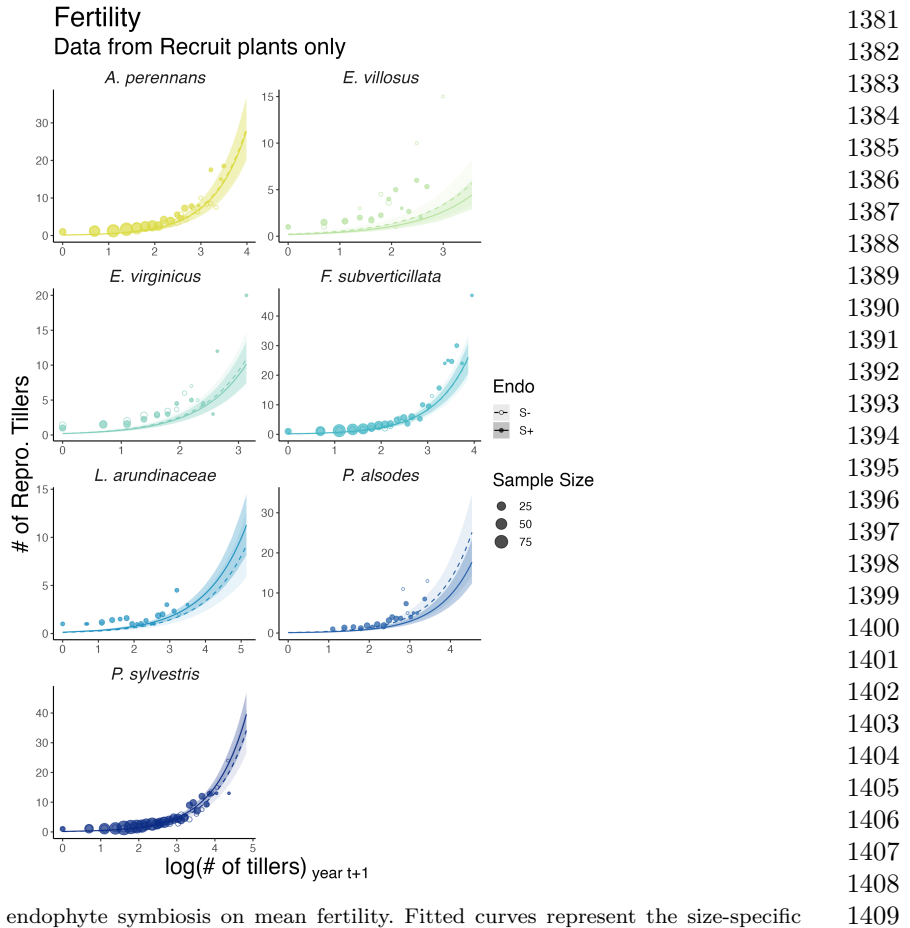
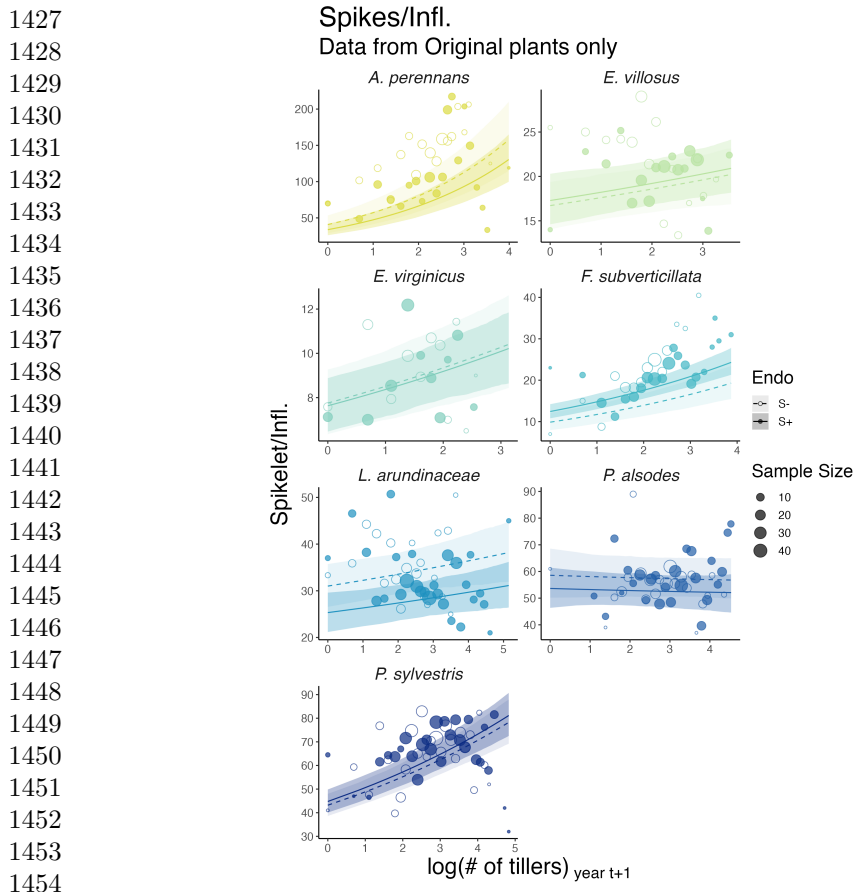


Fig. S8 Effect of endophyte symbiosis on mean fertility. Fitted curves represent the size-specific mean expected number of flowering tillers for recruited plants along with data binned by size shown as open circles with a dashed line for symbiont-free (S-) plants, while the solid line and filled circles represent symbiotic (S+) plants. 80% credible intervals are shown with dark shading for S+, or light shading for S-.



1455 **Fig. S9** Effect of endophyte symbiosis on mean spikelet production. Fitted curves represent the
1456 size-specific mean expected number of spikelets per inflorescence for original plants along with data
1457 binned by size shown as open circles with a dashed line for symbiont-free (S-) plants, while the solid
1458 line and filled circles represent symbiotic (S+) plants. 80% credible intervals are shown with dark
1459 shading for S+, or light shading for S-.

1460
1461
1462
1463
1464
1465
1466
1467
1468
1469
1470
1471
1472

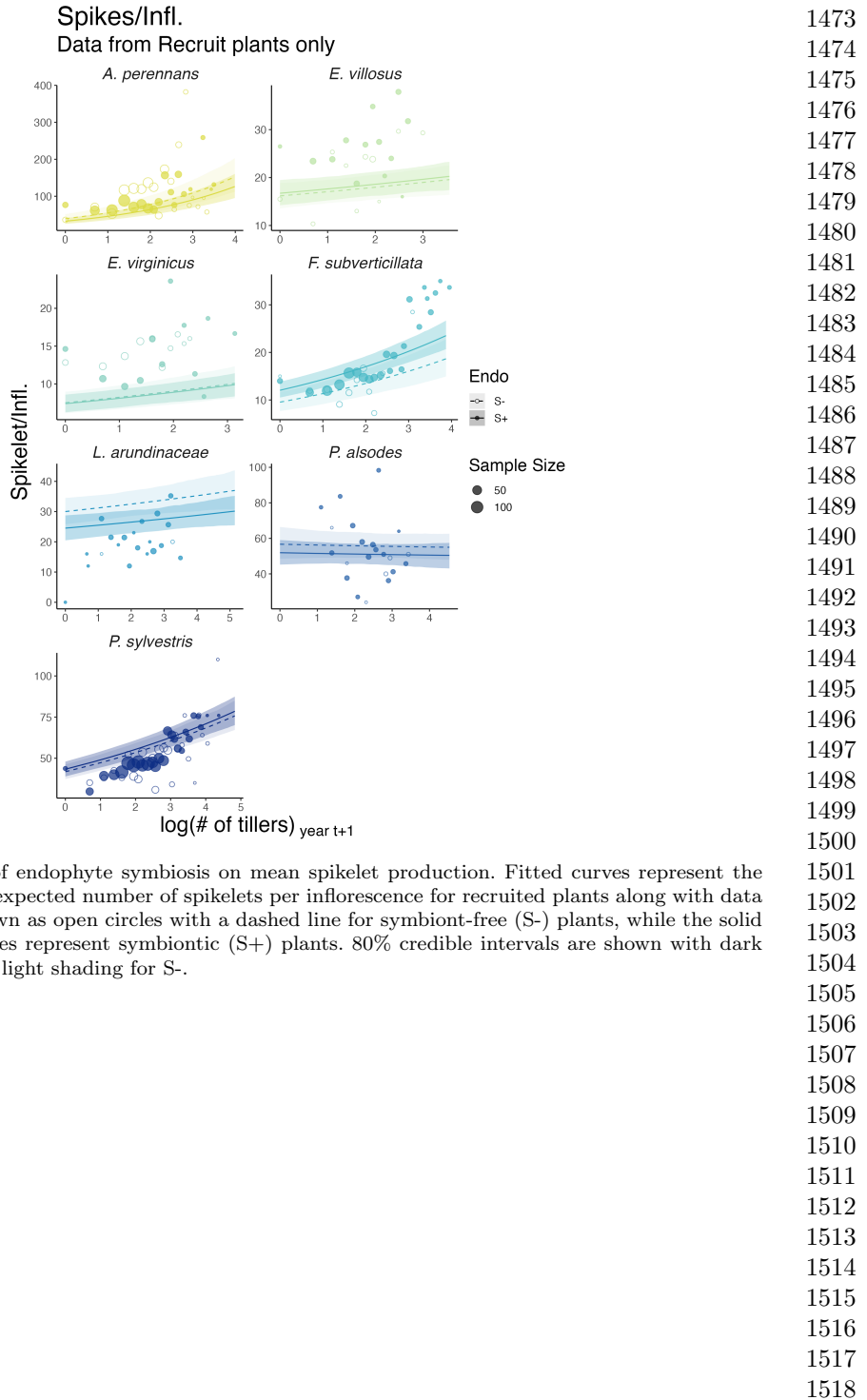
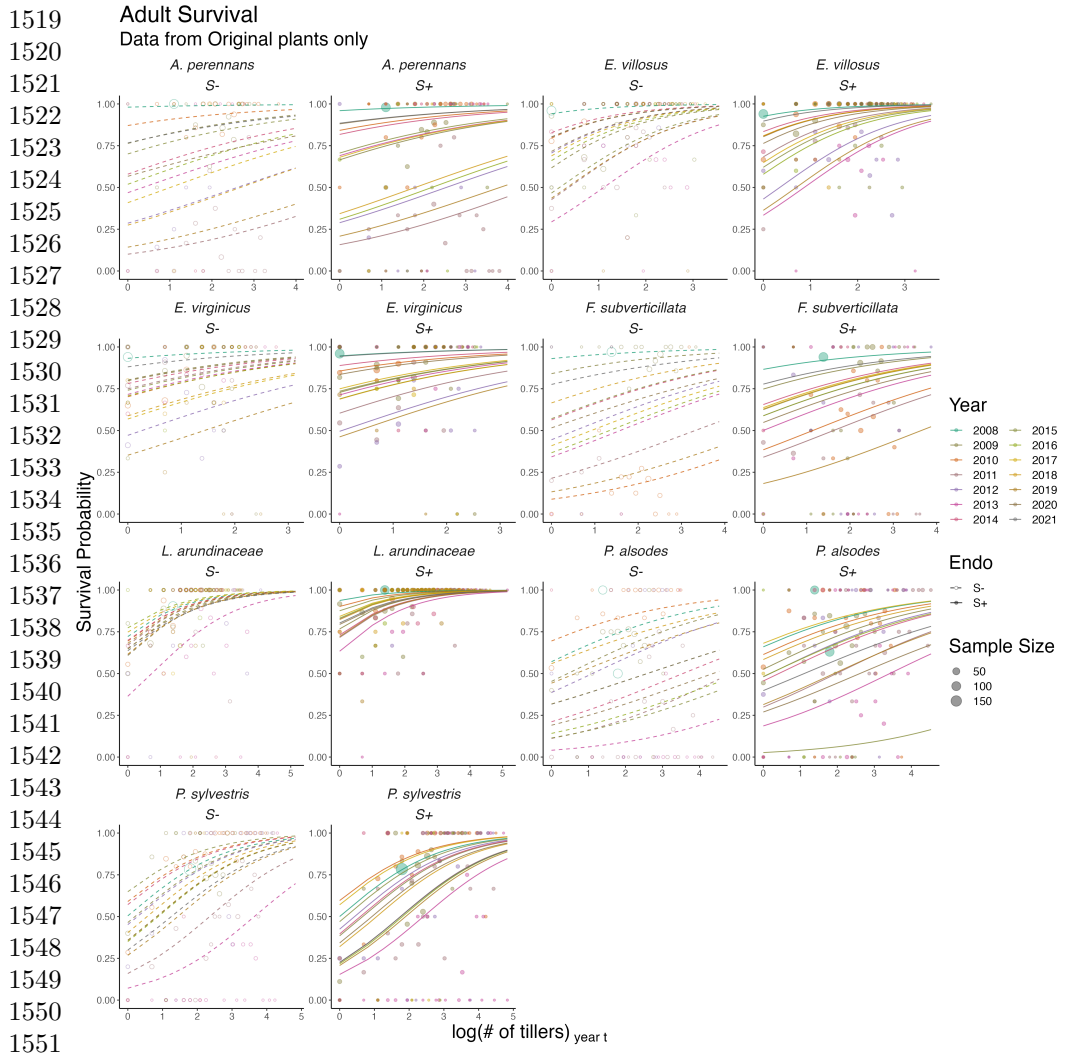


Fig. S10 Effect of endophyte symbiosis on mean spikelet production. Fitted curves represent the size-specific mean expected number of spikelets per inflorescence for recruited plants along with data binned by size shown as open circles with a dashed line for symbiont-free (S-) plants, while the solid line and filled circles represent symbiotic (S+) plants. 80% credible intervals are shown with dark shading for S+, or light shading for S-.



1553 **Fig. S11** Effect of endophyte symbiosis on yearly adult survival. Fitted curves represent the size-
1554 specific annual survival probability for original plants along with data binned by size and census year
1555 shown as open circles with a dashed line for symbiont-free (S-) plants, while the solid line and filled
1556 circles represent symbiotic (S+) plants.

1556
1557
1558
1559
1560
1561
1562
1563
1564

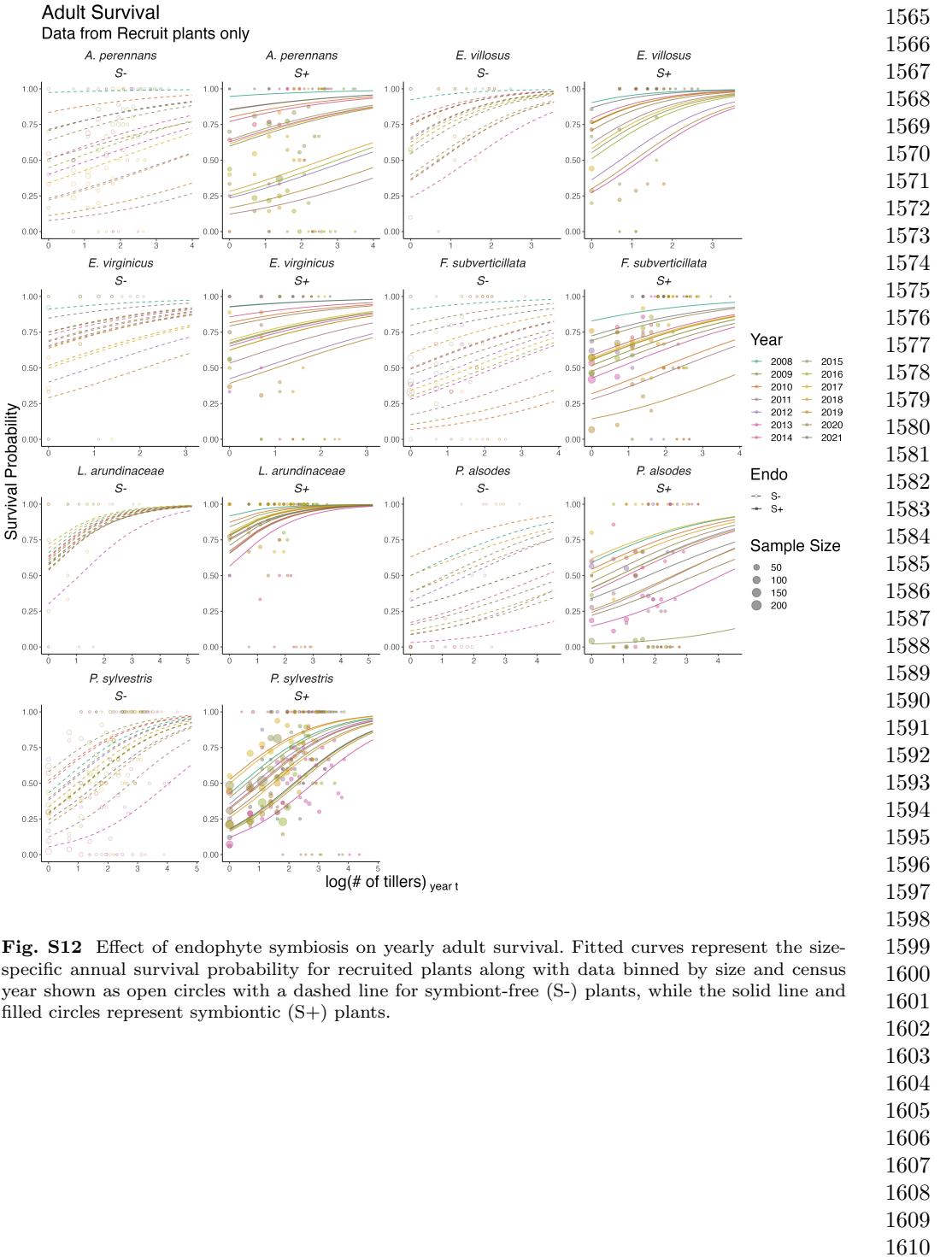
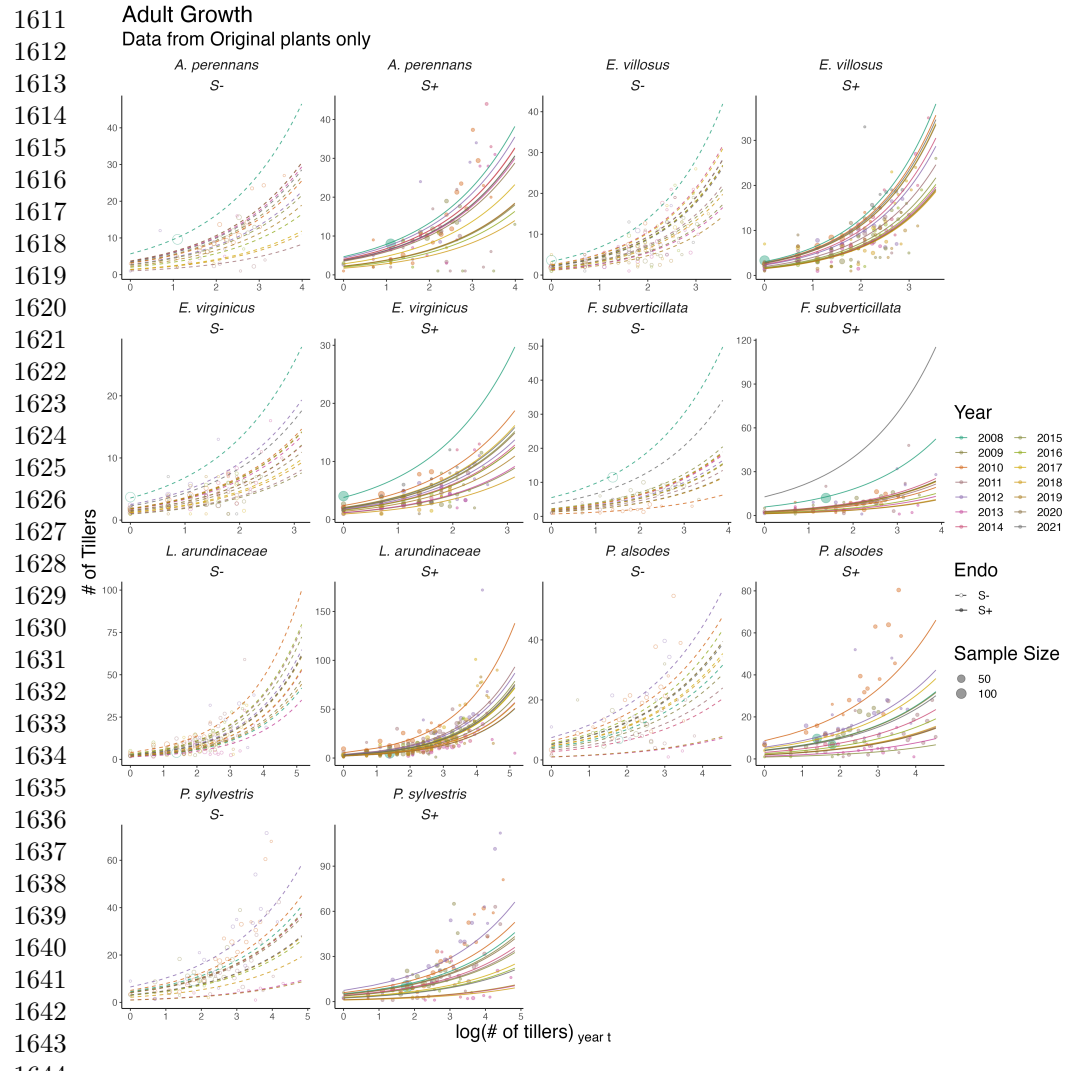


Fig. S12 Effect of endophyte symbiosis on yearly adult survival. Fitted curves represent the size-specific annual survival probability for recruited plants along with data binned by size and census year shown as open circles with a dashed line for symbiont-free (S-) plants, while the solid line and filled circles represent symbiotic (S+) plants.



1645 **Fig. S13** Effect of endophyte symbiosis on yearly adult growth. Fitted curves represent the size-
1646 specific annual expected plant size for original plants along with data binned by size and census year
1647 shown as open circles with a dashed line for symbiont-free (S-) plants, while the solid line and filled
1648 circles represent symbiotic (S+) plants.

1648
1649
1650
1651
1652
1653
1654
1655
1656

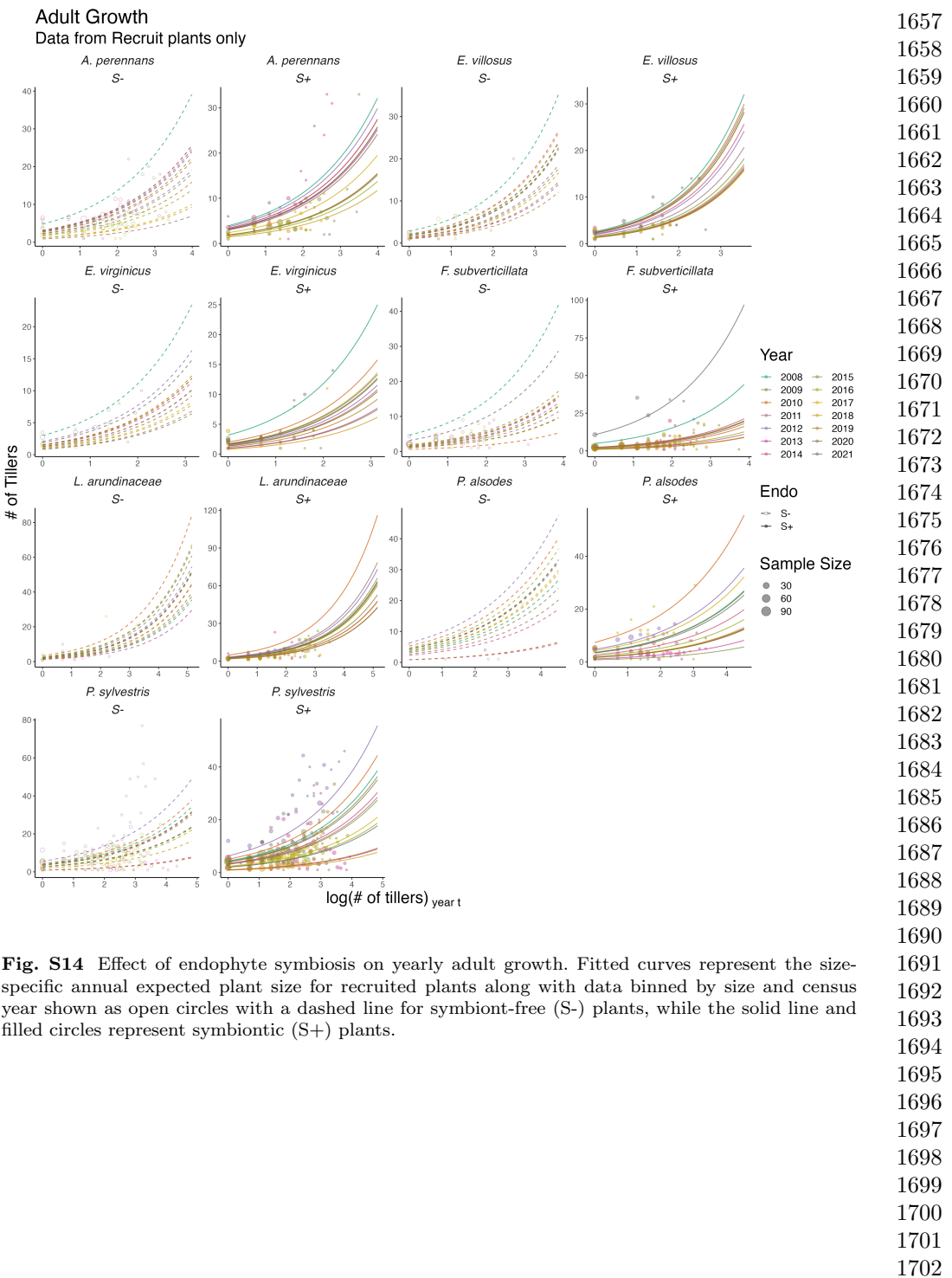
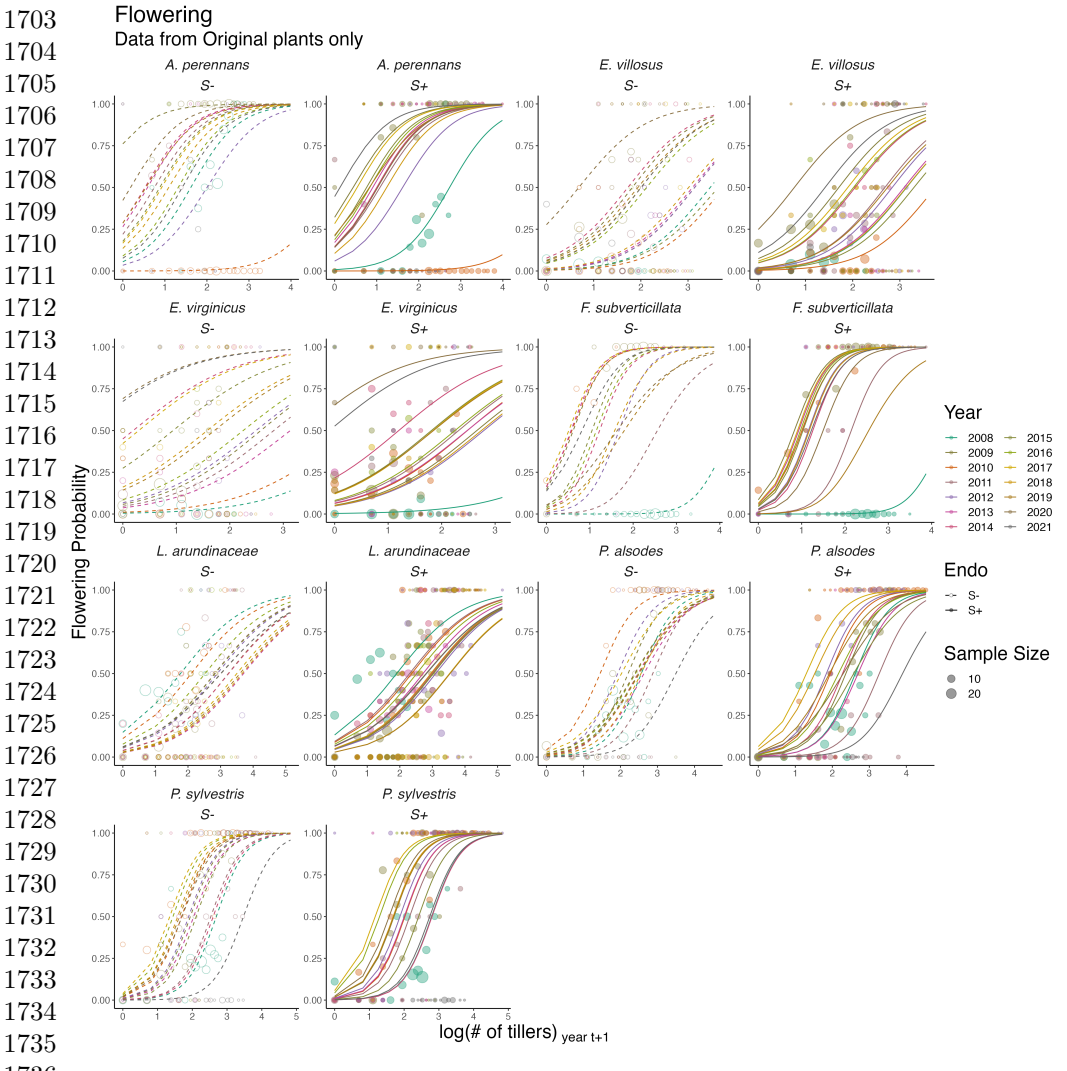


Fig. S14 Effect of endophyte symbiosis on yearly adult growth. Fitted curves represent the size-specific annual expected plant size for recruited plants along with data binned by size and census year shown as open circles with a dashed line for symbiont-free (S-) plants, while the solid line and filled circles represent symbiotic (S+) plants.



1737 **Fig. S15** Effect of endophyte symbiosis on yearly flowering. Fitted curves represent the size-specific
1738 annual flowering probability for original plants along with data binned by size and census year shown
1739 as open circles with a dashed line for symbiont-free (S-) plants, while the solid line and filled circles
1740 represent symbiotic (S+) plants.

1741
1742
1743
1744
1745
1746
1747
1748

Flowering
Data from Recruit plants only

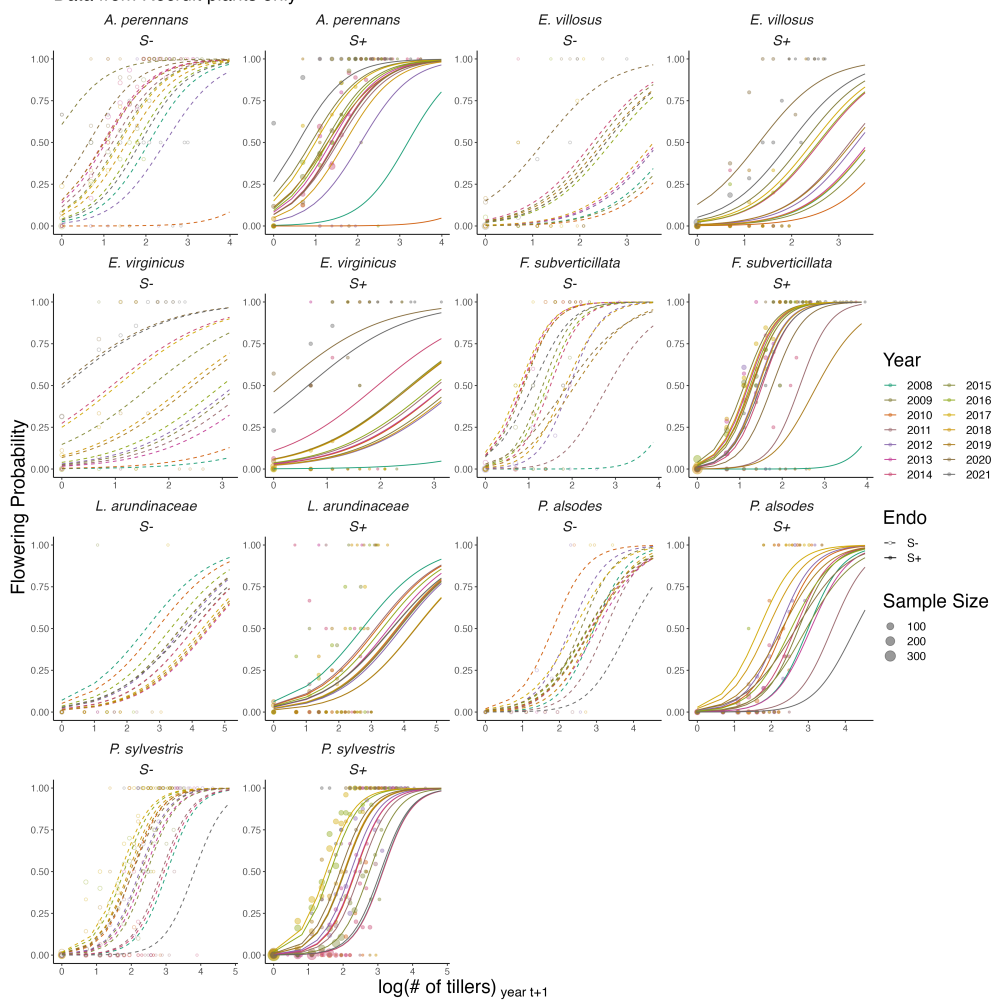
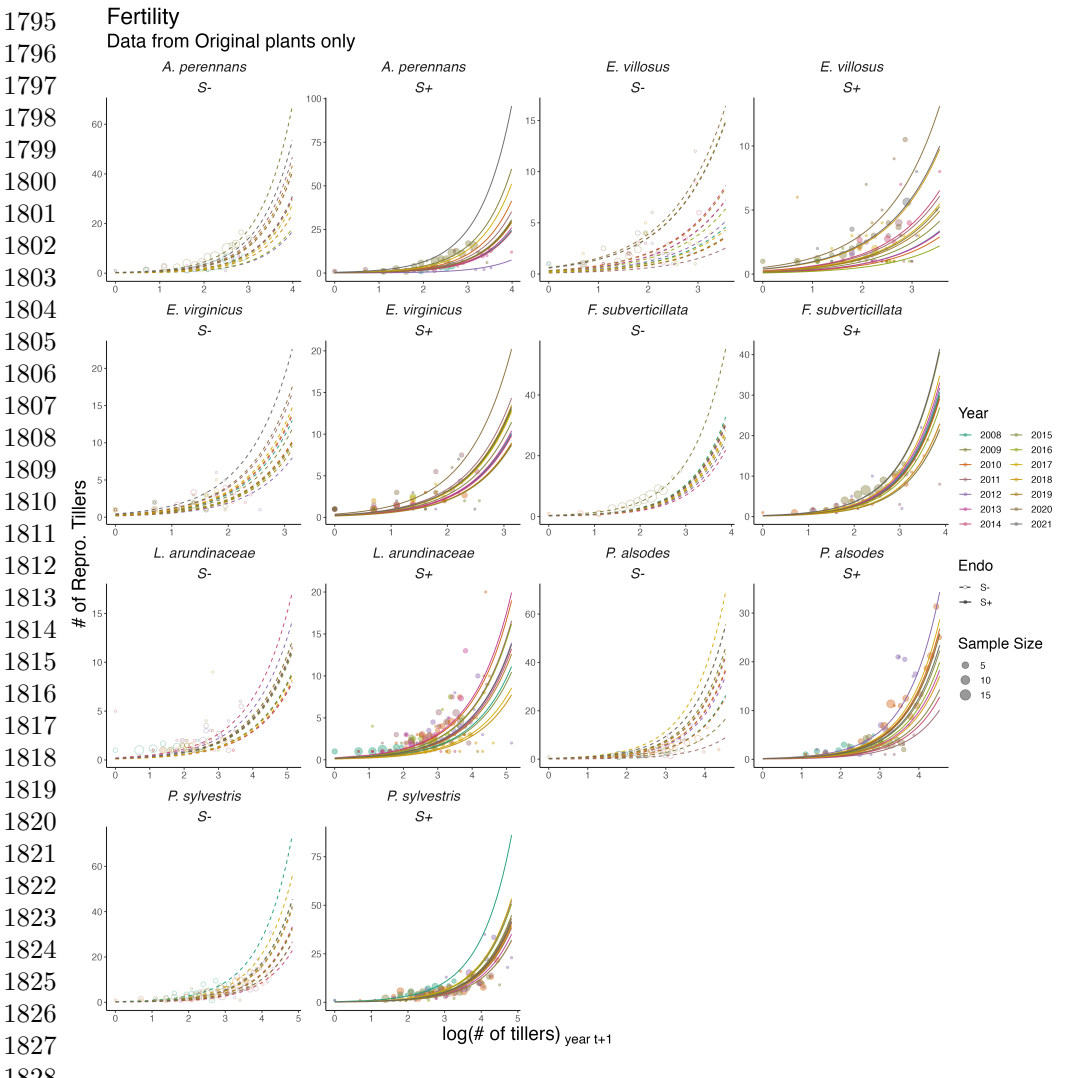


Fig. S16 Effect of endophyte symbiosis on yearly flowering. Fitted curves represent the size-specific annual flowering probability for recruited plants along with data binned by size and census year shown as open circles with a dashed line for symbiont-free (S-) plants, while the solid line and filled circles represent symbiotic (S+) plants.

1749
1750
1751
1752
1753
1754
1755
1756
1757
1758
1759
1760
1761
1762
1763
1764
1765
1766
1767
1768
1769
1770
1771
1772
1773
1774
1775
1776
1777
1778
1779
1780
1781
1782
1783
1784
1785
1786
1787
1788
1789
1790
1791
1792
1793
1794



1829 **Fig. S17** Effect of endophyte symbiosis on yearly fertility. Fitted curves represent the size-specific
 1830 annual expected number of flowering tillers for original plants along with data binned by size and
 1831 census year shown as open circles with a dashed line for symbiont-free (S-) plants, while the solid line
 1832 and filled circles represent symbiotic (S+) plants.

1833
 1834
 1835
 1836
 1837
 1838
 1839
 1840

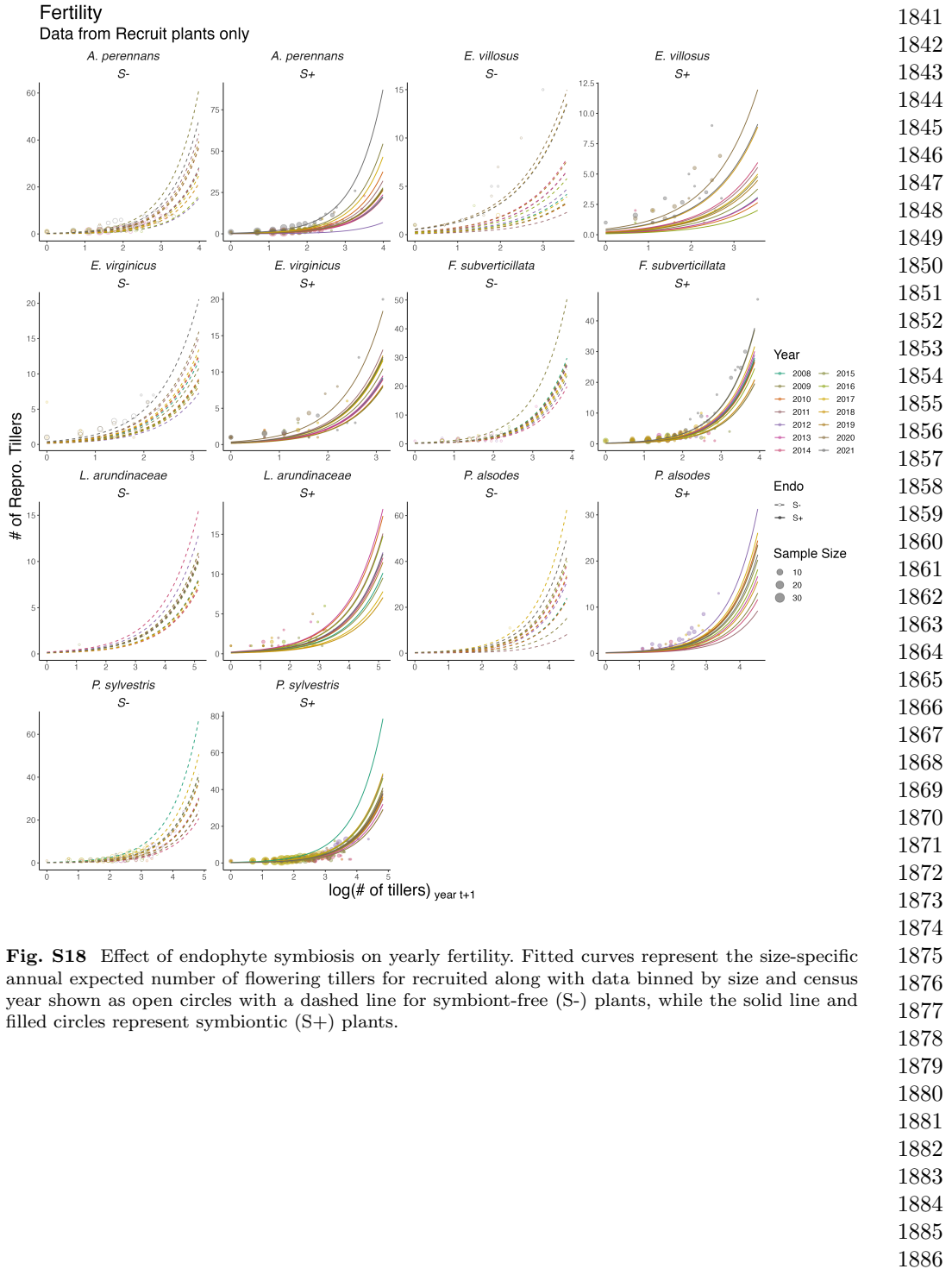


Fig. S18 Effect of endophyte symbiosis on yearly fertility. Fitted curves represent the size-specific annual expected number of flowering tillers for recruited along with data binned by size and census year shown as open circles with a dashed line for symbiont-free (S-) plants, while the solid line and filled circles represent symbiotic (S+) plants.

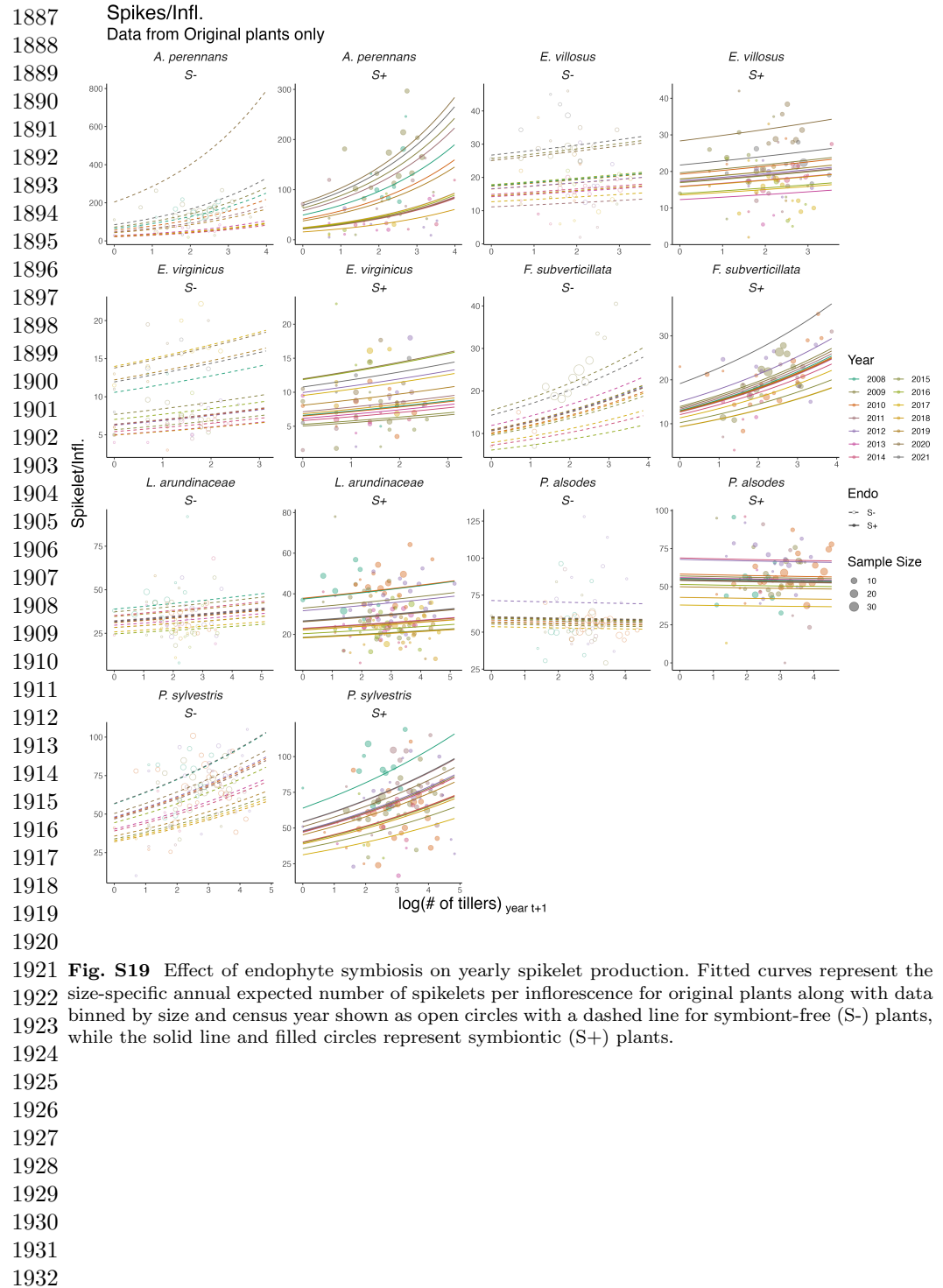


Fig. S19 Effect of endophyte symbiosis on yearly spikelet production. Fitted curves represent the size-specific annual expected number of spikelets per inflorescence for original plants along with data binned by size and census year shown as open circles with a dashed line for symbiont-free (S-) plants, while the solid line and filled circles represent symbiotic (S+) plants.

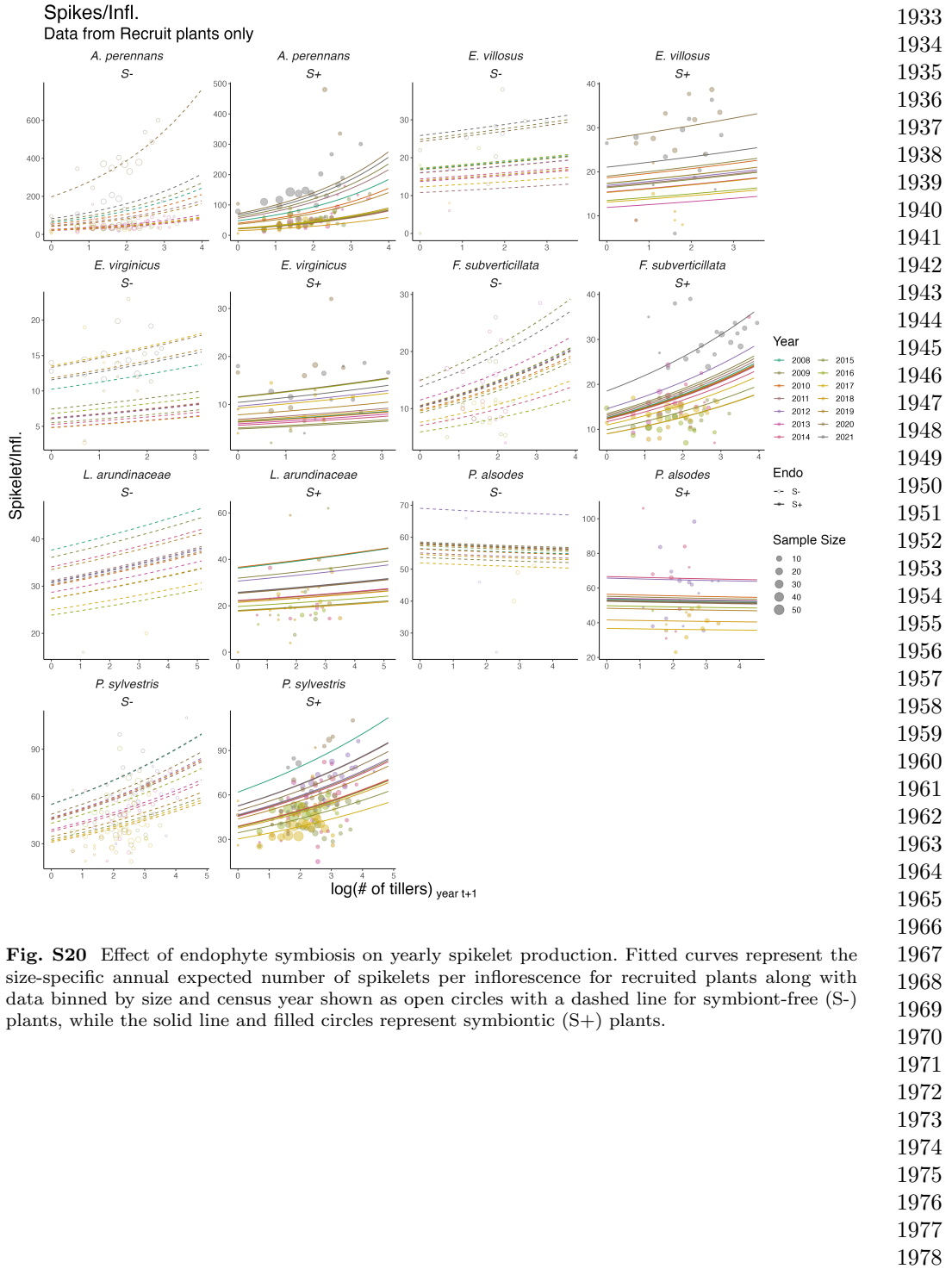
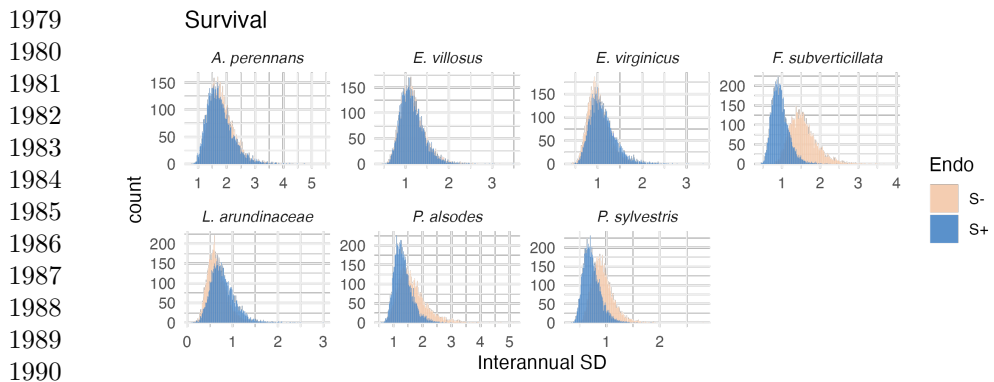


Fig. S20 Effect of endophyte symbiosis on yearly spikelet production. Fitted curves represent the size-specific annual expected number of spikelets per inflorescence for recruited plants along with data binned by size and census year shown as open circles with a dashed line for symbiont-free (S-) plants, while the solid line and filled circles represent symbiotic (S+) plants.



1991 **Fig. S21** Posterior distributions of the standard deviations of inter-annual year effects for survival.

1992 Histograms include 7500 post-warmup MCMC samples for symbiotic (S+; blue) and symbiont-free

1993 (S-; tan) plants from fitted vital rate model.

1994

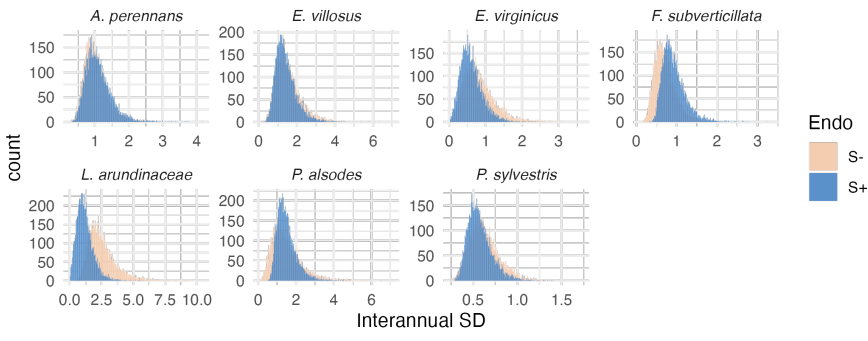
1995

1996

1997

Seedling Survival

1998



2009 **Fig. S22** Posterior distributions of the standard deviations of inter-annual year effects for seedling survival.

2010 Histograms include 7500 post-warmup MCMC samples for symbiotic (S+; blue) and symbiont-free

2011 (S-; tan) plants from fitted vital rate model.

2012

2013

2014

2015

2016

2017

2018

2019

2020

2021

2022

2023

2024

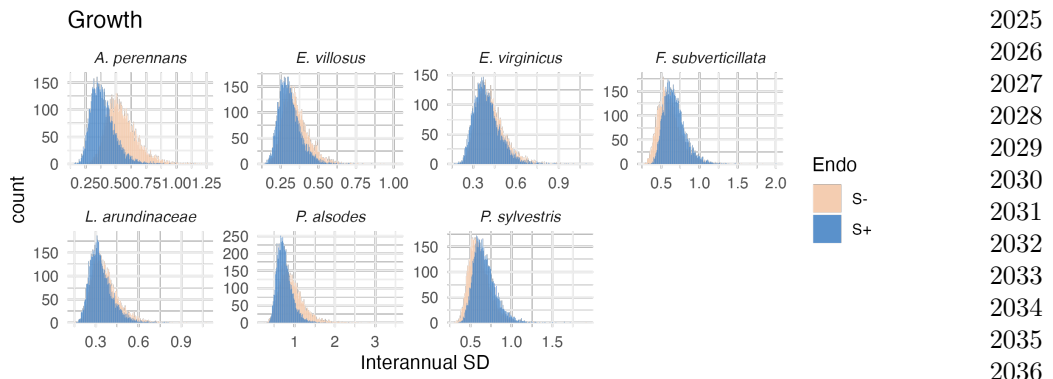


Fig. S23 Posterior distributions of the standard deviations of inter-annual year effects for growth. Histograms include 7500 post-warmup MCMC samples for symbiotic (S+; blue) and symbiont-free (S-; tan) plants from fitted vital rate model.

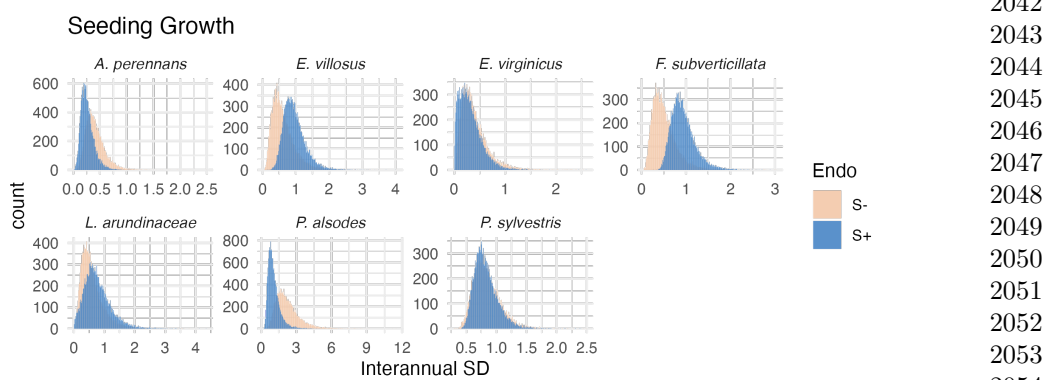
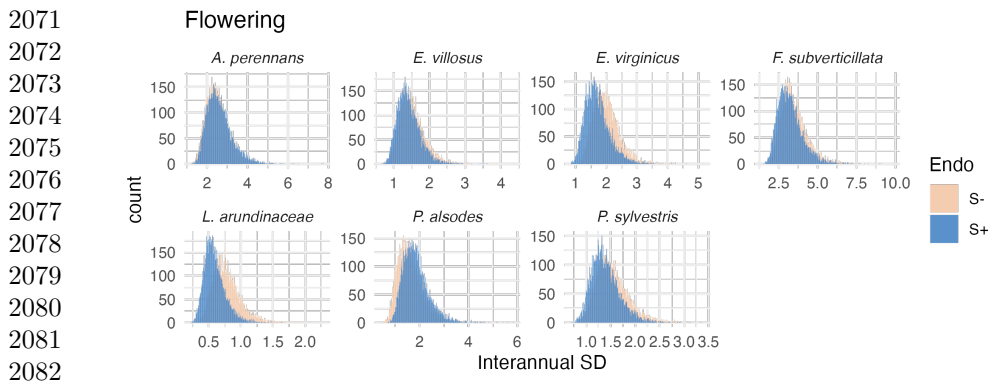


Fig. S24 Posterior distributions of the standard deviations of inter-annual year effects for seedling growth. Histograms include 7500 post-warmup MCMC samples for symbiotic (S+; blue) and symbiont-free (S-; tan) plants from fitted vital rate model.

2025
2026
2027
2028
2029
2030
2031
2032
2033
2034
2035
2036
2037
2038
2039
2040
2041
2042
2043
2044
2045
2046
2047
2048
2049
2050
2051
2052
2053
2054
2055
2056
2057
2058
2059
2060
2061
2062
2063
2064
2065
2066
2067
2068
2069
2070



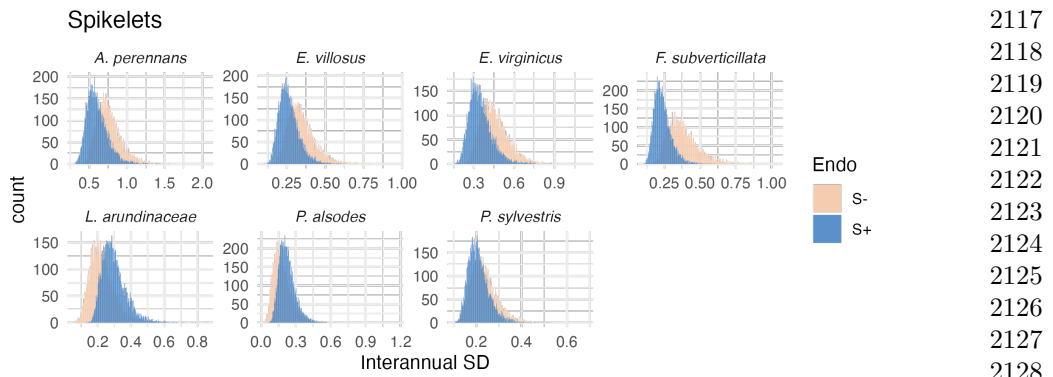


Fig. S27 Posterior distributions of the standard deviations of inter-annual year effects for spikelets per inflorescence. Histograms include 7500 post-warmup MCMC samples for symbiotic (S+; blue) and symbiont-free (S-; tan) plants from fitted vital rate model.

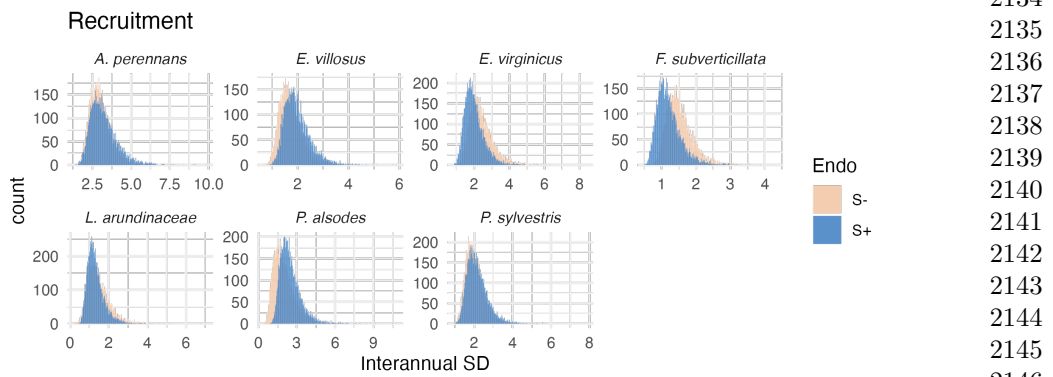


Fig. S28 Posterior distributions of the standard deviations of inter-annual year effects for recruitment. Histograms include 7500 post-warmup MCMC samples for symbiotic (S+; blue) and symbiont-free (S-; tan) plants from fitted vital rate model.

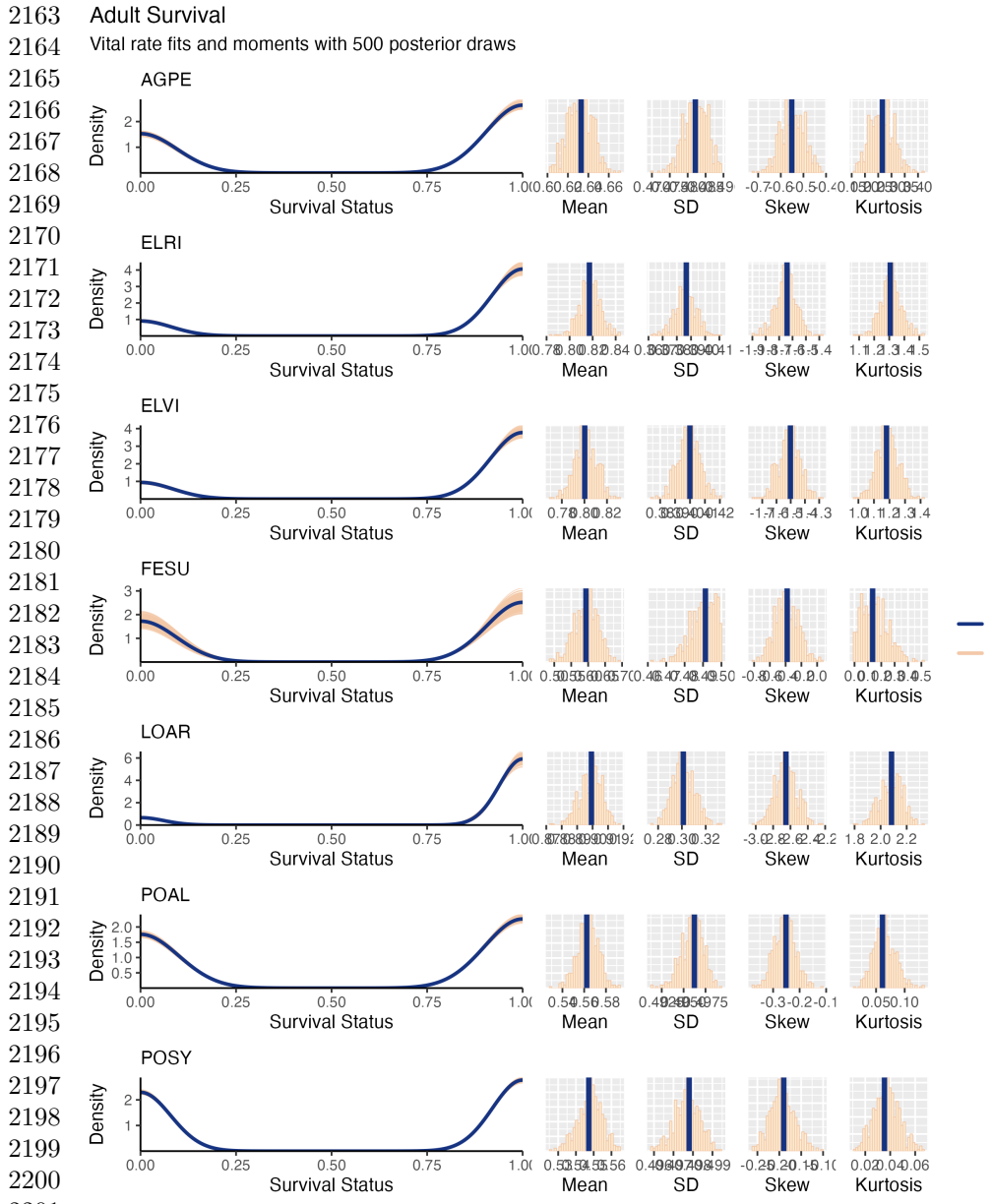


Fig. S29 Posterior predictive check for statistical model of Adult Survival. Consistency between real data and simulated values indicates that fitted models describe the data well. Lines show density distributions of observed data (blue line) compared to data simulated from fitted models (tan lines) generated from 500 draws from posterior distributions of model parameters along with the distribution's moments.

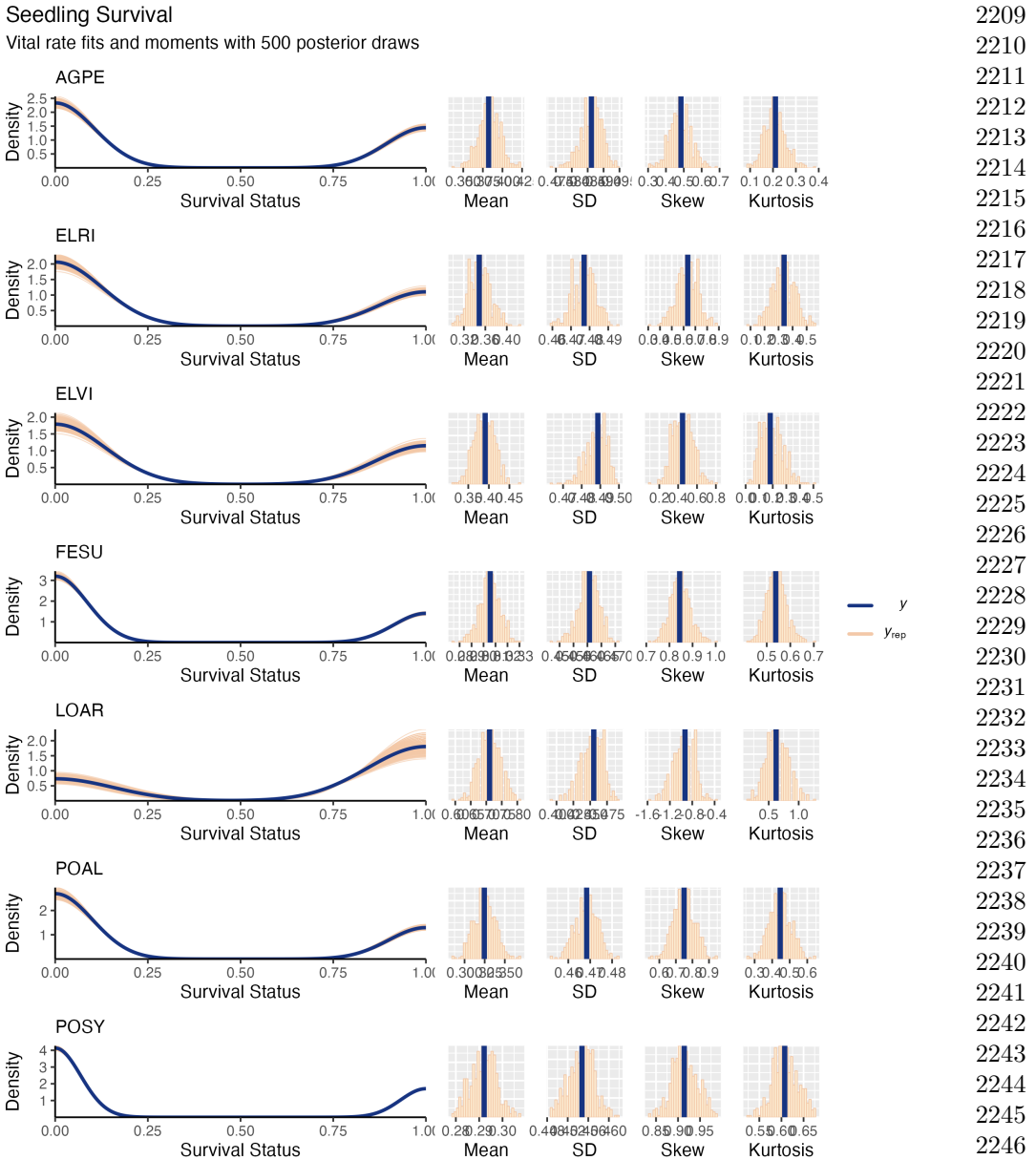
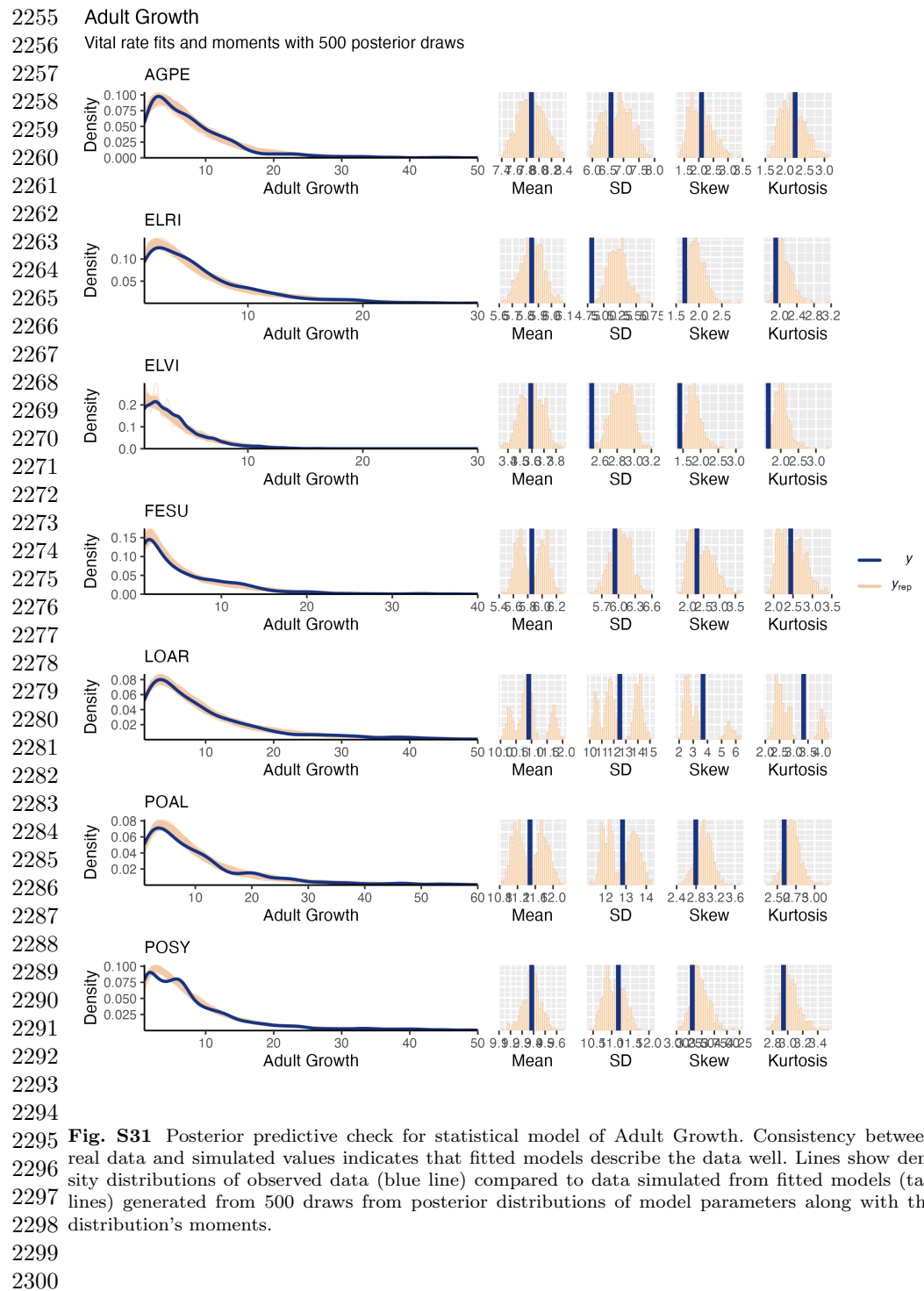


Fig. S30 Posterior predictive check for statistical model of Seedling Survival. Consistency between real data and simulated values indicates that fitted models describe the data well. Lines show density distributions of observed data (blue line) compared to data simulated from fitted models (tan lines) generated from 500 draws from posterior distributions of model parameters along with the distribution's moments.



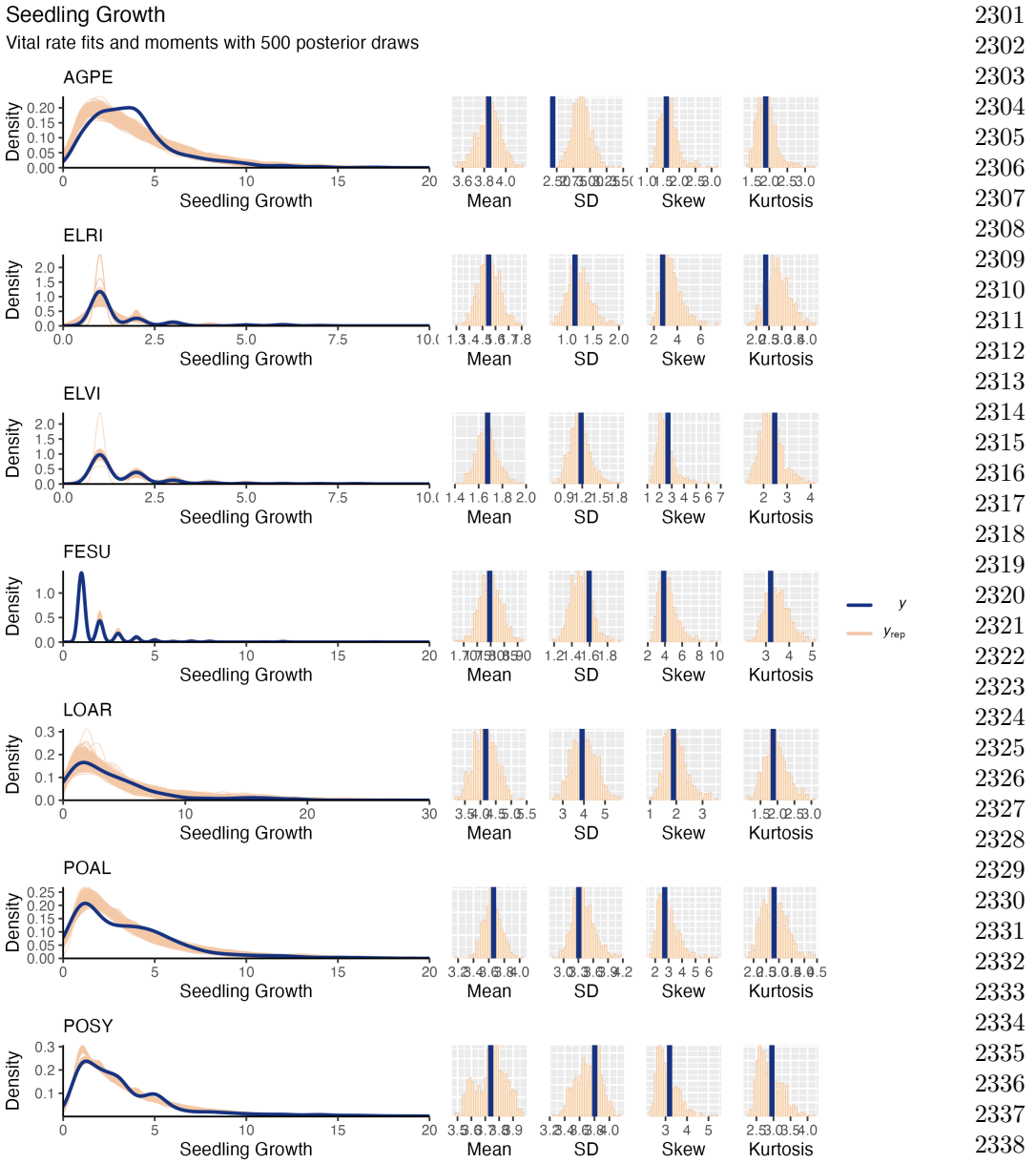
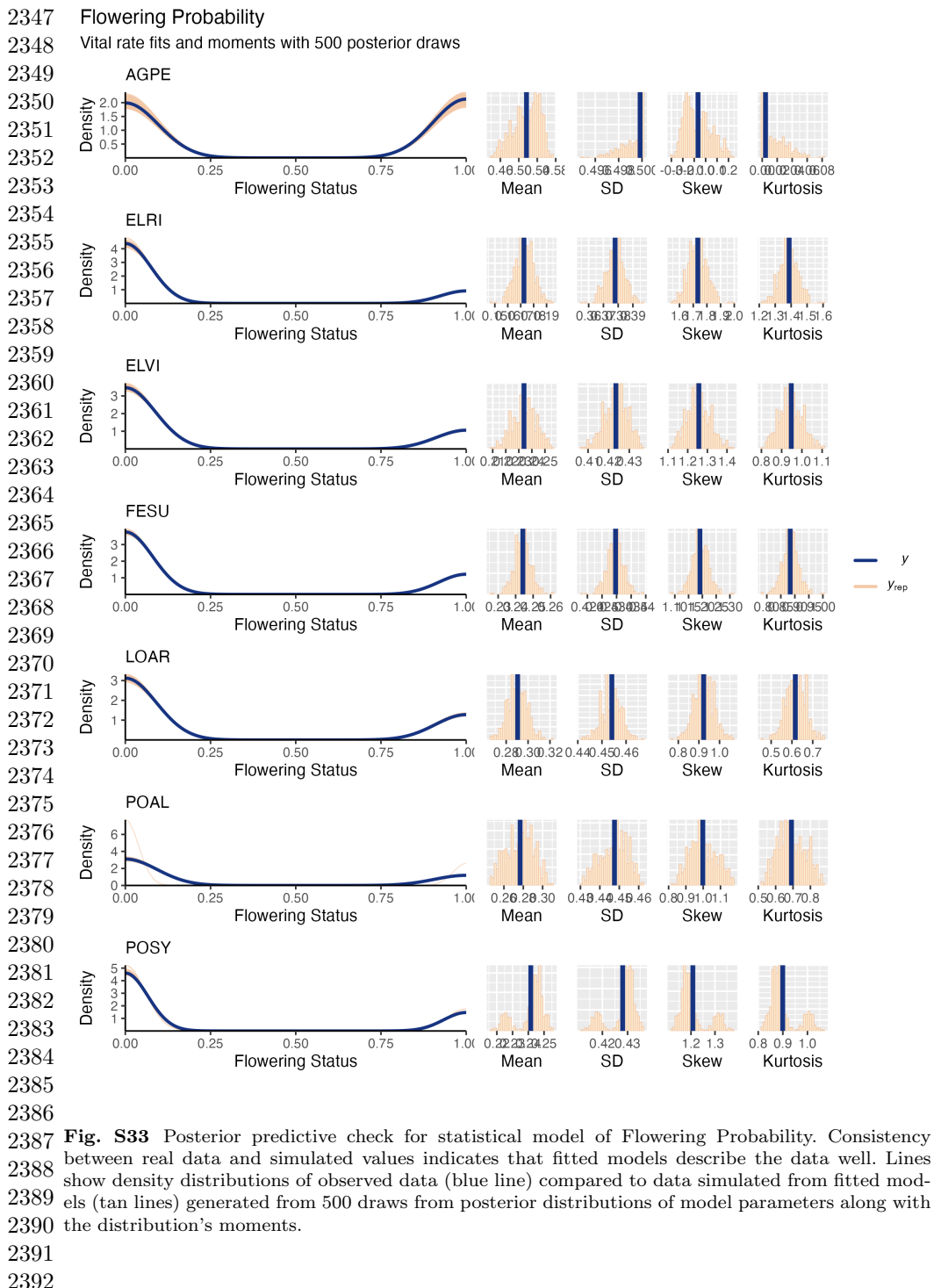


Fig. S32 Posterior predictive check for statistical model of Seedling Growth. Consistency between real data and simulated values indicates that fitted models describe the data well. Lines show density distributions of observed data (blue line) compared to data simulated from fitted models (tan lines) generated from 500 draws from posterior distributions of model parameters along with the distribution's moments.



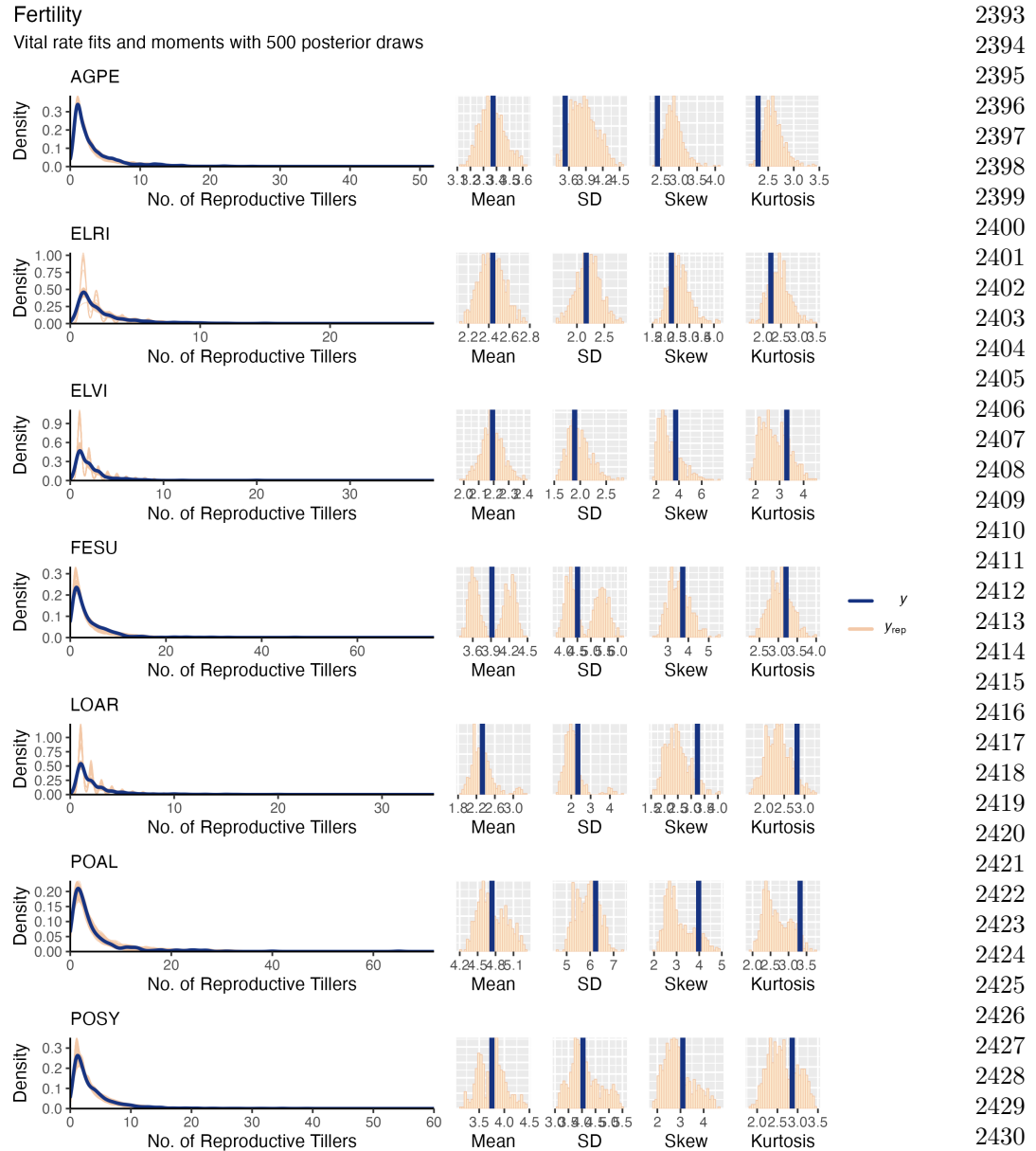
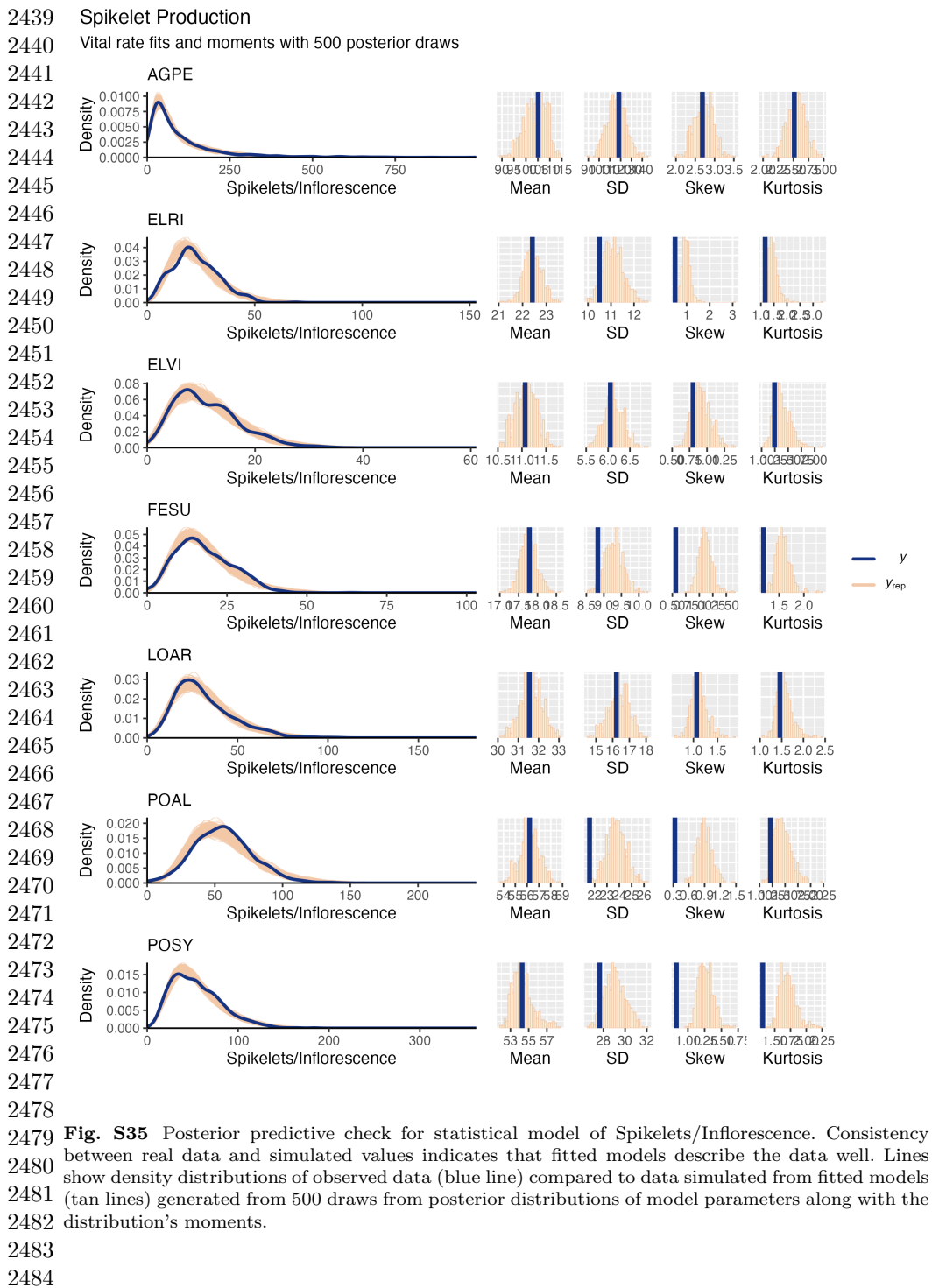


Fig. S34 Posterior predictive check for statistical model of Flowering Tiller production. Consistency between real data and simulated values indicates that fitted models describe the data well. Lines show density distributions of observed data (blue line) compared to data simulated from fitted models (tan lines) generated from 500 draws from posterior distributions of model parameters along with the distribution's moments.



Seed Production
Vital rate fits and moments with 500 posterior draws

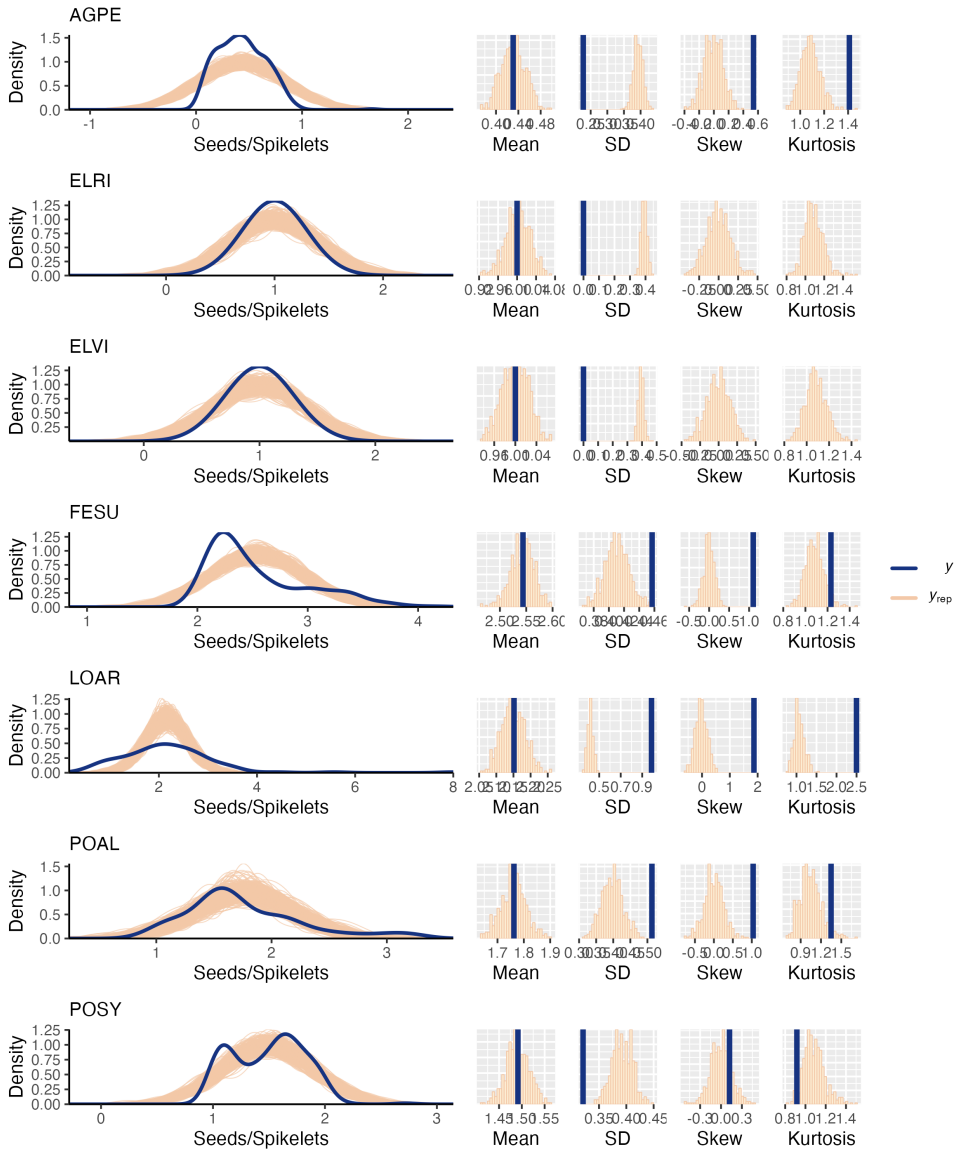
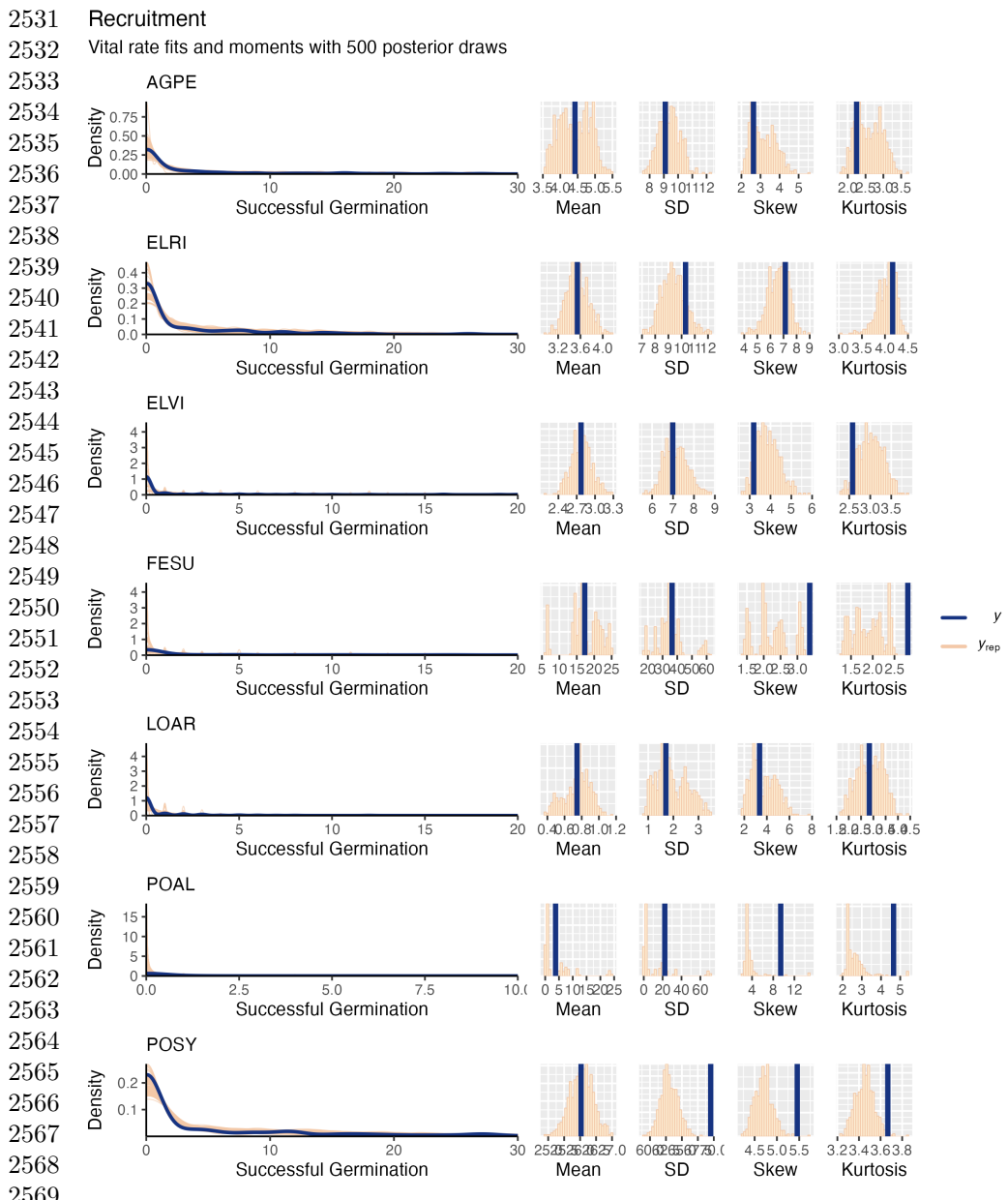


Fig. S36 Posterior predictive check for statistical model of Mean Seeds/Spikelet. Consistency between real data and simulated values indicates that fitted models describe the data well. Lines show density distributions of observed data (blue line) compared to data simulated from fitted models (tan lines) generated from 500 draws from posterior distributions of model parameters along with the distribution's moments.

2485
2486
2487
2488
2489
2490
2491
2492
2493
2494
2495
2496
2497
2498
2499
2500
2501
2502
2503
2504
2505
2506
2507
2508
2509
2510
2511
2512
2513
2514
2515
2516
2517
2518
2519
2520
2521
2522
2523
2524
2525
2526
2527
2528
2529
2530



2571 **Fig. S37** Posterior predictive check for statistical model of Recruitment. Consistency between real
 2572 data and simulated values indicates that fitted models describe the data well. Lines show den-
 2573 sity distributions of observed data (blue line) compared to data simulated from fitted models (tan
 2574 lines) generated from 500 draws from posterior distributions of model parameters along with the
 2575 distribution's moments.

2575
2576

Size specific vital rate moments

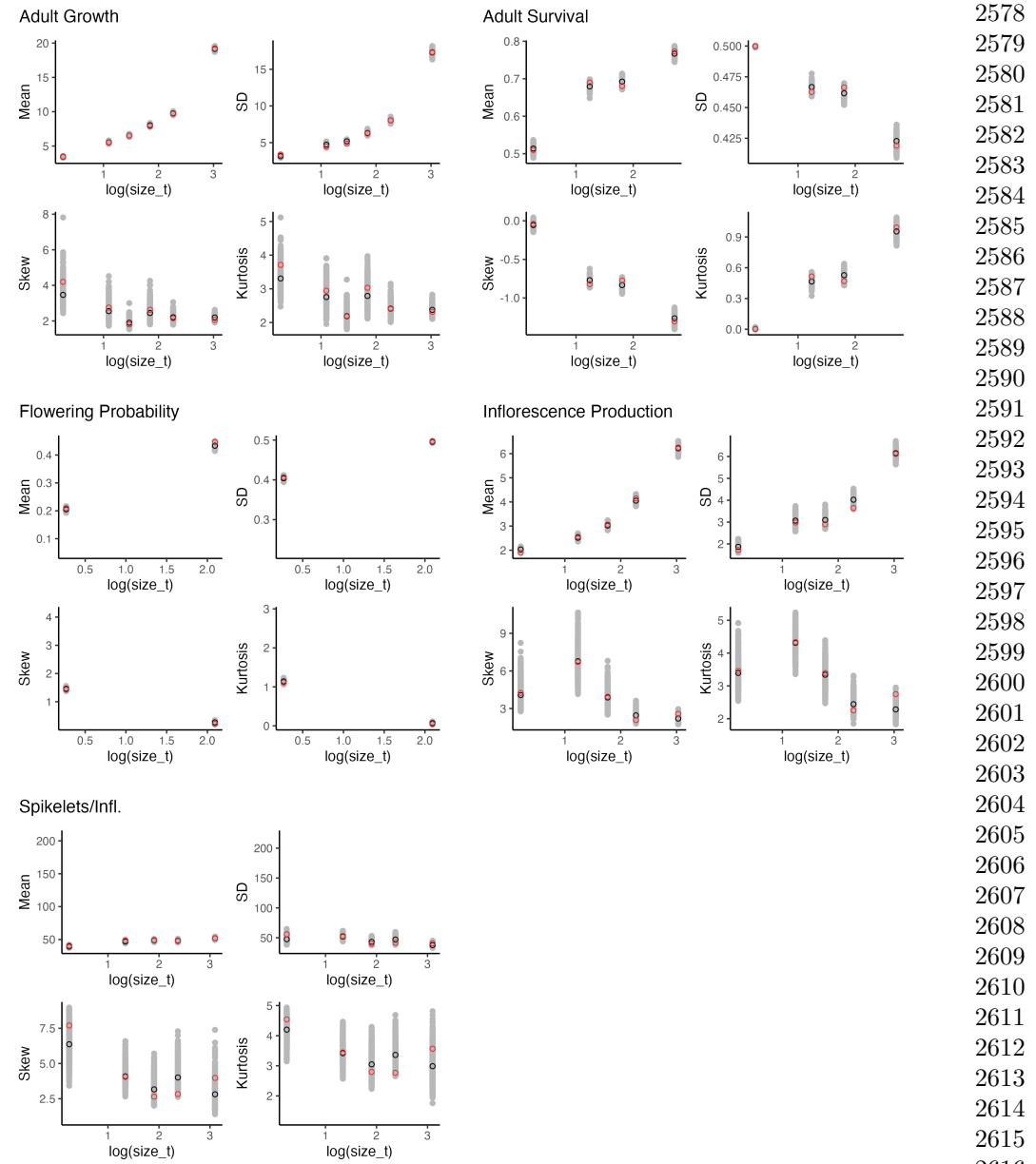
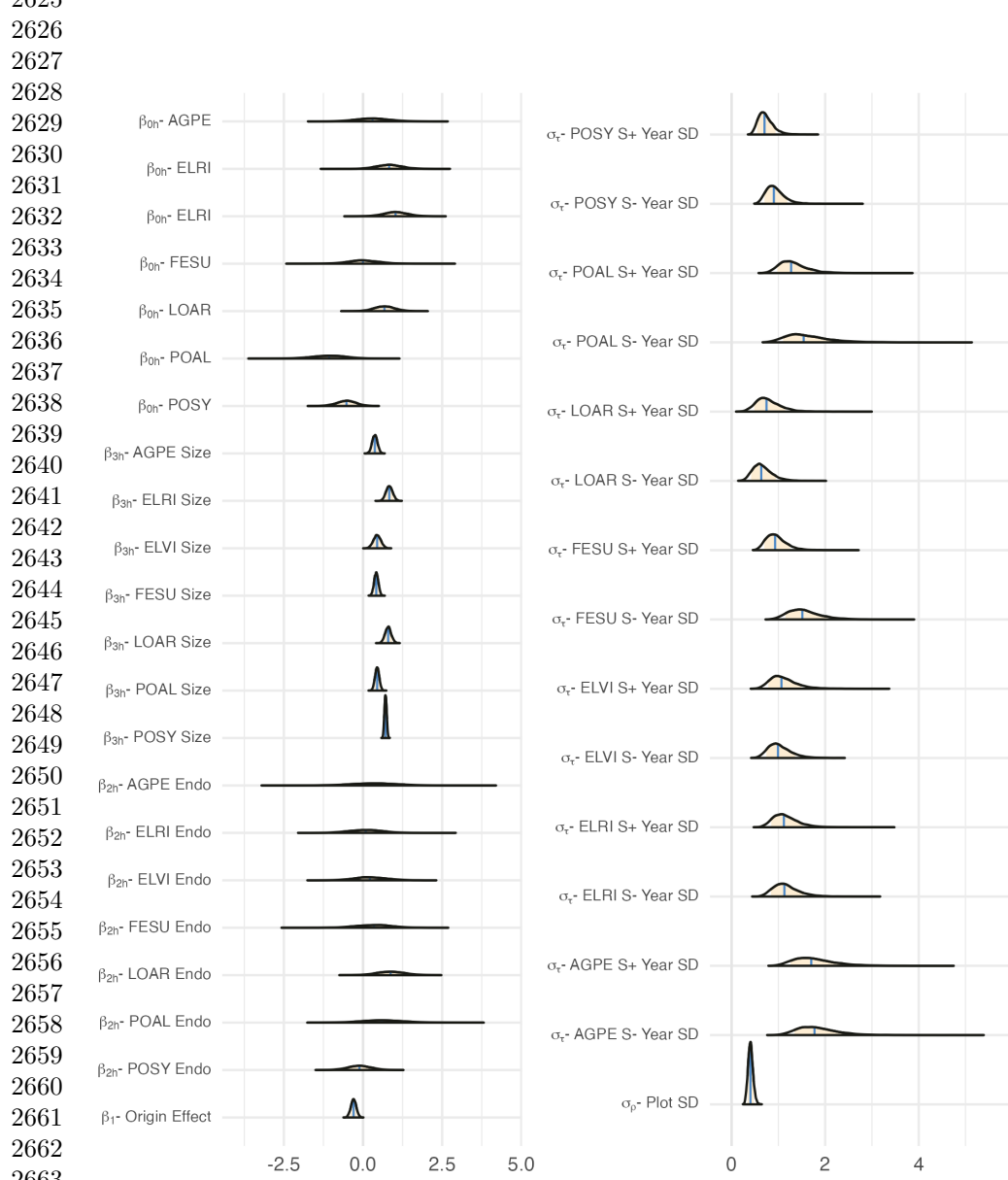


Fig. S38 Consistency between real data and fitted values across sizes indicates that the vital rate models are accurately capturing size dependence. Graphs of posterior predictive check for mean and higher moments of the vital rate models across size. Points show the value of statistical moments binned across size for the observed data (red circles) compared to the simulated datasets (grey circles) and the median of the simulated values (black circles) generated from 500 posterior draws from the fitted model.

2623 Adult Survival
 2624 Posterior mean with 80% credible intervals
 2625



2665 Fig. S39 Posterior distributions of the vital rate regressions for Adult Survival. Density curves show
 2666 80% credible interval along with the posterior posterior mean.
 2667
 2668

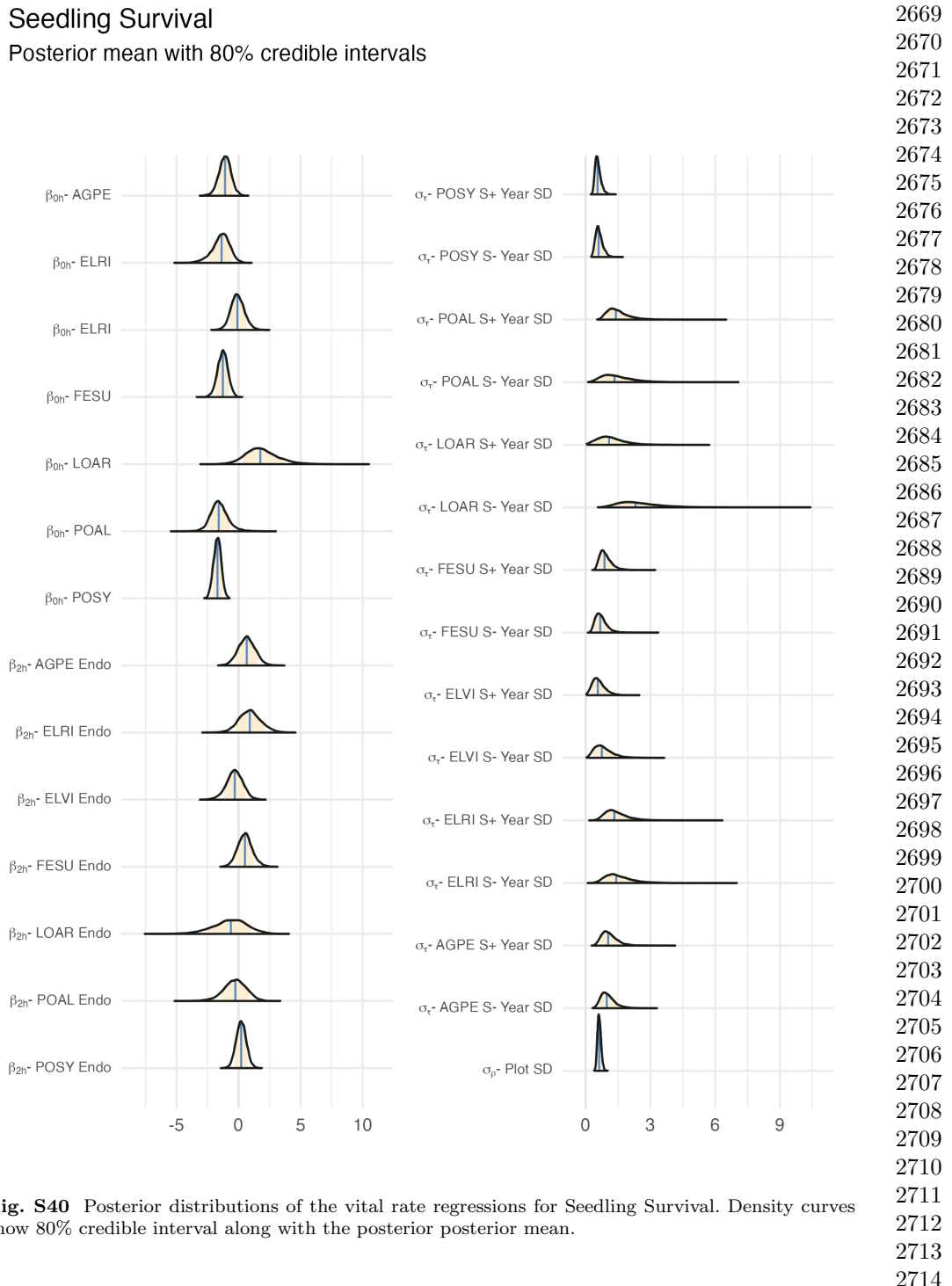
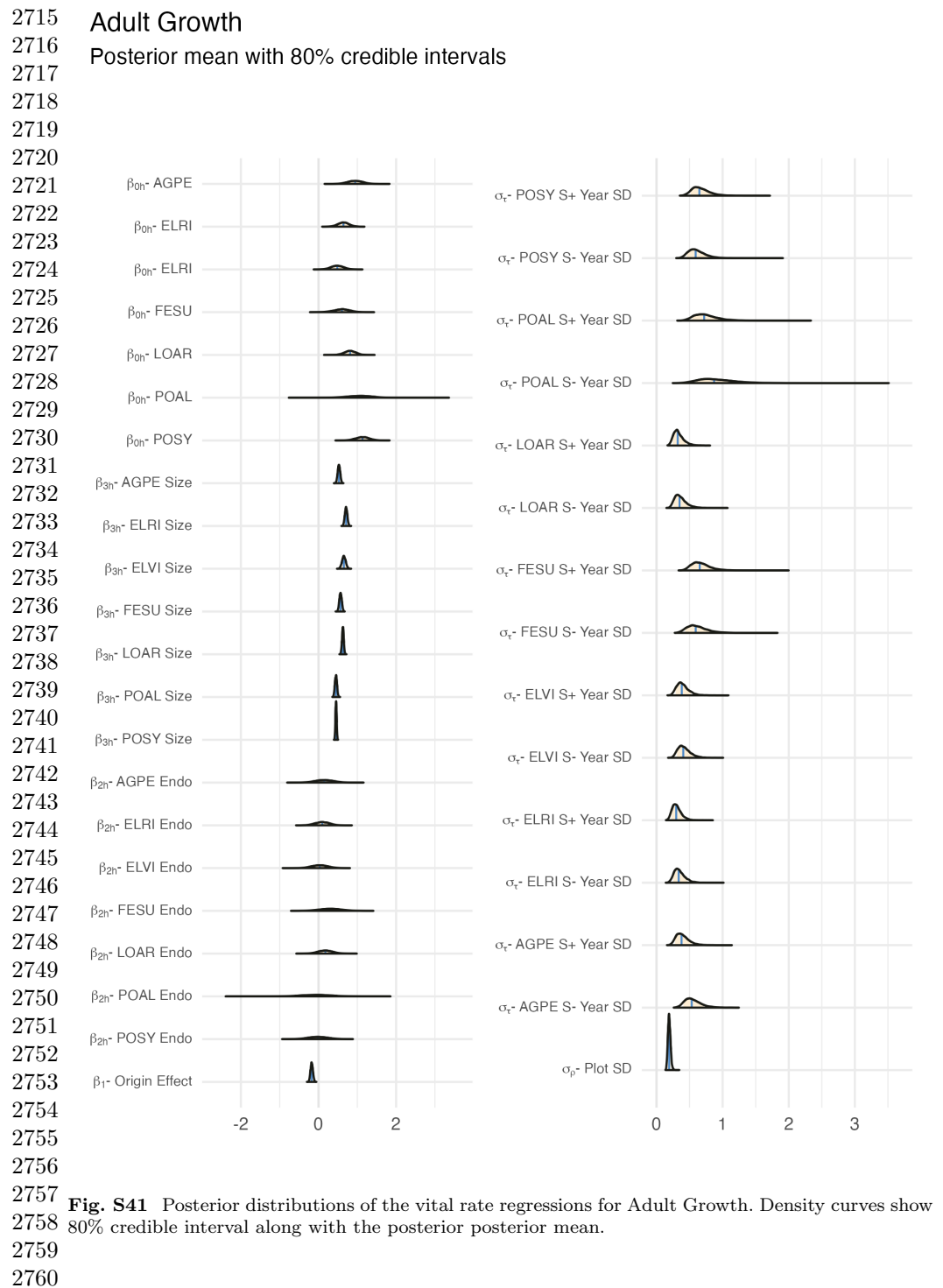


Fig. S40 Posterior distributions of the vital rate regressions for Seedling Survival. Density curves show 80% credible interval along with the posterior posterior mean.



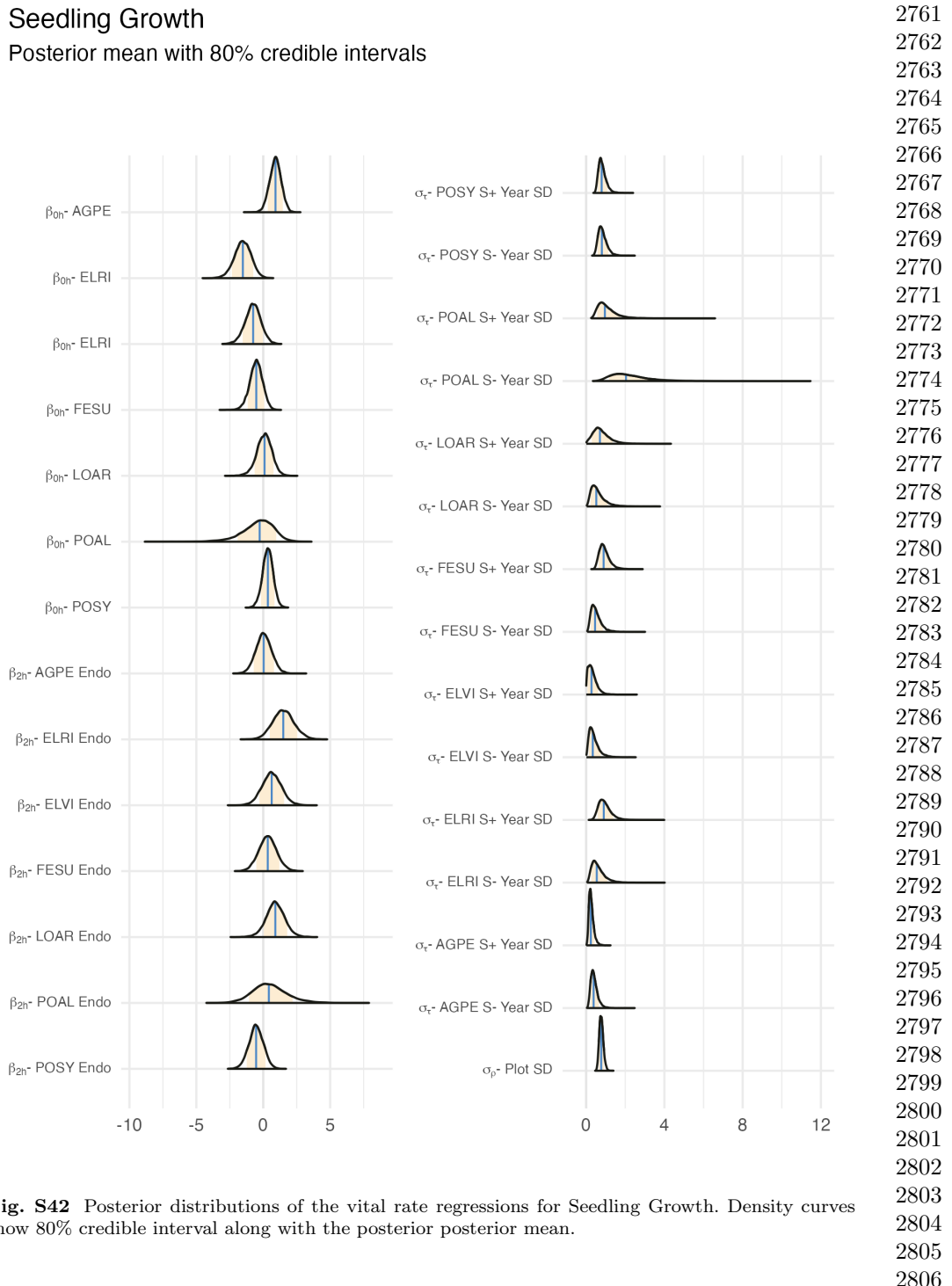
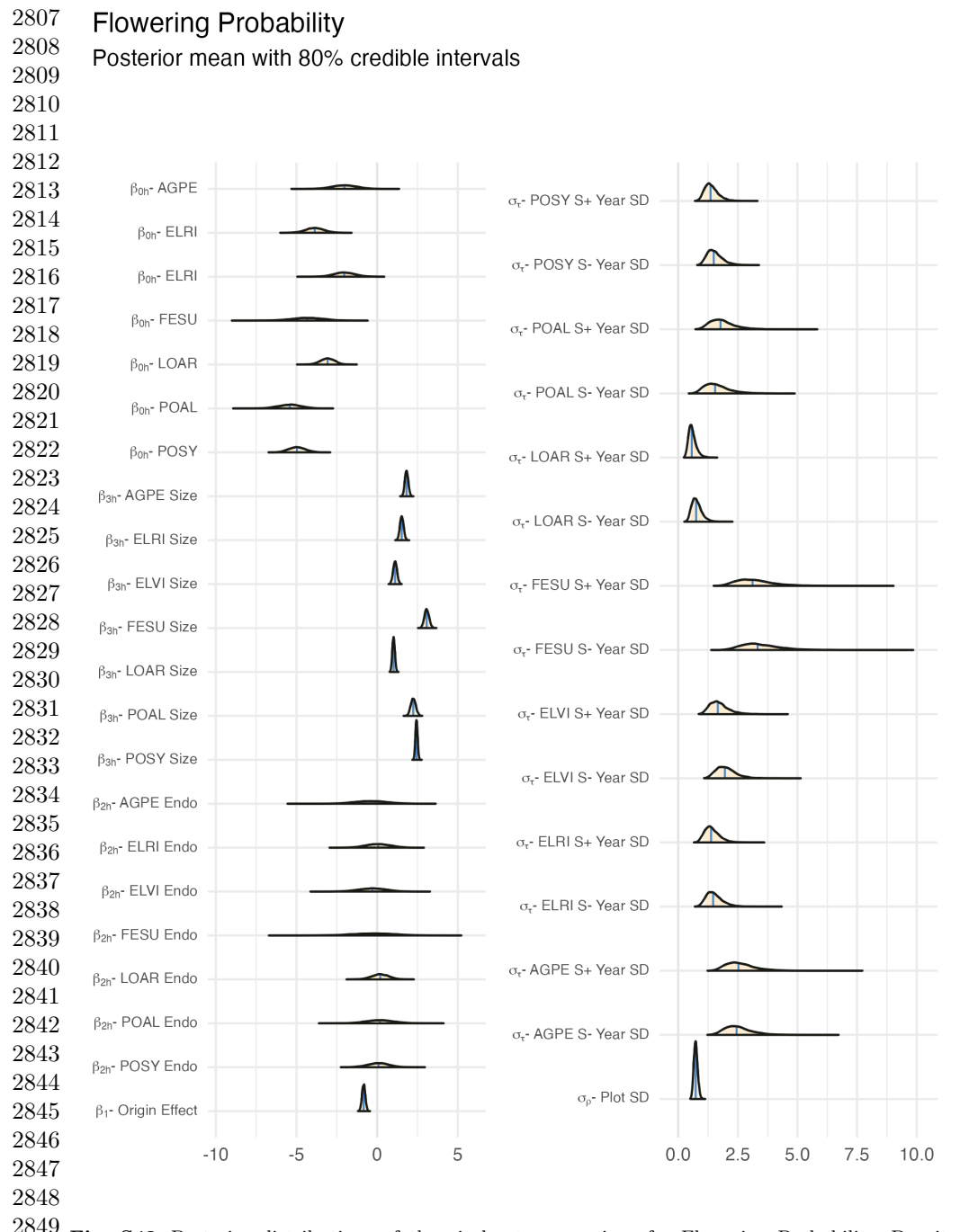


Fig. S42 Posterior distributions of the vital rate regressions for Seedling Growth. Density curves show 80% credible interval along with the posterior posterior mean.



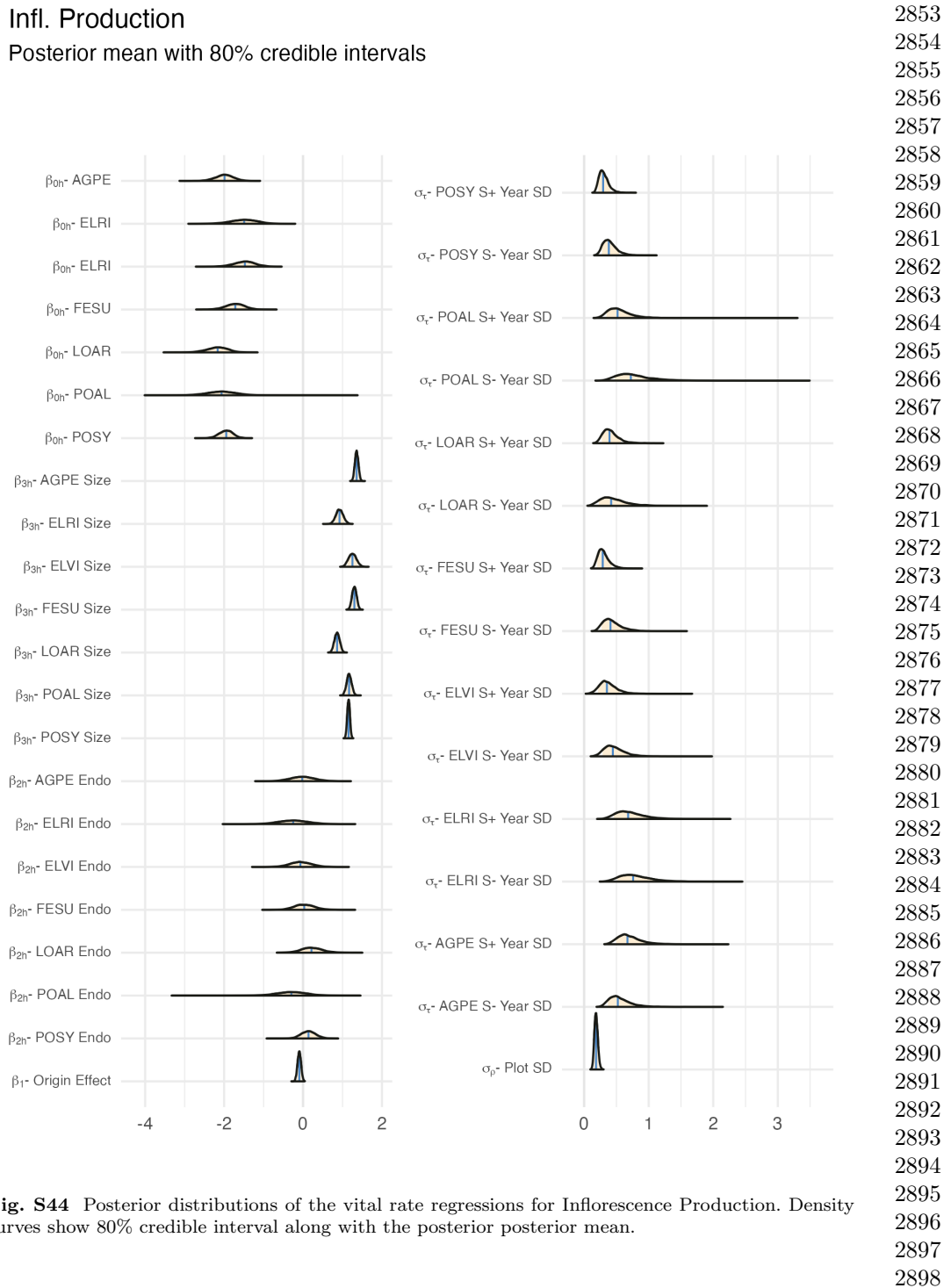
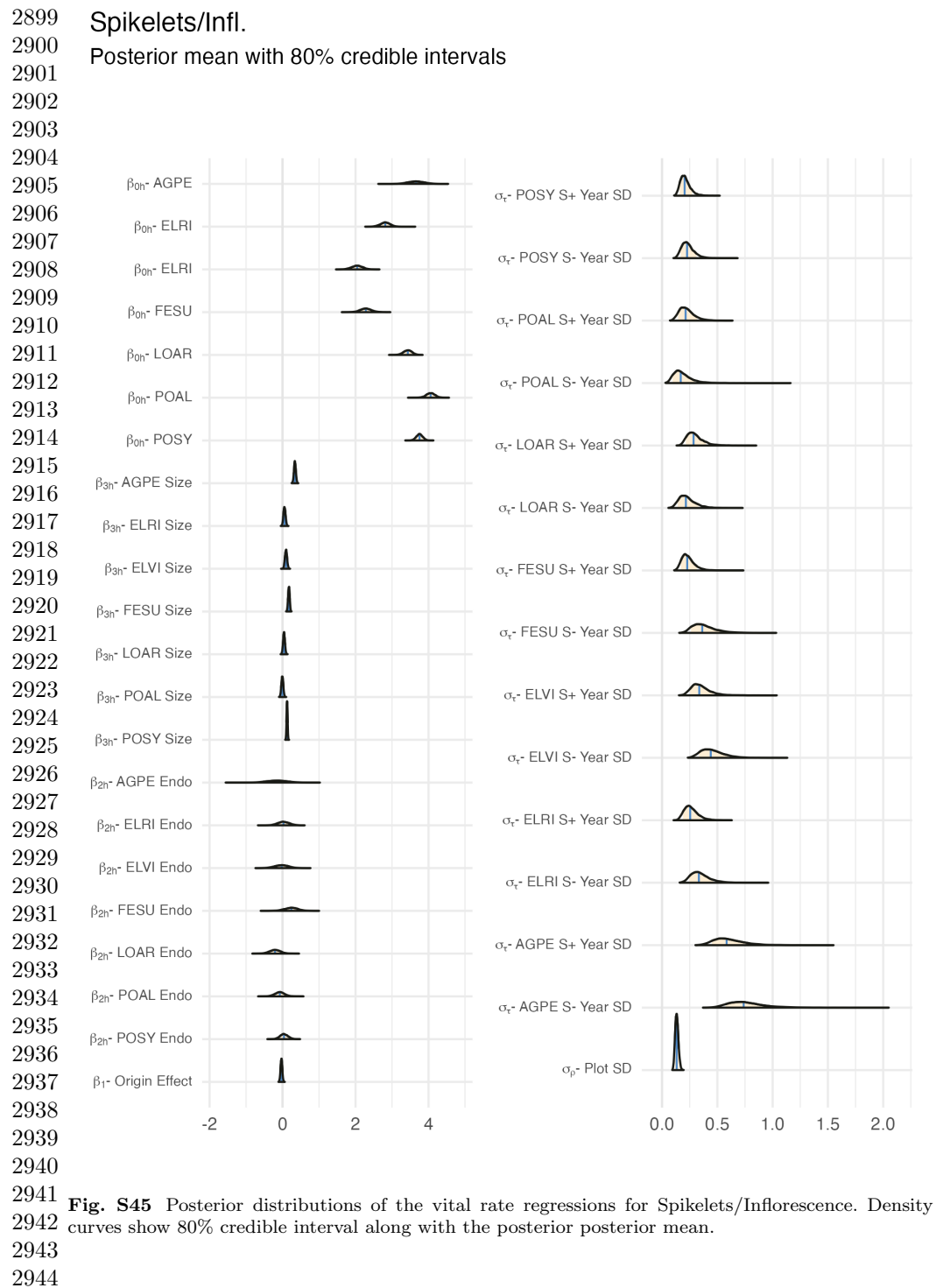


Fig. S44 Posterior distributions of the vital rate regressions for Inflorescence Production. Density curves show 80% credible interval along with the posterior posterior mean.



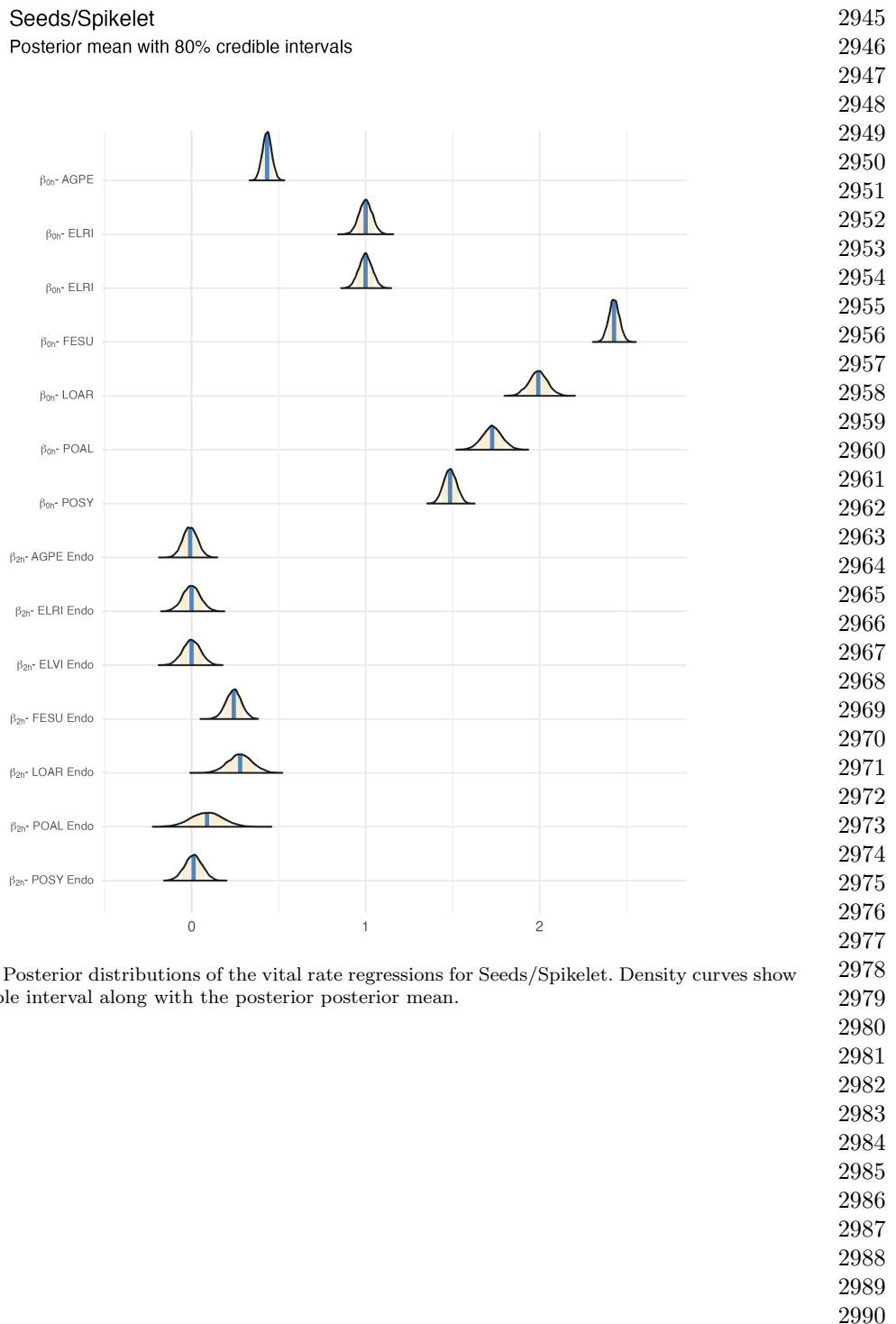
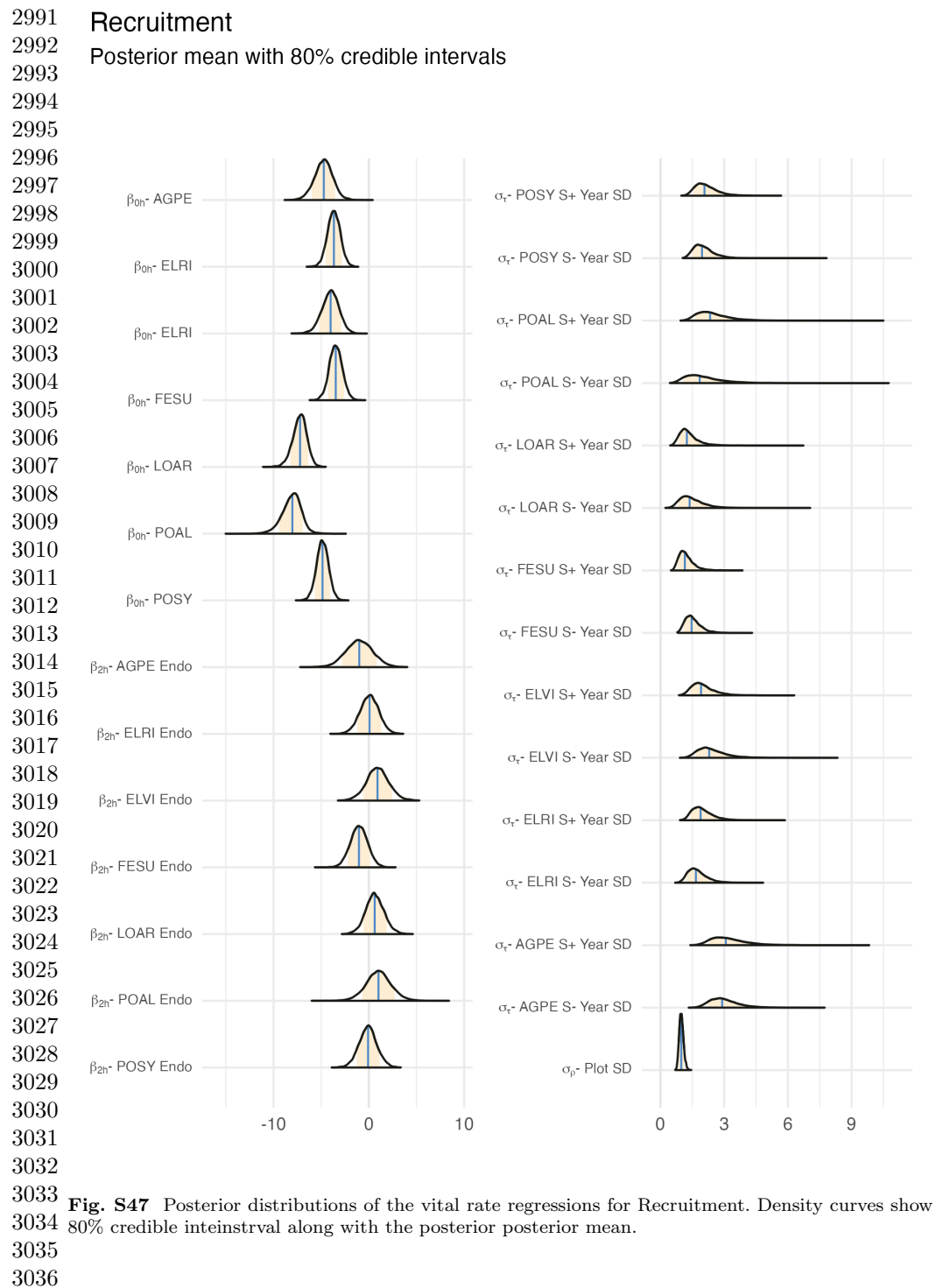
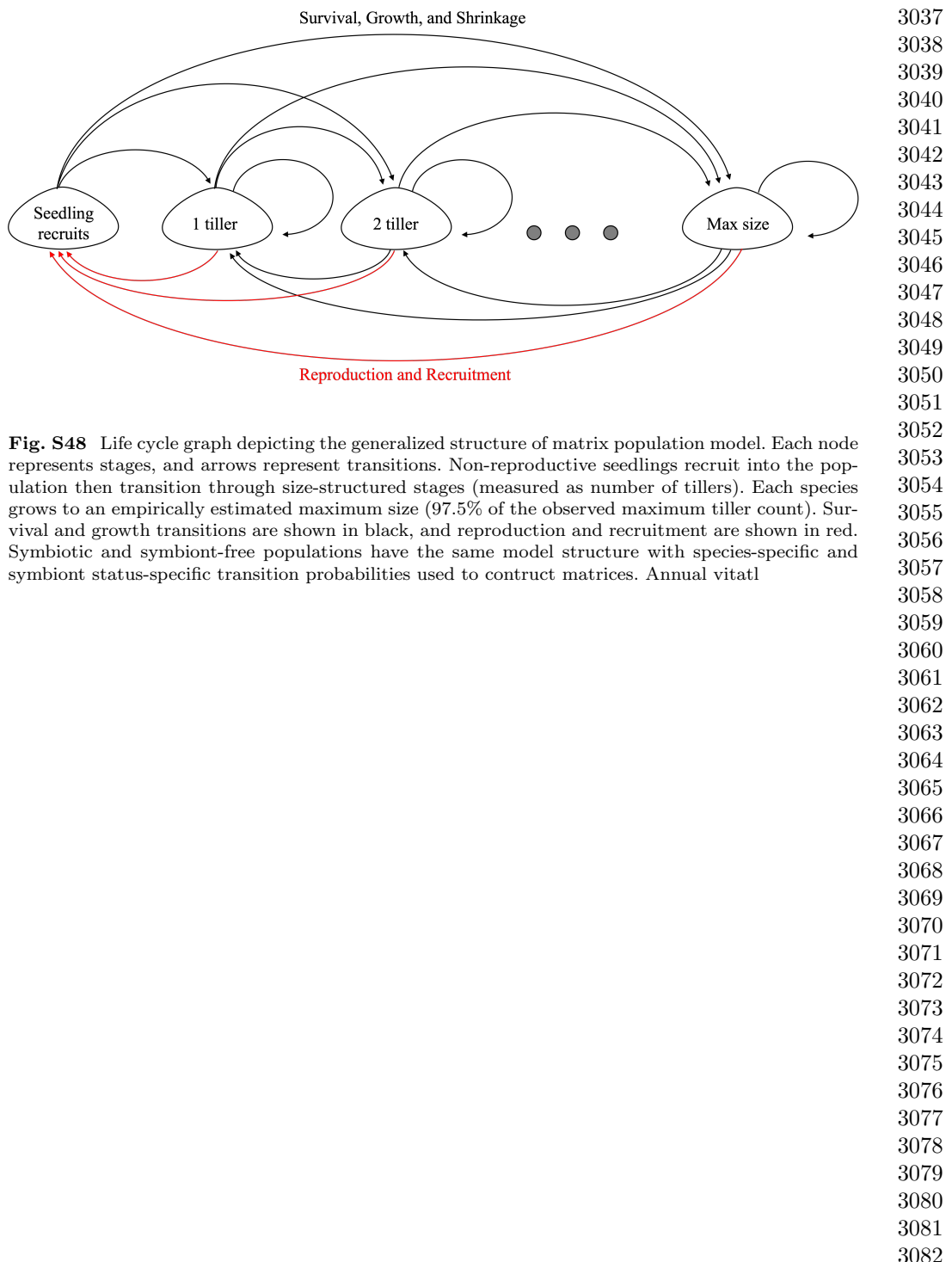
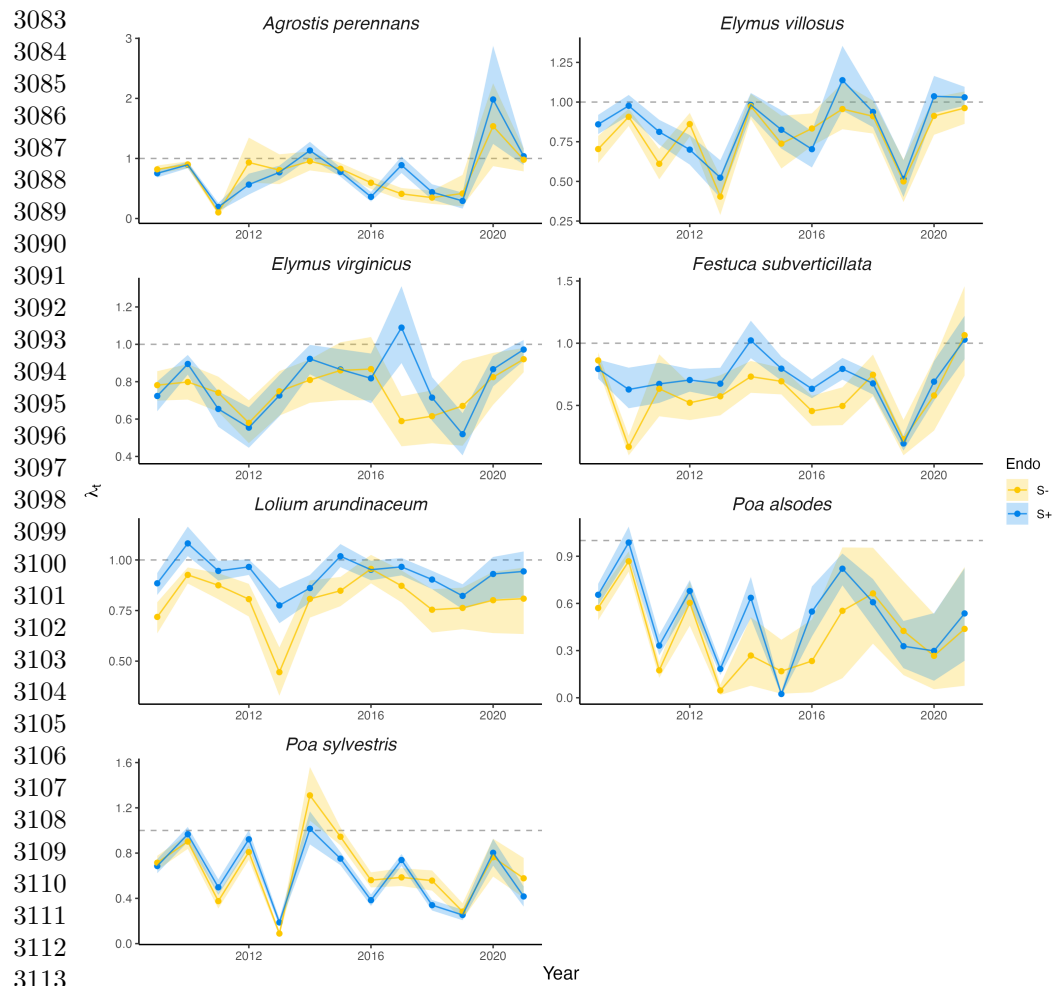


Fig. S46 Posterior distributions of the vital rate regressions for Seeds/Spikelet. Density curves show 80% credible interval along with the posterior posterior mean.



3033 Fig. S47 Posterior distributions of the vital rate regressions for Recruitment. Density curves show
 3034 80% credible interval along with the posterior mean.
 3035
 3036





3115 **Fig. S49** Annual growth rate values (λ_t) over thirteen years. Mean values for symbiotic (blue) and
 3116 symbiont-free (yellow) population growth rates are shown along with 80% credible intervals. Dashed
 3117 line at ($\lambda_t = 1$) indicates stable population growth rate. All values are calculated from matrix models
 representing recruit plants.

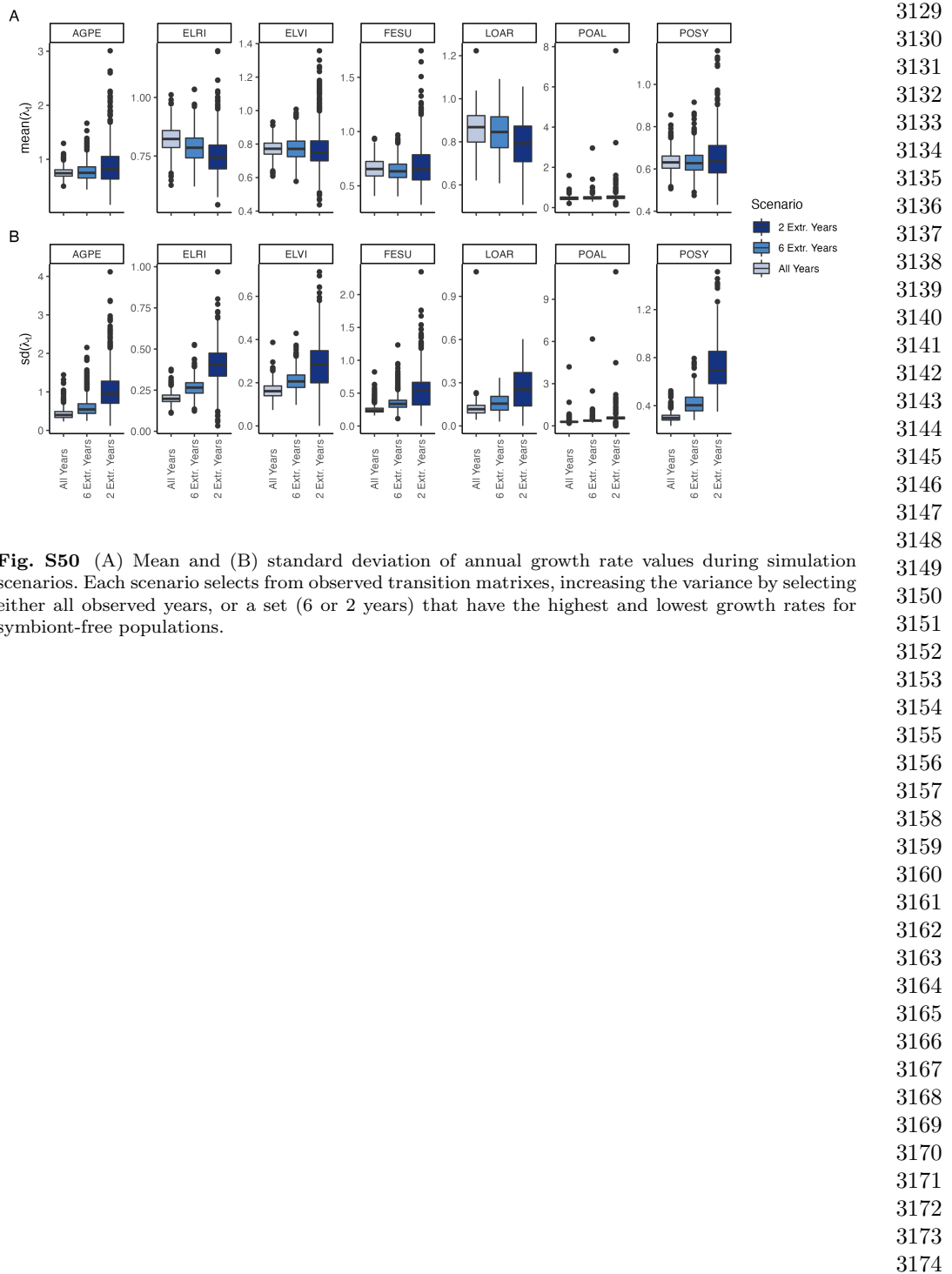


Fig. S50 (A) Mean and (B) standard deviation of annual growth rate values during simulation scenarios. Each scenario selects from observed transition matrixes, increasing the variance by selecting either all observed years, or a set (6 or 2 years) that have the highest and lowest growth rates for symbiont-free populations.

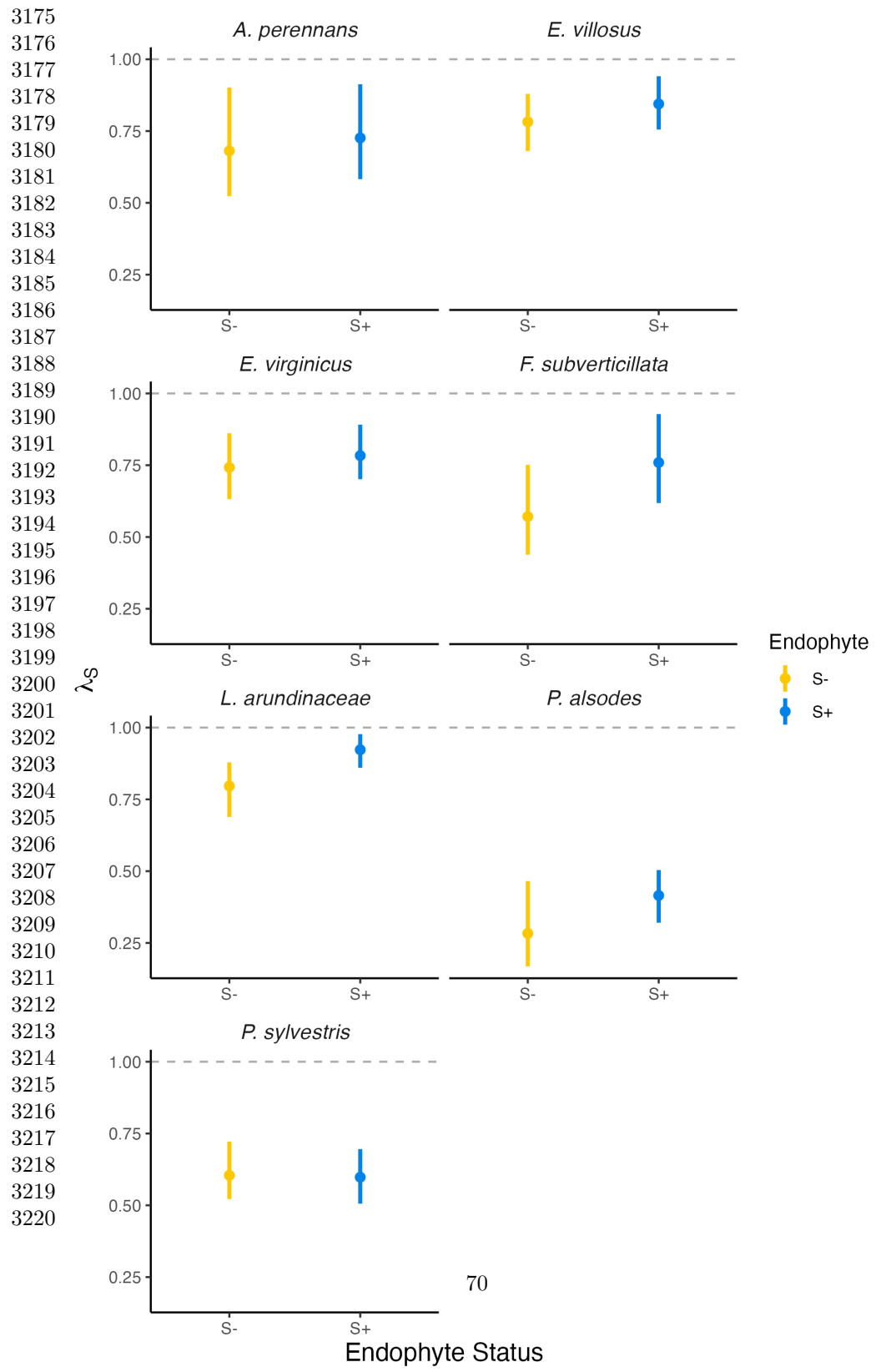
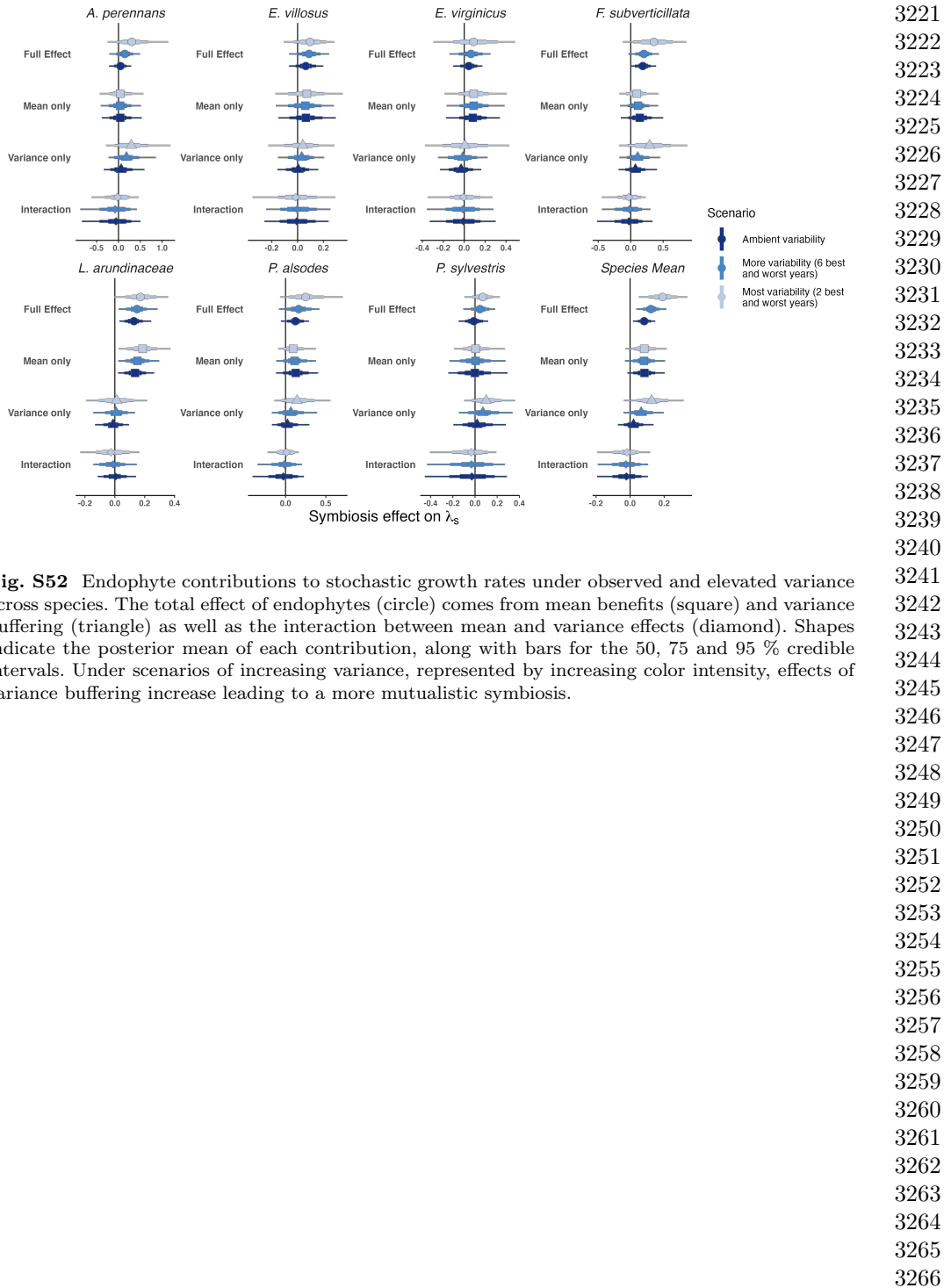
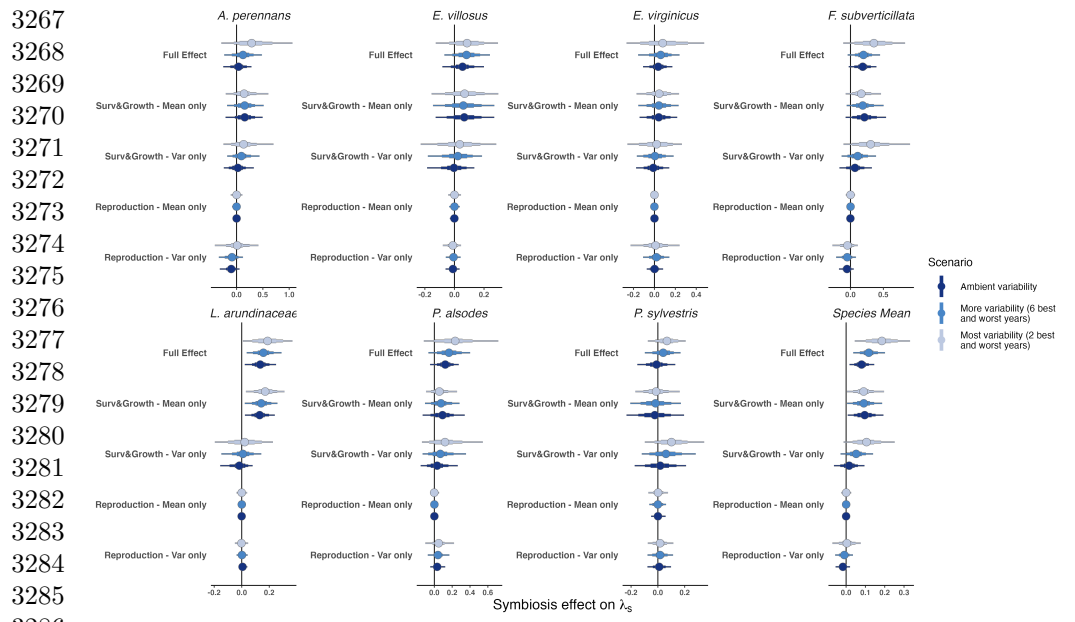


Fig. S51 Stochastic population growth rates (λ_s) for symbiotic (blue) and symbiont-free (yellow) populations. Points show posterior medians along with the 95% credible interval 50% and posterior medians. All values are calculated from matrix models representing recruit plants.





Endophyte Status Checks

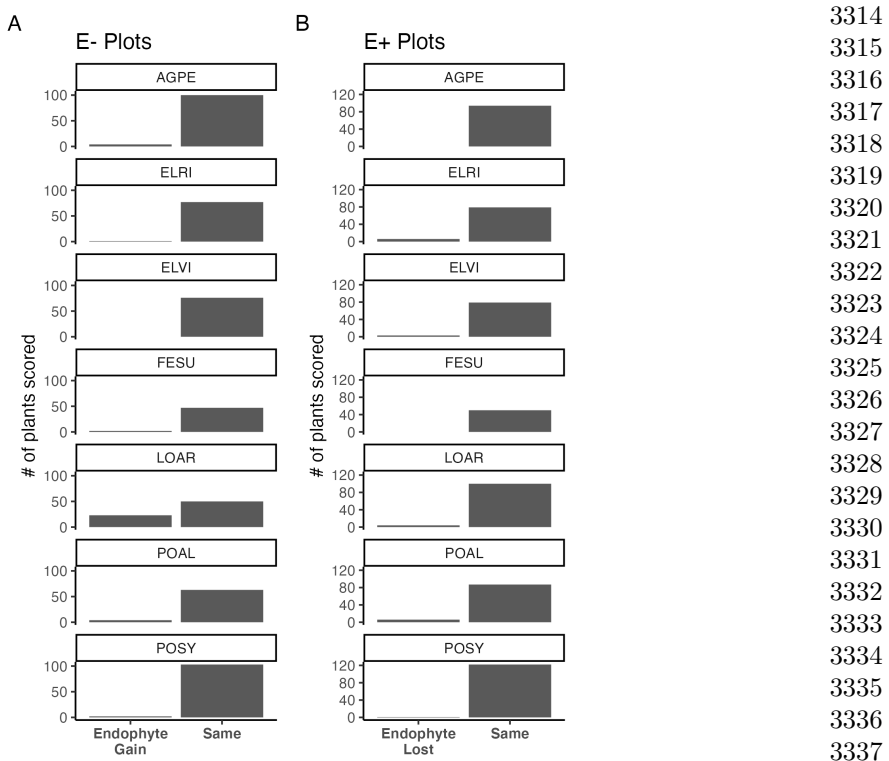
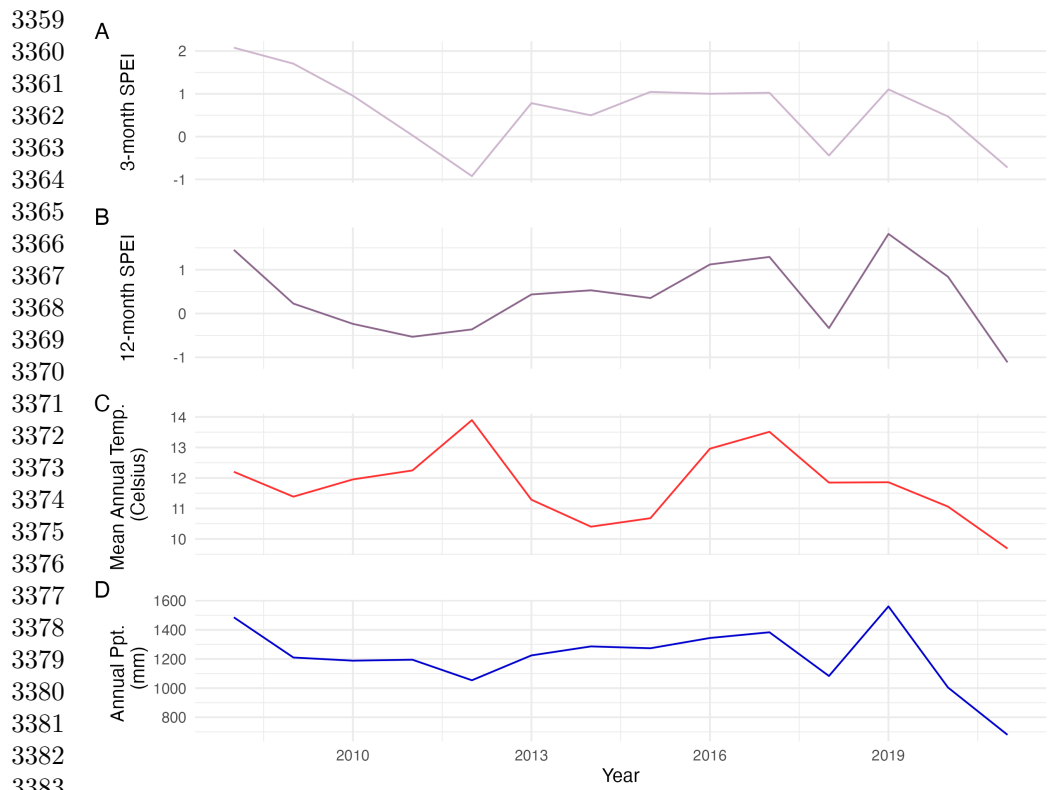


Fig. S54 Faithfulness of experimental plots to assigned endophyte status. Counts of plants scored with leaf peels or seed squashes to check the faithfulness of recruits to the assigned plot-level endophyte status. (A) Endophytic plants may be gained in initially S- plots, or (B) lost in initially S+ plots.



3385 **Fig. S55** Weather station time-series for Bloomington, IN. The Seasonal Precipitation-
 3386 Evapotranspiration Index (SPEI) calculated for the (A) three month growing season and (B) annually
 3387 from daily weather station observations of (C) average temperatures and (D) cumulative precipitation.
 3388 Climatic data shown are determined by the census year centered on the month of July.
 3389
 3390
 3391
 3392
 3393
 3394
 3395
 3396
 3397
 3398
 3399
 3400
 3401
 3402
 3403
 3404

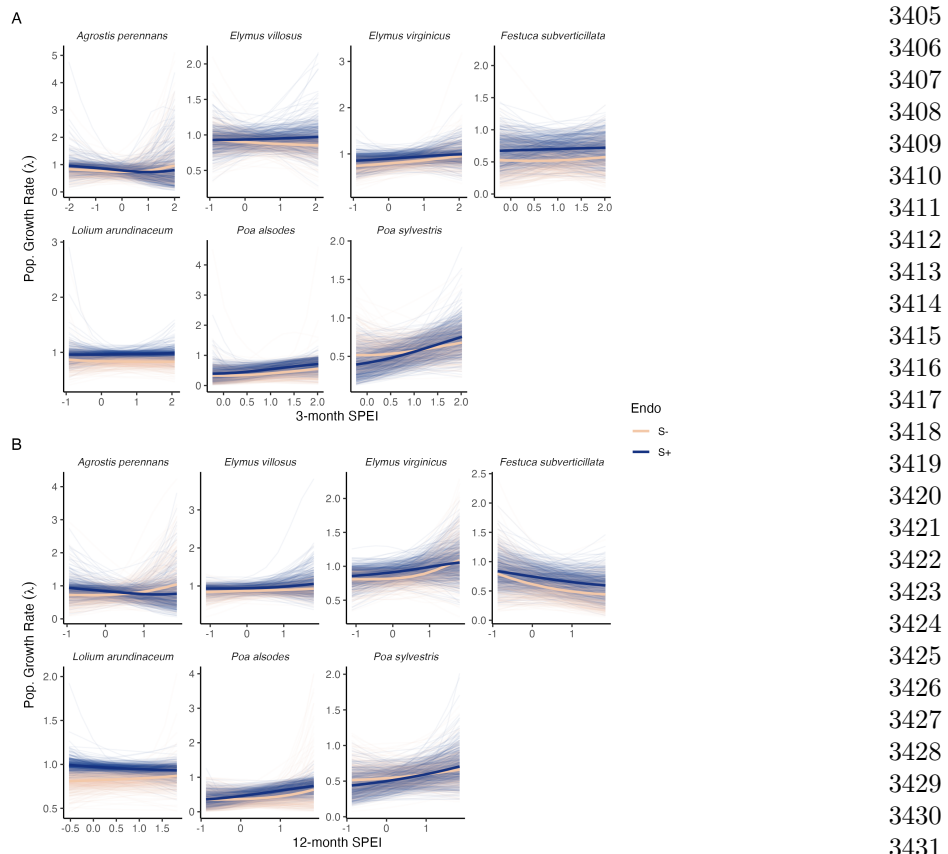


Fig. S56 Predicted population growth rates across drought indices. Symbiotic (S+; blue) and symbiont-free (S-; tan) populations respond differently to climate as measured by the (A) 3-month SPEI and (B) 12-month SPEI. Thick lines represent the predicted mean growth rate and thin lines show 500 posterior draws.

3405
3406
3407
3408
3409
3410
3411
3412
3413
3414
3415
3416
3417
3418
3419
3420
3421
3422
3423
3424
3425
3426
3427
3428
3429
3430
3431
3432
3433
3434
3435
3436
3437
3438
3439
3440
3441
3442
3443
3444
3445
3446
3447
3448
3449
3450

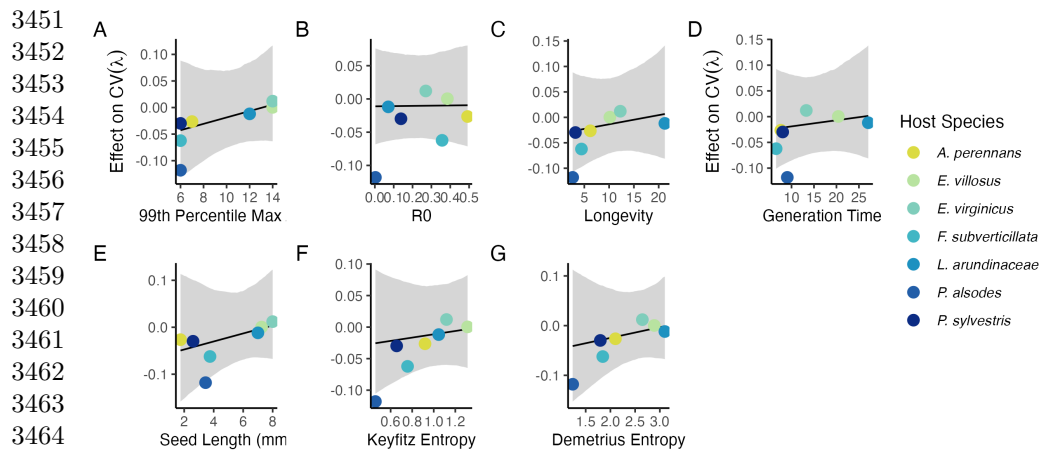


Fig. S57 Relationship between variance buffering and life history traits describing the fast-slow life history continuum accounting for phylogenetic covariance between grass host species. Regressions between life history traits describing the fast-slow life history continuum ((A) 99th percentile maximum age observed during long term censuses in years; (B) Net reproductive rate; (C) Longevity; (D) Generation time in years; (G) Seed size) and the effect of endophyte symbiosis on the coefficient of variation in population growth rate (λ). Each panel shows the fitted mean relationship (line) along with the 95% credible interval.

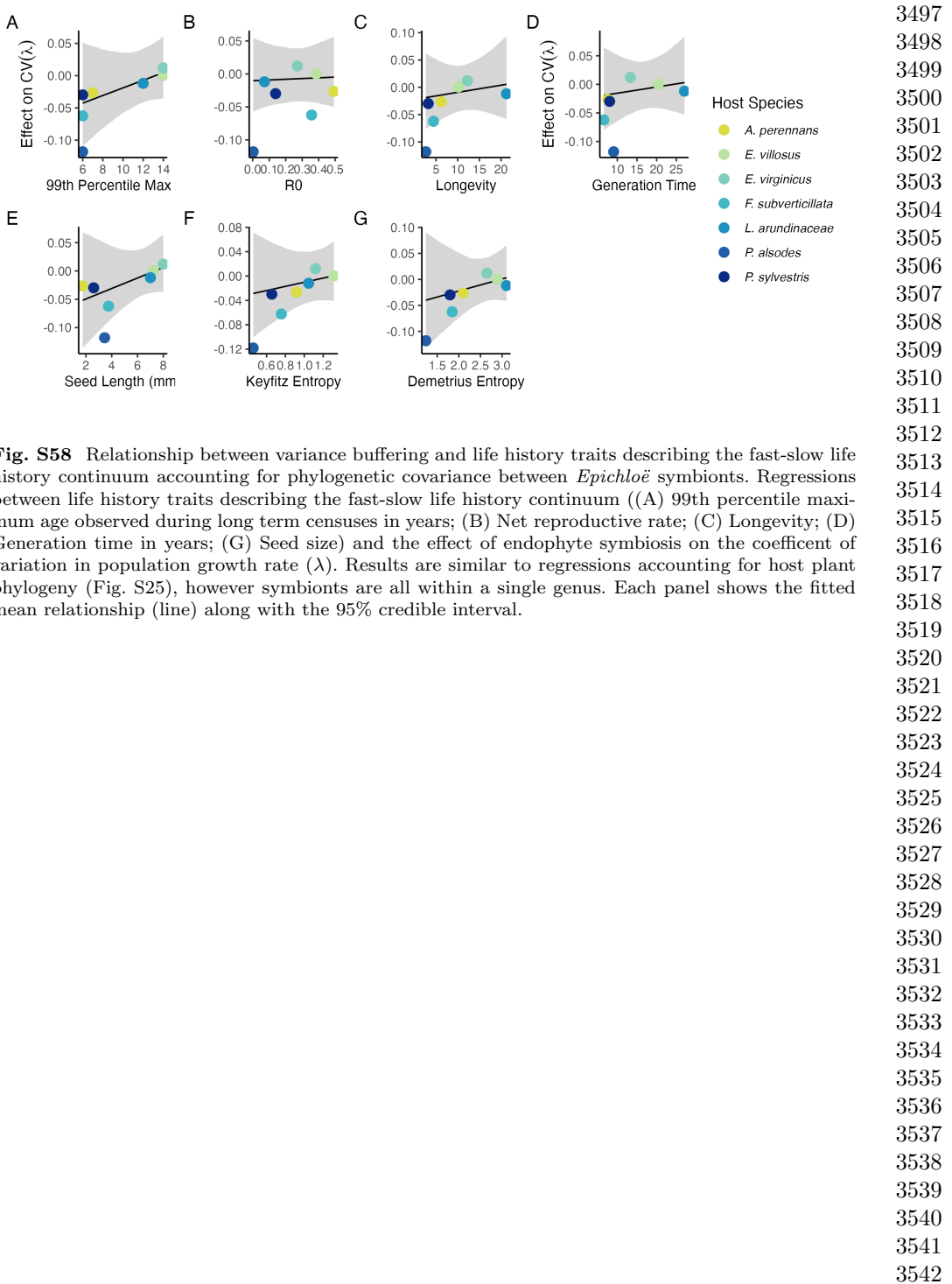
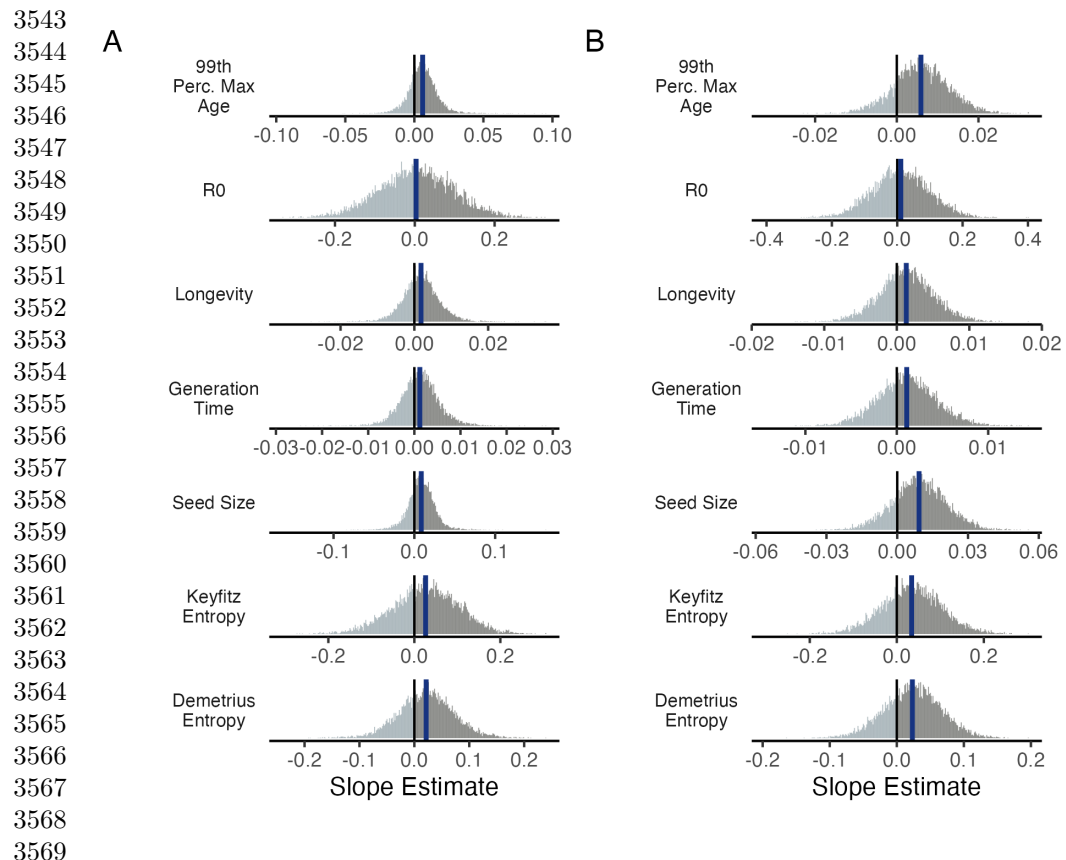
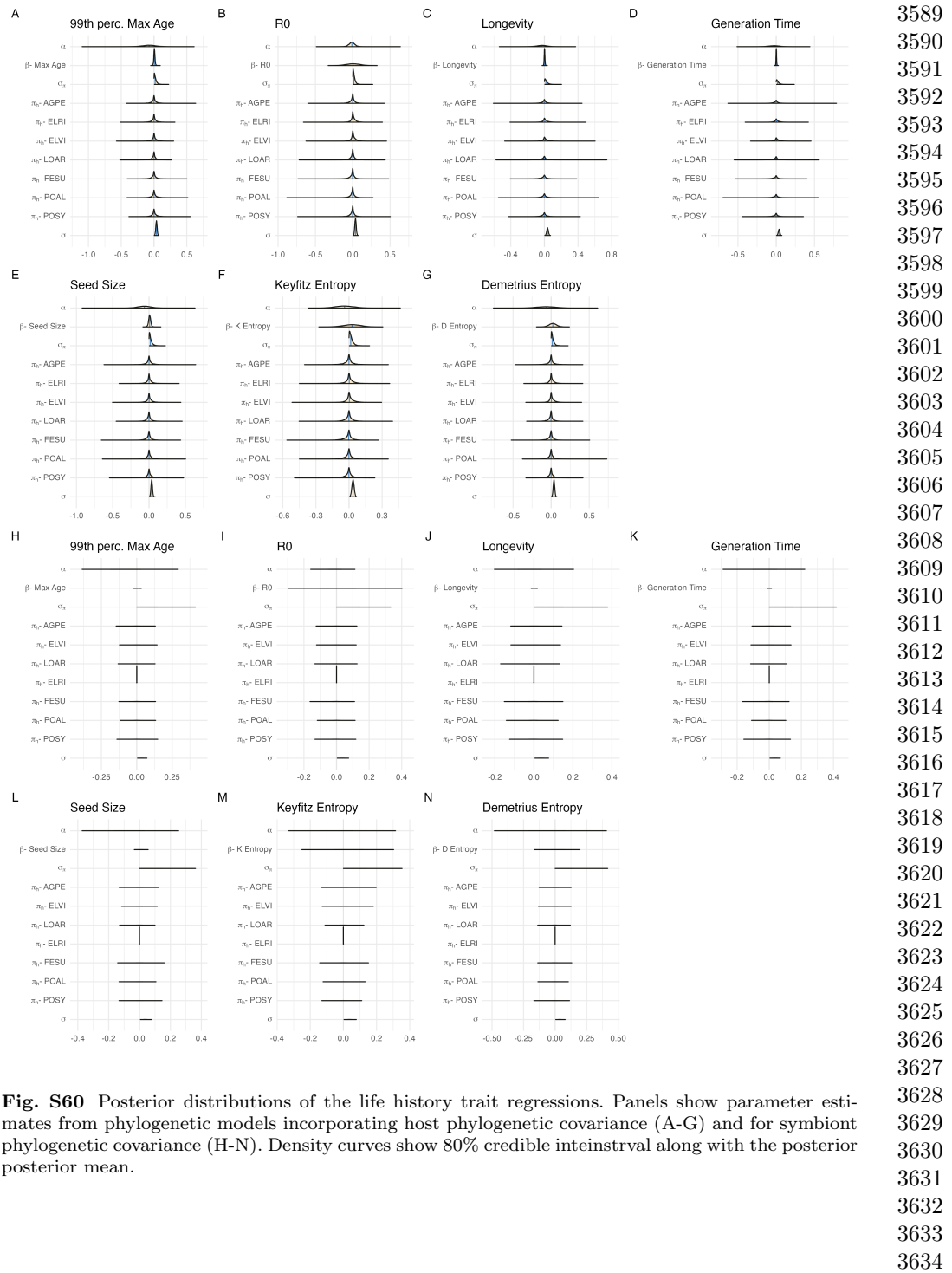


Fig. S58 Relationship between variance buffering and life history traits describing the fast-slow life history continuum accounting for phylogenetic covariance between *Epichloë* symbionts. Regressions between life history traits describing the fast-slow life history continuum ((A) 99th percentile maximum age observed during long term censuses in years; (B) Net reproductive rate; (C) Longevity; (D) Generation time in years; (G) Seed size) and the effect of endophyte symbiosis on the coefficient of variation in population growth rate (λ). Results are similar to regressions accounting for host plant phylogeny (Fig. S25), however symbionts are all within a single genus. Each panel shows the fitted mean relationship (line) along with the 95% credible interval.



3570 **Fig. S59** Posterior estimates of life history trait effects on variance buffering. Grey histograms
3571 show the posterior distribution of the slope parameter from models incorporating (A) host plant
3572 phylogenetic covariance and (B) symbiont phylogenetic covariance for each life history trait with blue
3573 bars showing the posterior mean.

3573
3574
3575
3576
3577
3578
3579
3580
3581
3582
3583
3584
3585
3586
3587
3588



3635 Supplemental Tables S1-S3

3636

3637

3638

3639

3640

3641

3642

3643

3644

3645

3646

3647

3648

3649

3650

3651

3652

3653

3654

3655

3656

3657

3658

3659

3660

3661

3662

3663

3664

3665

3666

3667

3668

3669

3670

3671

3672

3673

3674

3675

3676

3677

3678

3679

3680

Table S1 Summary of host-endophyte propagule and transplant methods

Host Species	Symbiont Species	Heat treatment duration (Temp.)	Transplant date
<i>Agrostis perennans</i>	<i>E. amarillans</i>	12 min. hot water bath (60 °C)	April 2008 (10 plots)
<i>Elymus villosus</i>	<i>E. elymi</i>	6 days drying oven (60 °C)	April 2008 (10 plots)
<i>Elymus virginicus</i>	<i>E. elymi</i> or <i>EviTG-1</i>	6 days drying oven (60 °C)	April 2008 (10 plots)
<i>Festuca subverticillata</i>	<i>E. starrii</i>	6 days drying oven (60 °C)	April 2008 (10 plots)
<i>Lolium arundinaceum</i>	<i>E. coenophiala</i>	6 days drying oven (60 °C)	Sept. 2007 (10 plots)
<i>Poa alsodes</i>	<i>E. alsodes</i>	7 days drying oven (60 °C)	Sept. 2007 (8 plots)/April 2008 (10 plots)
<i>Poa sylvestris</i>	<i>E. PsyTG-1</i>	7 days drying oven (60 °C)	Sept. 2007 (8 plots)/April 2008 (10 plots)
			3681
			3682
			3683
			3684
			3685
			3686
			3687
			3688
			3689
			3690
			3691
			3692
			3693
			3694
			3695
			3696
			3697
			3698
			3699
			3700
			3701
			3702
			3703
			3704
			3705
			3706
			3707
			3708
			3709
			3710
			3711
			3712
			3713
			3714
			3715
			3716
			3717
			3718
			3719
			3720
			3721
			3722
			3723
			3724
			3725
			3726

3727
 3728
 3729
 3730
 3731
 3732
 3733
 3734
 3735
 3736
 3737
 3738
 3739
 3740
 3741
 3742
 3743
 3744
 3745
 3746
 3747
 3748
 3749
 3750
 3751
 3752
 3753
 3754
 3755
 3756
 3757
 3758
 3759
 3760
 3761
 3762
 3763
 3764
 3765
 3766
 3767
 3768
 3769
 3770
 3771
 3772

Table S2 Summary of focal life history traits

Host Species	Observed max age (years)	99th percentile max age (years)	Generation time (years)	R_0	Longevity (years)	Seed length (mm.)	Keyfitz Entropy	Demetrius Entropy	Imperfect transmission rate (%)	Stromata Observed (% of individ. per species)
<i>Agrostis perennans</i>	11	7	7.6	0.58	6.4	1.75	0.9	2.1	69.8	0.0
<i>Elymus villosus</i>	14	14	20.7	0.35	9.8	7.25	1.3	2.9	100	4.6
<i>Elymus virginicus</i>	14	14	13.4	0.25	12.5	8	1.1	2.6	100	0.6
<i>Festuca subverticillata</i>	9	6	6.6	0.28	4.3	3.75	0.8	1.8	42.7	0.0
<i>Lolium arundinaceum</i>	12*	12*	27.4	0.08	21.3	7	1.1	3.1	100	0.0
<i>Poa alsodes</i>	8	6	9.2	0.003	2.6	3.45	0.5	1.2	99.9	0.0
<i>Poa sylvestris</i>	12	6	8.0	0.14	3.2	2.6	0.7	1.8	16.6	0.1
Page's λ (host)	—	0.27	0.28	0.23	0.28	0.27	0.25	0.25	—	—
Page's λ (symbiont)	—	0.63	0.63	0.63	0.63	0.62	0.62	0.62	—	—

*Censuses for *L. arundinaceum* plots stopped after year 12 of the experiment.

Table S3 Summary of host-endophyte drought sensitivities

Host Species	Effect on CV(λ)	Effect on Mean(λ)	$\frac{\Delta\lambda^-}{\Delta SPEI_3}$	$\frac{\Delta\lambda^+}{\Delta SPEI_3}$	3 month S- to S+ ratio	$\frac{\Delta\lambda^-}{\Delta SPEI_{12}}$	$\frac{\Delta\lambda^+}{\Delta SPEI_{12}}$	12 month S- to S+ ratio
<i>Agrostis perennans</i>	-0.0264	0.0441	0.03	-0.04	0.85	0.11	-0.06	1.82
<i>Elymus villosus</i>	0.0003	0.0509	-0.03	0.01	1.95	0.03	0.04	0.70
<i>Elymus virginicus</i>	0.0120	0.0578	0.07	0.05	1.50	0.10	0.07	1.42
<i>Festuca subverticillata</i>	-0.0622	0.1639	0.02	0.02	1.01	-0.13	-0.09	1.43
<i>Lolium arundinaceum</i>	-0.0118	0.1022	-0.01	0.01	1.32	0.03	-0.03	1.02
<i>Poa alsodes</i>	-0.1179	0.1282	0.10	0.14	0.71	0.11	0.14	0.73
<i>Poa sylvestris</i>	-0.0298	-0.0085	0.07	0.16	0.44	0.05	0.10	0.55
								3773
								3774
								3775
								3776
								3777
								3778
								3779
								3780
								3781
								3782
								3783
								3784
								3785
								3786
								3787
								3788
								3789
								3790
								3791
								3792
								3793
								3794
								3795
								3796
								3797
								3798
								3799
								3800
								3801
								3802
								3803
								3804
								3805
								3806
								3807
								3808
								3809
								3810
								3811
								3812
								3813
								3814
								3815
								3816
								3817
								3818

3819 **References**

- 3820 [1] Seneviratne, S. *et al.* *Changes in climate extremes and their impacts on the*
3821 *natural physical environment* (Cambridge University Press, 2012).
- 3822 [2] Bathiany, S., Dakos, V., Scheffer, M. & Lenton, T. M. Climate models predict
3823 increasing temperature variability in poor countries. *Science advances* **4**, eaar5809
3824 (2018).
- 3825 [3] IPCC. Climate change 2021: The physical science basis (2021). URL <https://www.ipcc.ch/report/ar6/wg1/>.
- 3826 [4] Clark, J. S. Why environmental scientists are becoming bayesians. *Ecology letters*
3827 **8**, 2–14 (2005).
- 3828 [5] Lewontin, R. C. & Cohen, D. On Population Growth in a Randomly Varying Envi-
3829 ronment. *Proceedings of the National Academy of Sciences* **62**, 1056–1060 (1969).
3830 URL <https://www.pnas.org/content/62/4/1056>. Publisher: National Academy of
3831 Sciences Section: Biological Sciences: Zoology.
- 3832 [6] Tuljapurkar, S. D. Population dynamics in variable environments. III. Evolution-
3833 ary dynamics of r-selection. *Theoretical Population Biology* **21**, 141–165 (1982).
3834 URL <http://www.sciencedirect.com/science/article/pii/0040580982900107>.
- 3835 [7] Cohen, J. E. Comparative statics and stochastic dynamics of age-structured
3836 populations. *Theoretical population biology* **16**, 159–171 (1979).
- 3837 [8] Tuljapurkar, S. *Population dynamics in variable environments* Vol. 85 (Springer
3838 Science & Business Media, 2013).
- 3839 [9] Pfister, C. A. Patterns of variance in stage-structured populations: evolutionary
3840 predictions and ecological implications. *Proceedings of the National Academy of
3841 Sciences* **95**, 213–218 (1998).
- 3842 [10] Compagnoni, A. *et al.* The effect of demographic correlations on the stochastic
3843 population dynamics of perennial plants. *Ecological Monographs* **86**, 480–494
3844 (2016).
- 3845 [11] Ellis, M. M. & Crone, E. E. The role of transient dynamics in stochastic
3846 population growth for nine perennial plants. *Ecology* **94**, 1681–1686 (2013).
- 3847 [12] Murphy, G. I. Pattern in life history and the environment. *The American
3848 Naturalist* **102**, 391–403 (1968).
- 3849 [13] Davison, R., Stadman, M. & Jongejans, E. Stochastic effects contribute to
3850 population fitness differences. *Ecological Modelling* **408**, 108760 (2019).
- 3851
- 3852
- 3853
- 3854
- 3855
- 3856
- 3857
- 3858
- 3859
- 3860
- 3861
- 3862
- 3863
- 3864

- [14] Compagnoni, A. *et al.* Herbaceous perennial plants with short generation time have stronger responses to climate anomalies than those with longer generation time. *Nature communications* **12**, 1–8 (2021). 3865
3866
3867
3868
- [15] Le Coeur, C., Yoccoz, N. G., Salguero-Gómez, R. & Vindenes, Y. Life history adaptations to fluctuating environments: Combined effects of demographic buffering and lability. *Ecology Letters* **25**, 2107–2119 (2022). 3869
3870
3871
3872
- [16] Morris, W. F. *et al.* Longevity can buffer plant and animal populations against changing climatic variability. *Ecology* **89**, 19–25 (2008). 3873
3874
- [17] Rodríguez-Caro, R. C. *et al.* The limits of demographic buffering in coping with environmental variation. *Oikos* **130**, 1346–1358 (2021). 3875
3876
3877
- [18] Tuljapurkar, S. & Orzack, S. H. Population dynamics in variable environments i. long-run growth rates and extinction. *Theoretical Population Biology* **18**, 314–342 (1980). 3878
3879
3880
3881
- [19] Fieberg, J. & Ellner, S. P. Stochastic matrix models for conservation and management: a comparative review of methods. *Ecology letters* **4**, 244–266 (2001). 3882
3883
3884
- [20] Menges, E. S. Applications of population viability analyses in plant conservation. *Ecological Bulletins* 73–84 (2000). 3885
3886
3887
- [21] Kuparinen, A., Boit, A., Valdovinos, F. S., Lassaux, H. & Martinez, N. D. Fishing-induced life-history changes degrade and destabilize harvested ecosystems. *Scientific reports* **6**, 22245 (2016). 3888
3889
3890
3891
- [22] Hilde, C. H. *et al.* The Demographic Buffering Hypothesis: Evidence and Challenges. *Trends in Ecology & Evolution* **0** (2020). URL [https://www.cell.com/trends/ecology-evolution/abstract/S0169-5347\(20\)30050-1](https://www.cell.com/trends/ecology-evolution/abstract/S0169-5347(20)30050-1). Publisher: Elsevier. 3892
3893
3894
- [23] Dybala, K. E., Gardali, T. & Eadie, J. M. Dependent vs. independent juvenile survival: contrasting drivers of variation and the buffering effect of parental care. *Ecology* **94**, 1584–1593 (2013). 3895
3896
3897
3898
- [24] Colchero, F., Eckardt, W. & Stoinski, T. Evidence of demographic buffering in an endangered great ape: Social buffering on immature survival and the role of refined sex-age classes on population growth rate. *Journal of Animal Ecology* **90**, 1701–1713 (2021). 3899
3900
3901
3902
3903
- [25] Rodriguez, R., White Jr, J., Arnold, A. E. & Redman, a. R. a. Fungal endophytes: diversity and functional roles. *New phytologist* **182**, 314–330 (2009). 3904
3905
3906
- [26] McFall-Ngai, M. *et al.* Animals in a bacterial world, a new imperative for the life sciences. *Proceedings of the National Academy of Sciences* **110**, 3229–3236 (2013). 3907
3908
3909
3910

- 3911 [27] Funkhouser, L. J. & Bordenstein, S. R. Mom knows best: the universality of
3912 maternal microbial transmission. *PLoS biology* **11**, e1001631 (2013).
- 3913
- 3914 [28] Fine, P. E. Vectors and vertical transmission: an epidemiologic perspective.
3915 *Annals of the New York Academy of Sciences* **266**, 173–194 (1975).
- 3916
- 3917 [29] Russell, J. A. & Moran, N. A. Costs and benefits of symbiont infection in aphids:
3918 variation among symbionts and across temperatures. *Proceedings of the Royal
3919 Society B: Biological Sciences* **273**, 603–610 (2006).
- 3920
- 3921 [30] Kivlin, S. N., Emery, S. M. & Rudgers, J. A. Fungal symbionts alter plant
3922 responses to global change. *American Journal of Botany* **100**, 1445–1457 (2013).
- 3923
- 3924 [31] Dunbar, H. E., Wilson, A. C. C., Ferguson, N. R. & Moran, N. A. Aphid thermal
3925 tolerance is governed by a point mutation in bacterial symbionts. *PLoS biology*
3926 **5**, e96 (2007).
- 3927
- 3928 [32] Reyna, R., Cooke, P., Grum, D., Cook, D. & Creamer, R. Detection and local-
3929 ization of the endophyte *undifilum oxytropis* in locoweed tissues. *Botany* **90**,
3930 1229–1236 (2012).
- 3931
- 3932 [33] Saikkonen, K., Gundel, P. E. & Helander, M. Chemical ecology mediated by
3933 fungal endophytes in grasses. *Journal of chemical ecology* **39**, 962–968 (2013).
- 3934
- 3935 [34] Neyaz, M., Gardner, D. R., Creamer, R. & Cook, D. Localization of the
3936 swainsonine-producing chaetothyriales symbiont in the seed and shoot apical
3937 meristem in its host *ipomoea carnea*. *Microorganisms* **10**, 545 (2022).
- 3938
- 3939 [35] Chamberlain, S. A., Bronstein, J. L. & Rudgers, J. A. How context dependent
3940 are species interactions? *Ecology letters* **17**, 881–890 (2014).
- 3941
- 3942 [36] Catford, J. A., Wilson, J. R., Pyšek, P., Hulme, P. E. & Duncan, R. P. Address-
3943 ing context dependence in ecology. *Trends in Ecology & Evolution* **37**, 158–170
3944 (2022).
- 3945
- 3946 [37] Jordano, P. Spatial and temporal variation in the avian-frugivore assemblage of
3947 *prunus mahaleb*: patterns and consequences. *Oikos* 479–491 (1994).
- 3948
- 3949 [38] Leuchtmann, A. Systematics, distribution, and host specificity of grass endo-
3950 phytes. *Natural toxins* **1**, 150–162 (1992).
- 3951
- 3952 [39] Cheplick, G. P., Faeth, S. & Faeth, S. H. *Ecology and evolution of the grass-*
3953 *endophyte symbiosis* (OUP USA, 2009).
- 3954
- 3955 [40] Brem, D. & Leuchtmann, A. Epichloë grass endophytes increase herbivore resis-
3956 tance in the woodland grass *brachypodium sylvaticum*. *Oecologia* **126**, 522–530
3957 (2001).

- [41] Decunta, F. A., Pérez, L. I., Malinowski, D. P., Molina-Montenegro, M. A. & Gundel, P. E. A systematic review on the effects of epichloë fungal endophytes on drought tolerance in cool-season grasses. *Frontiers in plant science* **12**, 644731 (2021). 3957
3958
3959
3960
3961
3962
3963
3964
3965
3966
3967
3968
3969
3970
3971
3972
3973
3974
3975
3976
3977
3978
3979
3980
3981
3982
3983
3984
3985
3986
3987
3988
3989
3990
3991
3992
3993
3994
3995
3996
3997
3998
3999
4000
4001
4002
- [42] Bacon, C. W. & White, J. F. in *Stains, media, and procedures for analyzing endophytes* 47–56 (CRC Press, 2018).
- [43] Rudgers, J. A. & Swafford, A. L. Benefits of a fungal endophyte in elymus virginicus decline under drought stress. *Basic and Applied Ecology* **10**, 43–51 (2009).
- [44] Bultman, T. L., White Jr, J. F., Bowdish, T. I., Welch, A. M. & Johnston, J. Mutualistic transfer of epichloë spermatia by phorbis flies. *Mycologia* **87**, 182–189 (1995).
- [45] Stan Development Team. RStan: the R interface to Stan (2022). URL <https://mc-stan.org/>. R package version 2.21.7.
- [46] Elderd, B. D. & Miller, T. E. Quantifying demographic uncertainty: Bayesian methods for integral projection models. *Ecological Monographs* **86**, 125–144 (2016).
- [47] Gabry, J., Simpson, D., Vehtari, A., Betancourt, M. & Gelman, A. Visualization in bayesian workflow. *Journal of the Royal Statistical Society Series A: Statistics in Society* **182**, 389–402 (2019).
- [48] Brooks, S. P. & Gelman, A. General methods for monitoring convergence of iterative simulations. *Journal of computational and graphical statistics* **7**, 434–455 (1998).
- [49] Gelman, A. & Hill, J. *Data analysis using regression and multilevel/hierarchical models* (Cambridge university press, 2006).
- [50] Williams, J. L., Miller, T. E. & Ellner, S. P. Avoiding unintentional eviction from integral projection models. *Ecology* **93**, 2008–2014 (2012).
- [51] Jones, O. R. *et al.* Rcompadre and rage—two r packages to facilitate the use of the compadre and comadre databases and calculation of life-history traits from matrix population models. *Methods in Ecology and Evolution* **13**, 770–781 (2022).
- [52] .
- [53] Bürkner, P.-C. brms: An R package for Bayesian multilevel models using Stan. *Journal of Statistical Software* **80**, 1–28 (2017).
- [54] Zanne, A. E. *et al.* Three keys to the radiation of angiosperms into freezing environments. *Nature* **506**, 89–92 (2014).

- 4003 [55] Leuchtmann, A., Bacon, C. W., Schardl, C. L., White Jr, J. F. & Tadych,
4004 M. Nomenclatural realignment of neotyphodium species with genus epichloë.
4005 *Mycologia* **106**, 202–215 (2014).
- 4006
4007 [56] Metcalf, C. J. E. *et al.* Statistical modelling of annual variation for inference
4008 on stochastic population dynamics using integral projection models. *Methods in*
4009 *Ecology and Evolution* **6**, 1007–1017 (2015).
- 4010
4011 [57] Caswell, H. Matrix population models: Construction, analysis, and interpretation.
4012 2nd edn sinauer associates. Inc., Sunderland, MA (2001).
- 4013
4014 [58] Rees, M. & Ellner, S. P. Integral projection models for populations in temporally
4015 varying environments. *Ecological Monographs* **79**, 575–594 (2009).
- 4016
4017 [59] Vandenkoornhuyse, P., Quaiser, A., Duhamel, M., Le Van, A. & Dufresne, A.
4018 The importance of the microbiome of the plant holobiont. *New Phytologist* **206**,
4019 1196–1206 (2015).
- 4020
4021 [60] Rees, M. Evolutionary ecology of seed dormancy and seed size. *Philosophical*
4022 *Transactions of the Royal Society of London. Series B: Biological Sciences* **351**,
4023 1299–1308 (1996).
- 4024
4025 [61] Moles, A. T. & Westoby, M. Seedling survival and seed size: a synthesis of the
4026 literature. *Journal of Ecology* **92**, 372–383 (2004).
- 4027
4028 [62] Afkhami, M. E. & Rudgers, J. A. Symbiosis lost: imperfect vertical transmission
4029 of fungal endophytes in grasses. *The American Naturalist* **172**, 405–416 (2008).
- 4030
4031 [63] Brown, A. & Akçay, E. Evolution of transmission mode in conditional mutualisms
4032 with spatial variation in symbiont quality. *Evolution* **73**, 128–144 (2019).
- 4033
4034 [64] Bruijning, M., Henry, L. P., Forsberg, S. K., Metcalf, C. J. E. & Ayroles, J. F.
4035 Natural selection for imprecise vertical transmission in host–microbiota systems.
Nature ecology & evolution **6**, 77–87 (2022).
- 4036
4037 [65] Leuchtmann, A. & Clay, K. in *The population biology of grass endophytes* 185–202
4038 (Springer, 1997).
- 4039
4040 [66] Lange, C. *et al.* Impact of intraspecific variation in insect microbiomes on host
4041 phenotype and evolution. *The ISME journal* **17**, 1798–1807 (2023).
- 4042
4043 [67] Jeschke, J. M. & Kokko, H. The roles of body size and phylogeny in fast and
4044 slow life histories. *Evolutionary Ecology* **23**, 867–878 (2009).
- 4045
4046 [68] Quintana-Ascencio, P. F., Menges, E. S., Cook, G. S., Ehrlé, J. & Afkhami,
4047 M. Drivers of demography: Past challenges and a promise for a changed future.
Demographic Methods across the Tree of Life; Salguero-Gómez, R., Gamelon, M.,
4048 *Eds* 115–129 (2021).

- [69] Evers, S. M. *et al.* Lagged and dormant season climate better predict plant vital rates than climate during the growing season. *Global Change Biology* **27**, 1927–1941 (2021). 4049
4050
4051
4052
4053
4054
4055
4056
4057
4058
4059
4060
4061
4062
4063
4064
4065
4066
4067
4068
4069
4070
4071
4072
4073
4074
4075
4076
4077
4078
4079
4080
4081
4082
4083
4084
4085
4086
4087
4088
4089
4090
4091
4092
4093
4094